



2023 DRAFT COASTAL MASTER PLAN

LANDSCAPE INPUT DATA

ATTACHMENT B1

REPORT: VERSION 04

DATE: AUGUST 2022

PREPARED BY: BRADY C. COUVILLION



COASTAL PROTECTION AND
RESTORATION AUTHORITY
150 TERRACE AVENUE
BATON ROUGE, LA 70802
WWW.COASTAL.LA.GOV

COASTAL PROTECTION AND RESTORATION AUTHORITY

This document was developed in support of the 2023 Coastal Master Plan being prepared by the Coastal Protection and Restoration Authority (CPRA). CPRA was established by the Louisiana Legislature in response to Hurricanes Katrina and Rita through Act 8 of the First Extraordinary Session of 2005. Act 8 of the First Extraordinary Session of 2005 expanded the membership, duties, and responsibilities of CPRA and charged the new authority to develop and implement a comprehensive coastal protection plan, consisting of a master plan (revised every six years) and annual plans. CPRA's mandate is to develop, implement, and enforce a comprehensive coastal protection and restoration master plan.

CITATION

Couvillion, B. C. (2022). 2023 Draft Coastal Master Plan: Attachment B1: Landscape Input Data. Version 4. (pp. 1-130). Baton Rouge, Louisiana: Coastal Protection and Restoration Authority.

ACKNOWLEDGEMENTS

This document was developed as part of a broader Model Improvement Plan in support of the 2023 Coastal Master Plan under the guidance of the Modeling Decision Team (MDT):

- Coastal Protection and Restoration Authority (CPRA) of Louisiana – Elizabeth Jarrell (formerly CPRA), Stuart Brown, Ashley Cobb, Catherine Fitzpatrick (formerly CPRA), Krista Jankowski, David Lindquist, Sam Martin, and Eric White
- University of New Orleans – Denise Reed

This document was prepared by the 2023 Coastal Master Plan Landscape Data Team:

- Brady R. Couvillion – U.S. Geological Survey (USGS)

EXECUTIVE SUMMARY

Coastal Louisiana is a complex landscape. The composition of the landscape, as well as the processes which influence said landscape, vary in both space and time. The models utilized in the 2023 Coastal Master Plan must attempt to reflect that spatial and temporal variability. It is therefore of the utmost importance that the spatial datasets upon which the models are initialized are of the highest quality.

This task focused on the compilation and creation of spatial datasets pertaining to parameters necessary to initialize models, calibrate their operations, and/or validate their results. Spatial datasets compiled and/or created as part of this effort include 1) an initial Landscape Composition and Configuration spatial dataset, 2) an Integrated Topo/Bathymetric Digital Elevation Model 3) a Wetland Vegetation Community Type data set, and 4) Historical Marsh Edge Erosion Rates.

Each of these datasets constitutes a fundamental descriptor of the coastal landscape, upon which the models depend. This document describes the datasets compiled and the methodologies utilized to create the best-available spatial data describing the landscape in coastal Louisiana. While data collection dates vary, the datasets created for this effort are intended to represent 2018. The data described herein form initialization data sets upon which most, if not all, models of the 2023 Coastal Master Plan depend in one way or another.

TABLE OF CONTENTS

COASTAL PROTECTION AND RESTORATION AUTHORITY	2
CITATION	2
ACKNOWLEDGEMENTS	3
EXECUTIVE SUMMARY	4
TABLE OF CONTENTS	5
LIST OF TABLES	6
LIST OF FIGURES	6
LIST OF ABBREVIATIONS	7
1.0 INTRODUCTION	9
2.0 METHODS	10
2.1 Study Area	10
2.2 Landscape Composition	10
2.3 Baseline Digital Elevation Model - Integrated Topo/Bathymetric Data	18
2.4 Initial Vegetation Community Type Classification	25
2.5 Historical Edge Erosion Rates	31
3.0 RESULTS	35
3.1 Landscape Composition Results	35
3.2 Digital Elevation model – integrated topo/ bathymetric data	36
3.3 Wetland Vegetation Community Type Results	37
3.4 Marsh Edge Erosion Rate Results	39
4.0 DISCUSSION	42
5.0 REFERENCES	43
APPENDIX A: DIGITAL ELEVATION MODEL GRIDDED VISUALIZATIONS	45
APPENDIX B: WETLAND VEGETATION COMMUNITY TYPE VISUALIZATIONS	89

LIST OF TABLES

Table 1. Sentinel-2 endmembers for sand and developed areas	17
Table 2. Herbaceous wetland community types of interest.....	26
Table 3. NOAA CCAP non-wetland LULC Categories.....	27
Table 4. Confusion Matrix – Herbaceous Wetland Types - 2018	39

LIST OF FIGURES

Figure 1. Domain for the Landscape Data task and the hydrologic compartments... 10	
Figure 2. An example of a Sentinel-2 composite image (bands 8,4,3) in various stages of pre-processing.	12
Figure 3. Mean 2018 composite Sentinel-2 image (bands 8,4,3).	14
Figure 4. Standard deviations of the mNDWI (upper) and NDVI (lower) during 2018 from Sentinel-2 imagery.	15
Figure 5. Sentinel-2 based mNDWI values versus 1-meter aerial imagery-based fractional water.....	17
Figure 6. Topographic source projects used in the CoNED2 Integrated Topo/Bathymetric DEM.	19
Figure 7. Integrated bathy/topo source projects used in the CoNED2 Integrated Topo/Bathymetric DEM.	20
Figure 8. Bathymetric source projects used in the CoNED2 Integrated Topo/Bathymetric DEM.	21
Figure 9. Year of acquisition of data used in the NGOM2 CoNED Integrated Topo/Bathymetric DEM.	22
Figure 10. Hydro-flattened locations in the NGOM2 Topobathymetric Digital Elevation Model.	24
Figure 11. 2018 Sentinel-2 based NDVI harmonic image displaying phase, amplitude, and value on R,G,B.	29
Figure 12. Example area from 2018 Sentinel-2 based PCA image.	30
Figure 13. An example area of the land area change matrix – 2005, 2008, 2012, 2015/16, and 2018.	32
Figure 14. An example area of the Euclidean distance calculation.	33
Figure 15. Landscape Composition (fractional land is showing in red, fractional FAV in green, fractional SAV in blue, and fractional water in black).	35
Figure 16. DEM.	36
Figure 17. 2018 LULC Classification.	38
Figure 18. Marsh Edge Erosion Rates – 1-m resolution.....	40
Figure 19. Generalized (100-m) marsh edge erosion rates.	41

LIST OF ABBREVIATIONS

CART	CLASSIFICATION AND REGRESSION TREES
CCAP	COASTAL CHANGE ANALYSIS PROGRAM
CONED	COASTAL NATIONAL ELEVATION DATASET
CPRA	COASTAL PROTECTION AND RESTORATION AUTHORITY
CRMS	COASTWIDE REFERENCE MONITORING SYSTEM
CWPPRA.....	COASTAL WETLANDS PLANNING, PROTECTION, AND RESTORATION ACT
DEM	DIGITAL ELEVATION MODEL
DOA	DATES OF ACQUISITION
DTMS	DIGITAL TERRAIN MODELS
FAV	FLOATING AQUATIC VEGETATION
GPS.....	GLOBAL POSITIONING SYSTEM
GPSONBM	GLOBAL POSITIONING SYSTEM ON BENCHMARKS
GRS80	GEODETIC REFERENCE SYSTEM
HUC	HYDROLOGIC UNIT CODES
ICM	INTEGRATED COMPARTMENT MODEL
KM	KILOMETER
LADOT	LOUISIANA DEPARTMENT OF TRANSPORTATION
LAVEGMOD.....	ICM VEGETATION MODEL
LMRMP	LOWER MOST MISSISSIPPI RIVER MANAGEMENT PROGRAM
LPBF	LAKE PONTCHARTRAIN BASIN FOUNDATION
LSU	LINEAR SPECTRAL UNMIXING
LULC	LAND USE OR LAND COVER
M	METER
MESMA	MULTIPLE ENDMEMBER SPECTRAL MIXTURE ANALYSIS
MNDWI	MODIFIED NORMALIZED DIFFERENCE WATER INDEX
NDVI	NORMALIZED DIFFERENCE VEGETATION INDEX
NGS	NATIONAL GEODETIC SURVEY
NWI.....	NATIONAL WETLANDS INVENTORY
PCA	PRINCIPAL COMPONENTS ANALYSIS
POR.....	PERIOD OF RECORD

1.0 INTRODUCTION

The data upon which models are initiated and/or calibrated is an important determinant of the quality and utility of the modeling results. Flawed input data will inevitably produce flawed output data. Consequently, the accuracy of those input and calibration datasets directly influences the confidence that can be placed in the results.

As such, this effort compiled and created input datasets pertaining to the coastal Louisiana landscape from the best data available. As the 2023 Coastal Master Plan models are representing spatially variable phenomena, the data representing those landscapes and processes must also be spatial data. The data used in this effort have been created from, or informed by, a variety of sources including field data, aerial, and satellite imagery.

This document details the data sets compiled, and the methodologies utilized, to create the best available input datasets pertaining to the coastal Louisiana landscape as input data to various models utilized in the 2023 Coastal Master Plan. These include 1) a spatial representation of the initial land-water composition and configuration, 2) an integrated Topo/Bathymetric Digital Elevation Model 3) a spatial representation of land use/land cover (LULC) and wetland vegetation community types, and 4) historical marsh edge erosion rates. These datasets form vital input data upon which many of the models used in the 2023 Coastal Master Plan depend.

2.0 METHODS

2.1 STUDY AREA

While the models utilized for the 2023 Coastal Master Plan typically utilize a domain consistent with the hydrologic compartments shown in Figure 1, the intent for this effort was to create landscape data for an area larger than the hydrologic compartment domain to provide information regarding the conditions present in boundary areas of each hydrologic compartment. As such, the domain for this effort (Figure 1) is delineated by all 10-digit Hydrologic Unit Codes (HUCs) intersecting a 10-m elevation contour landward and a seaward boundary which extended into the Gulf of Mexico to alleviate boundary condition concerns. The domain extends beyond Sabine Lake to the west and beyond Mobile Bay to the east (Figure 1).

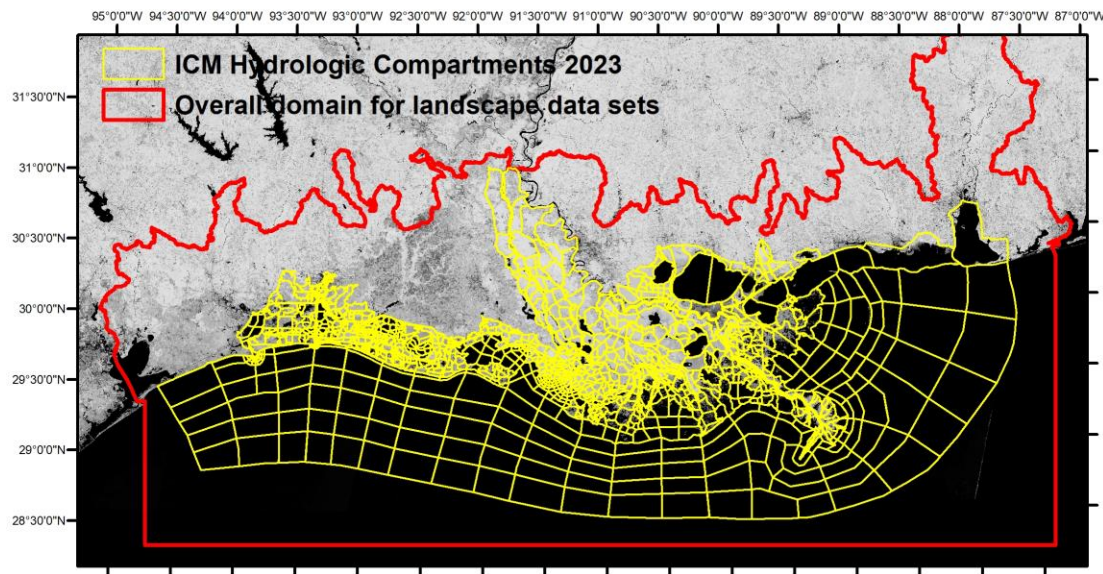


Figure 1. Domain for the Landscape Data task and the hydrologic compartments. Background imagery is a 2018 Normalized Difference Vegetation Index median composite from Landsat 8 included for visual reference only.

2.2 LANDSCAPE COMPOSITION

The initial composition and configuration of the landscape forms an important baseline from which models are initiated and forms a baseline of comparison for model results. As land area is an important parameter to many ecological processes and outcomes, accuracy in describing this initial

composition is paramount. While a parameter as simple as land area seems simplistic, the dynamic nature of wetland environments necessitates sophisticated techniques are utilized to accurately describe the landscape.

IMAGERY

Whereas previous iterations of the Louisiana Coastal Master Plan have utilized Landsat imagery to quantify the initial landscape composition and configuration, a newly available satellite from the European Space Agency, Copernicus Sentinel-2, was chosen for this assessment. The sensors on board Sentinel-2 are superior to those of Landsat in several respects including spatial, spectral, and temporal resolution. In terms of spatial resolution, Sentinel-2 has four bands at 10-m resolution and an additional 6 bands at 20-m resolution. This is compared to the spatial resolution of Landsat which is ~30-m resolution in most bands.

Temporal resolution refers to the revisit period of the satellite. Sentinel-2 has a revisit period of five days (as opposed to 16 days for the Landsat series of satellites). This increased temporal resolution increases the likelihood of coverage during a given season, and also provides additional data regarding temporal variation, useful in the classification of targets such as vegetation. One of the only facets in which Sentinel-2 is not superior to Landsat is period of record (POR). Sentinel-2 imagery is only available from mid-2015 through present whereas Landsat is available from 1984-present. As the objective of this particular task was to create a 2018 baseline landscape composition and configuration data set, Sentinel-2 was identified as a superior choice for that particular purpose.

Imagery for this effort therefore consisted of Sentinel-2 imagery from 2018. The surface reflectance corrected collection of Sentinel-2 imagery was utilized. As the revisit period of the Sentinel-2 satellite is five days, in theory this led to a collection of 73 images, or more (considering overlap), at any given location. The following sections will discuss preprocessing techniques which reduced that collection of images down to only images and pixels which contain quality data.

PRE-PROCESSING / CLOUD EXCLUSION

Initial pre-processing of the collection of Sentinel-2 imagery from 2018 consisted of filtering the collection of all available images during 2018 using the “CLOUDY_PIXEL_PERCENTAGE” metric provided in the metadata of each image. This metric was used to filter the collection of images to contain only those which were estimated to contain less than 40% cloud cover throughout each entire image. This initial step filters the collection to remove images that are exceptionally cloudy and likely contaminated.

While portions of an image may be cloudy, that does not mean that image does not still contain valuable data in other regions. As such, the next step in preprocessing was to conduct cloud recognition and exclusion on a per-pixel basis. This step attempts to recognize clouds, clouds shadows, and other sources of noise or erroneous values, and mask out just those specific pixels, leaving uncontaminated pixels unmasked and available for utilization. For this process, a multi-stage

approach was taken. The first step was to use the “QA60” band contained in the Sentinel-2 imagery to recognize and exclude clouds and other sources of contamination. This initial masking step is done on a pixel-by-pixel basis, so, at this stage, a given pixel likely has a different number of observations remaining than its neighbors. Those remaining values should be cloud-free; however, the QA60 band is not infallible. Previous investigations have shown that clouds and other erroneous values often remain after masking using the QA60 band. A second iteration of masking was therefore conducted by calculating standard deviations from the mean of the remaining values at each pixel and excluding dates or observations in which the pixel values are more than 2 standard deviations from the mean. This step identifies and excludes pixels which are likely contaminated in some manner.

Following this iteration of masking, the remaining observations should be relatively cloud and contamination free, and those pixels were used as the final population from which a mean composite was created. Figure 2 below is an illustration of a mean composite of Sentinel-2 imagery at each stage of preprocessing. Figure 2a is the mean composite following solely filtering on the basis of the “CLOUDY_PIXEL_PERCENTAGE” metric. Figure 2b shows a mean composite following filtering based on the “CLOUDY_PIXEL_PERCENTAGE” pixel percentage, as well as masking on the basis of the “QA60” band. Figure 2c is a mean composite of Sentinel imagery following all three iterations of filtering and masking.

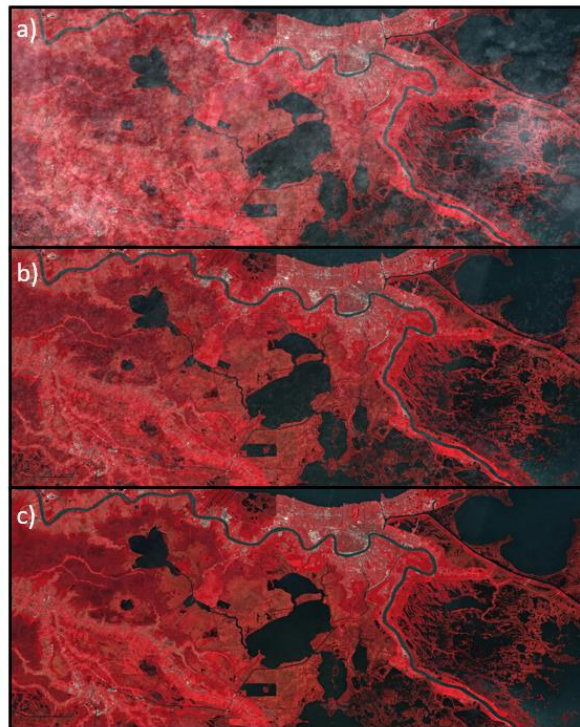


Figure 2. An example of a Sentinel-2 composite image (bands 8,4,3) in various stages of pre-processing.

INDICES

MODIFIED NORMALIZED DIFFERENCE WATER INDEX

The Modified Normalized Difference Water Index (mNDWI) (Xu 2005, 2006) was calculated as this index is particularly informative when distinguishing between land and water categories. The mNDWI enhances water features while reducing noise from land, vegetation, and soil (Xu, 2006). This index is a ratio of green and short-wave infrared (SWIR) wavelengths of light. The mNDWI is seen in Equation 1 below (Green: ~0.52–0.60 μm ; SWIR: ~1.55–1.75 μm):

$$\text{mNDWI} = (\text{Green} - \text{SWIR}) / (\text{Green} + \text{SWIR}) \quad (1)$$

The mNDWI results in a dataset with a bimodal distribution representing land and water. The values of this metric used in the Linear Spectral Unmixing methodology are discussed in the High-Resolution Imagery for Endmember Development in Wetland Areas section.

NORMALIZED DIFFERENCE VEGETATION INDEX

A Normalized Difference Vegetation Index (NDVI) was also used as an informative index indicating the presence (or absence) and vigor of vegetation. This index, and the variability of this index, was primarily used to identify floating aquatic vegetation, discussed further in the Aquatic Vegetation section. The NDVI formula is detailed in Equation 2 below (NIR: 0.772-0.898 μm ; Red: 0.631-0.692 μm):

$$\text{NDVI} = (\text{NIR} - \text{Red}) / (\text{NIR} + \text{Red}) \quad (2)$$

ANNUAL COMPOSITE

Following the previously discussed preprocessing and calculation of indices, a mean composite was calculated from all remaining values during the 2018 observation period. By utilizing a mean composite to quantify landscape composition and configuration, this helps ensure the resulting data set is more indicative of “normal” conditions and lessens the chance of including ephemeral events such as flooding. A visualization of the 2018 mean annual composite Sentinel-2 imagery is shown below in Figure 3.

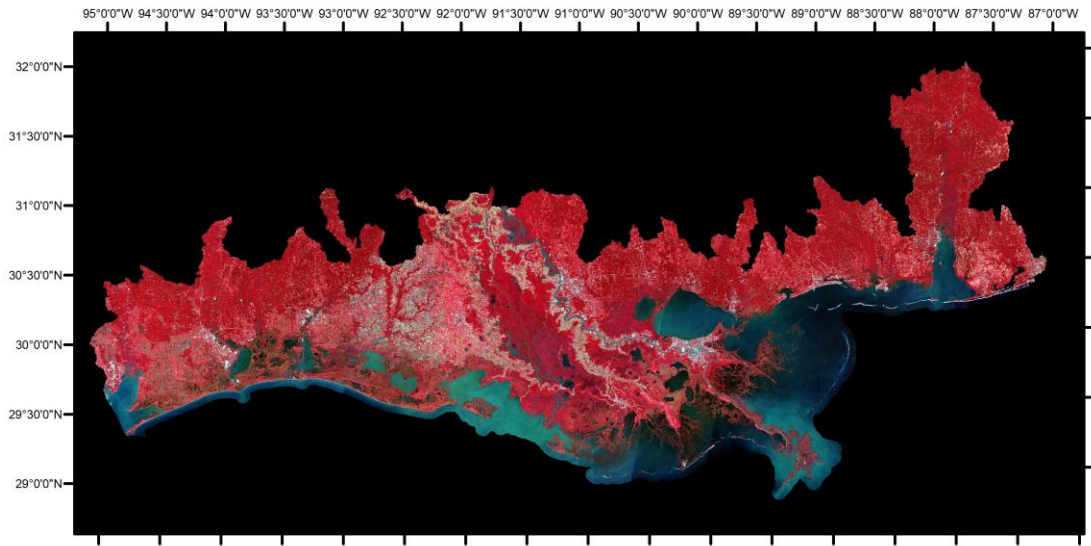


Figure 3. Mean 2018 composite Sentinel-2 image (bands 8,4,3).

AQUATIC VEGETATION

Aquatic vegetation, particularly floating aquatic vegetation (FAV) is one of the greatest obstacles to accurately categorizing land and water categories in coastal Louisiana. Targets containing FAV have strong vegetation signals, a characteristic usually indicative of land. Unless FAV is identified correctly and recoded to water, a transient vegetation signal can be misinterpreted as land change. In the past, areas of FAV have often been recoded via user-interpretation. In this case, the scale of the analysis made user-interaction with each image impractical. For this reason, we sought to recognize and account for aquatic vegetation in an automated manner.

The recognition or classification of aquatic vegetation can however be complicated by the fact that species that can occur in free-floating, aquatic conditions can either also occur in attached marsh and/or appear spectrally similar to other species of marsh that occur in attached conditions. We therefore developed an approach based on variability in both the NDVI and mNDWI indices. Our approach is based largely on the observation that targets containing aquatic vegetation are generally characterized by variation in these indices signals through time. In other words, as the vegetation moves or dies during various times of year, the reflectance values with respect to vegetation and water signals will vary tremendously. We therefore created an aquatic vegetation mask by querying pixels that contained a combination of variable NDVI and mNDWI signals through the period of record. An example of the datasets quantifying this variability is shown in Figure 4 below which displays standard deviations of all NDVI values (remaining after pre-processing) during 2018, and is a similar measure for the mNDWI in 2018. The higher values in the light gray and white symbologies indicate

higher variability in these indices throughout the year and are indicative of the possibility of aquatic vegetation in those locations.

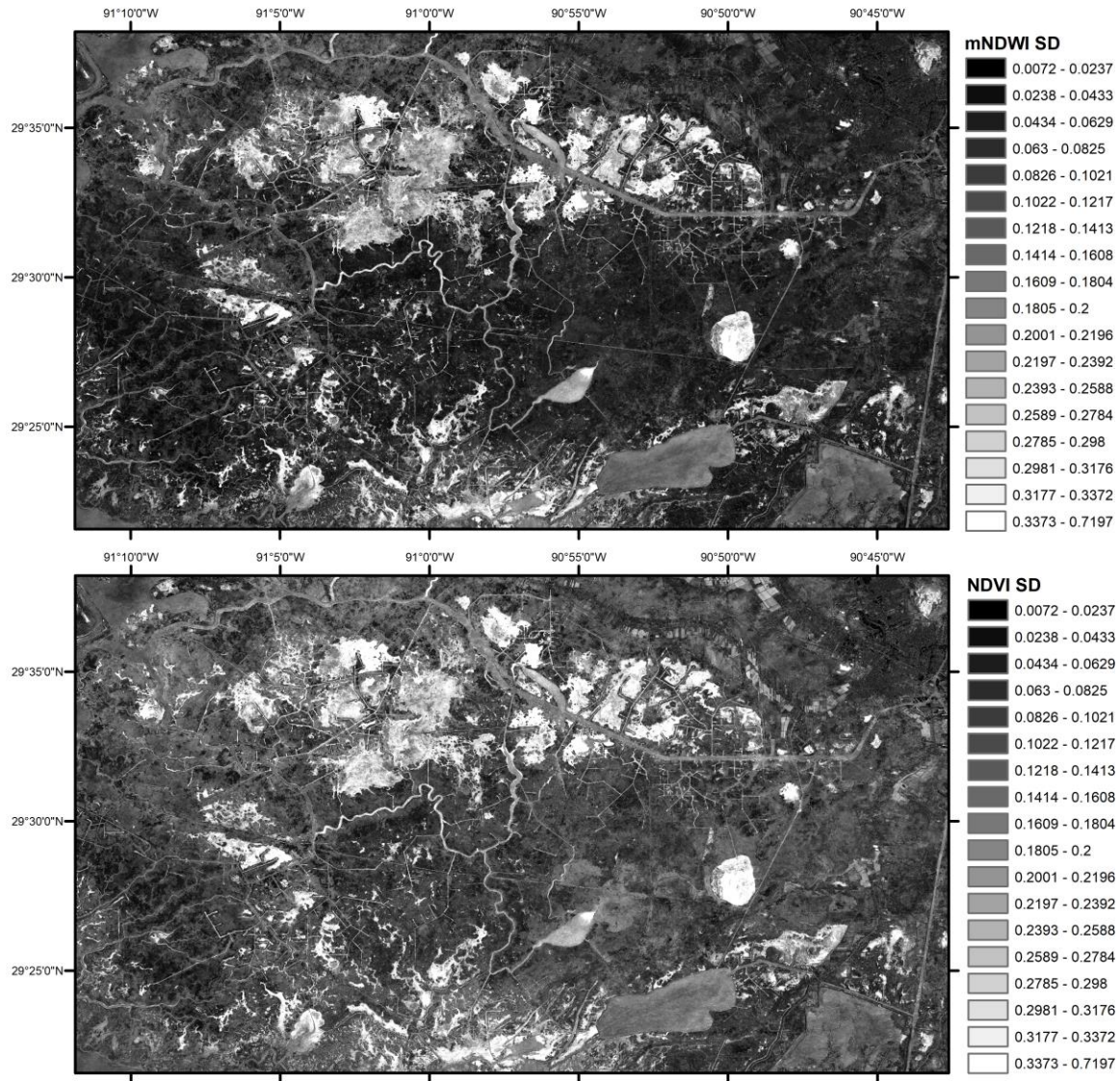


Figure 4. Standard deviations of the mNDWI (upper) and NDVI (lower) during 2018 from Sentinel-2 imagery.

A mask was created to identify areas in which the standard deviation of NDVI values in 2018 exceeded a value of 0.22, and the standard deviation of the mNDWI in 2018 exceeded a value of 0.2. Spectral unmixing was then utilized to identify and quantify aquatic vegetation within this mask and

will be further discussed in the Endmember Development in Developed and Sandy Areas section.

HIGH-RESOLUTION IMAGERY FOR ENDMEMBER DEVELOPMENT IN WETLAND AREAS

“Endmembers” are spectral values (in particular bands or indices) representative of a pixel of homogenous composition of a class of interest. Endmember values for Sentinel-2 were developed using aerial imagery-based land/water classifications (1-meter resolution) to calibrate the mNDWI values representing fractional land and water categories. The land/water products used for calibration consisted of 2015/2016 land/water classifications of coastal Louisiana created for the Coastwide Reference Monitoring System (CRMS) (Couvillion et al., 2018a; 2018b). While there is now a 2018 high-resolution data set for CRMS land/water, it was not available at the time of endmember development for this effort and as such, the 2015/16 CRMS data was compared to 2015/16 Sentinel-2 imagery.

Mean mNDWI values were calculated during time periods which most closely matched the periods of acquisition the high-resolution assessments. Aerial imagery-based land/water products were aggregated from 1-m resolution to 10-m resolution to match the Sentinel-2 pixels and the percent land/water in each 10-m pixel was recorded. Mean and standard deviation values of mNDWI were recorded in 1% intervals from 1% water to 99% water. The results are shown in Figure 5.

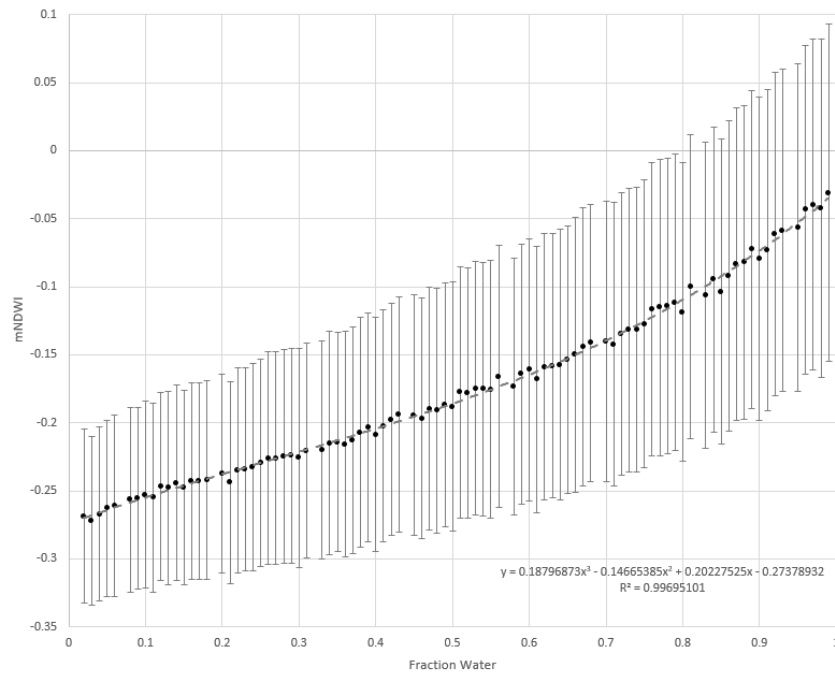


Figure 5. Sentinel-2 based mNDWI values versus 1-meter aerial imagery-based fractional water.

Endmember values were calculated from the line which best fit the calibration data. The values of these lines at 0% water and 100% water were -0.2738 and +0.0302, respectively.

ENDMEMBER DEVELOPMENT IN DEVELOPED AND SANDY AREAS

While the above endmembers work well in vegetated wetland environments, they do not work well in developed or sandy areas. The mNDWI value alone can lead to misclassification of these areas as containing high amounts of water. As such, it is important to recognize developed and sandy targets and estimate their composition by other means. Through a process similar to that described above, endmembers were developed for sandy and developed areas using National Oceanic and Atmospheric Administration (NOAA) Coastal Change Analysis Program (C-CAP) 2015-2017 Beta-level data (NOAA, 2022). The endmembers for sand and developed areas are shown below in Table 1. Sentinel-2 endmembers for sand and developed areas.

Table 1. Sentinel-2 endmembers for sand and developed areas

Code	Description	B3	B4	B5	B6	B7	B8	B11	B12	NDVI	mNDWI
SND	Sand	2129.58	2355.42	2535.90	2598.51	2673.43	2738.41	3178.59	2861.81	0.0710	-0.1223
DLI	Developed, Low Intensity	900.37	863.51	1299.27	2194.32	2498.89	2665.60	2277.34	1551.78	0.2550	-0.2460
DMI	Developed, Medium Intensity	1151.33	1184.90	1502.22	2065.22	2272.16	2392.48	2354.22	1818.86	0.1694	-0.1742
DHI	Developed, High Intensity	1684.21	1802.76	2017.48	2243.51	2357.42	2447.43	2738.57	2307.47	0.0823	-0.0986

FRACTIONAL LAND/WATER ESTIMATION

A combination of Linear Spectral Unmixing (LSU) and Multiple Endmember Spectral Mixture Analysis (MESMA) was used to estimate the relative abundance of targets of interest in a given pixel of imagery. In this case those targets of interest were the fraction of land, floating aquatic vegetation, submerged aquatic vegetation, and water in a given pixel. The determination of a pixel's contents are based on the targets' spectral characteristics, informed by the endmember discussed in previous sections. This method assumes the reflectance of each pixel of the image is a linear combination of the reflectance of each target (or endmember) within that pixel. The result of linear spectral unmixing is an image in which pixel values indicate a fractional estimate of the composition of the target class within that pixel. The output of this step was a 4-band raster data set, with the four bands representing the fraction of land, water, floating aquatic vegetation (FAV) and submerged aquatic vegetation (SAV) in each pixel.

POST-PROCESSING

While the landscape composition data was originally created at 10-m spatial resolution, some models of the ICM require input data at coarser resolutions. The 10-m fractional land water data was aggregated to 30-m and 500-m resolution and then thresholded to classify anything with greater than 50% land as a thematic land category, and greater than or equal to 50% water, FAV, or SAV as water.

2.3 BASELINE DIGITAL ELEVATION MODEL - INTEGRATED TOPO/BATHYMETRIC DATA

The elevation of a given wetland is one of the most important determinants of the fate of said wetland. In many respects, the survival of a given wetland is determined by its elevation, and its ability to maintain an elevation suitable to wetland survival. As elevation decreases relative to water level, inundation depth, duration, and frequency increases. Beyond certain thresholds, this can lead to inundation stress, which increases the susceptibility of that particular wetland to loss. Conversely, in open water areas, the bathymetry of a given location is one of the most fundamental and important determinants of the land building or restoration potential at a given location.

Prior to this effort, the best available Digital Elevation Model consisted of the Coastal National Elevation Dataset, version 1 (CoNED, 2015), which was heavily utilized in the creation of the 2017 baseline digital elevation model (Couvillion, 2017). The topographic portion of this data set utilized primarily Lidar from the Louisiana Statewide Lidar Acquisition Project with dates of acquisition ranging from approximately 2001 through 2007. Not only is this data somewhat removed from the base period for the 2023 Coastal Master Plan (2018), there were known issues with many of the Lidar acquisitions including seamlines and water level fluctuations. Recognizing the limitations of this data, an effort was already underway to acquire new Lidar throughout much of coastal Louisiana and incorporate these newly available datasets into a CoNED version 2. This effort, termed the "NGOM2

TBDEM”, was a joint effort of the U.S. Geological Survey, the Louisiana Coastal Protection and Restoration Authority (CPRA), and the Lowermost Mississippi River Management Program (LMRMP), to create an improved version of integrated 1-m topo/bathymetric digital elevation model (TBDEM) for the Northern Gulf of Mexico (NGOM)-2. The new NGOM2 CoNED TBDEM utilized the best available multi-source topographic and bathymetric elevation data for NGOM. The 2023 Coastal Master Plan baseline digital elevation model (DEM) is largely based off of the surface resulting from this effort, with a few exceptions which will be discussed in the Integration section.

DATA SOURCES

The NGOM-2 TBDEM utilized 286 different data sets from a variety of sources including the USGS 3D Elevation Program (3DEP), the National Oceanic and Atmospheric Administration (NOAA), U.S. Army Corps of Engineers (USACE), U.S. Department of Agriculture Natural Resources Conservation Service (USDA NRCS), CPRA, Louisiana Department of Transportation (LA DOT), Lake Pontchartrain Basin Foundation (LPBF), and the Texas Natural Resources Information System. Spatial metadata is available detailing the source data for any given location (Danielson et al., 2022). Visualizing 286 sources is difficult in one visualization and as such, Figures 6-8 below split the data sources into three categories; topographic sources (Figure 6) topo/bathymetric sources (Figure 7), and bathymetric sources (Figure 8).

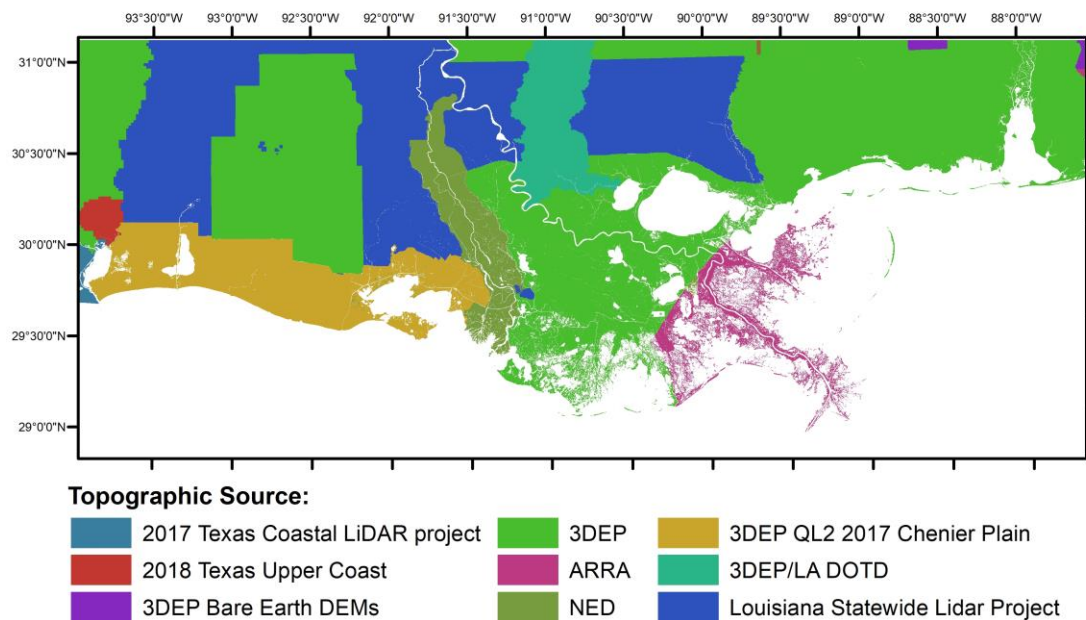


Figure 6. Topographic source projects used in the CoNED2 Integrated Topo/Bathymetric DEM.

The topographic data sources utilized in this effort consist primarily of newly collected, high density

Lidar data from a variety of sources shown in Figure 6. In certain, non-coastal areas, the older Lidar from the Louisiana Statewide Lidar project was utilized however these areas are of lesser importance in coastal modeling efforts. Additionally, the areas in which this older Lidar was used were less susceptible to some of the issues observed in wetland areas.

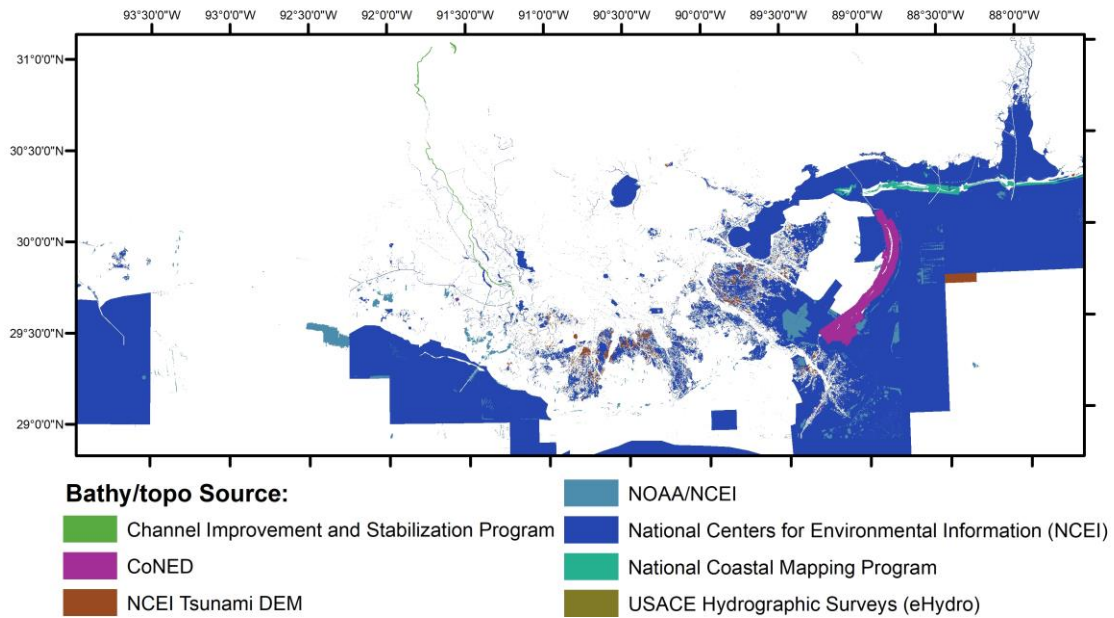


Figure 7. Integrated bathy/topo source projects used in the CoNED2 Integrated Topo/Bathymetric DEM.

The data sources visualized in Figure 7 include topo/bathymetric sources from a variety of agencies. Typically, these datasets consisted of previous combined bathymetric and topographic data sources.

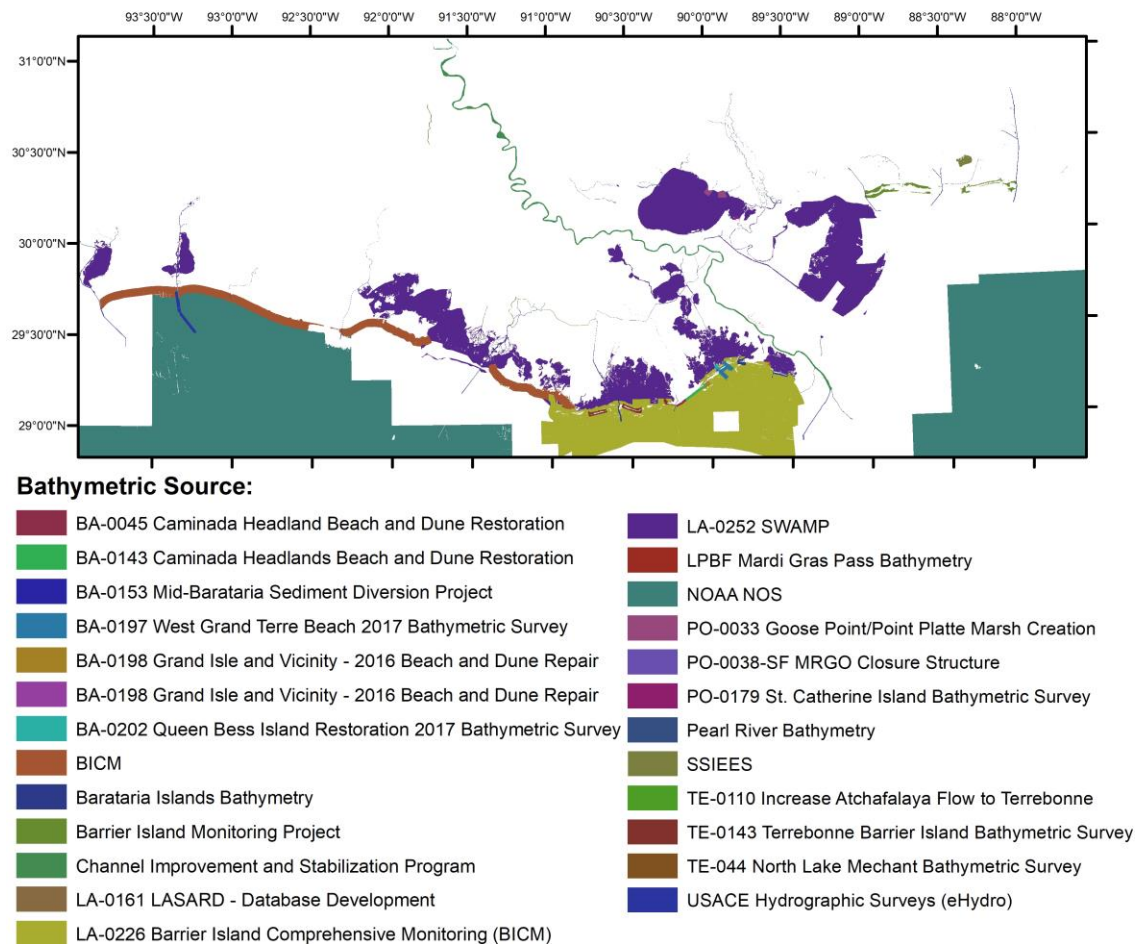


Figure 8. Bathymetric source projects used in the CoNED2 Integrated Topo/Bathymetric DEM.

The dates of acquisition (DOA) of the various elevation sources ranged from 1851 through 2021. Spatial metadata (Danielson et al., 2022) detailing the date of acquisition by location is available in the “Date Acquired” attribute of the metadata and is visualized in Figure 9. This figure symbolizes the older data sets in red and the newest data sets in green. In general, the topographic data sources are more recent and many of the bathymetric sources, particularly those far offshore are often older. While the age of many of these bathymetric data sources appears concerning, most of the locations in which the bathymetry is exceptionally old are in areas far offshore. The bathymetric values in these locations are of lesser consequence to most of the models of the 2023 Coastal Master Plan than near-shore water bodies.

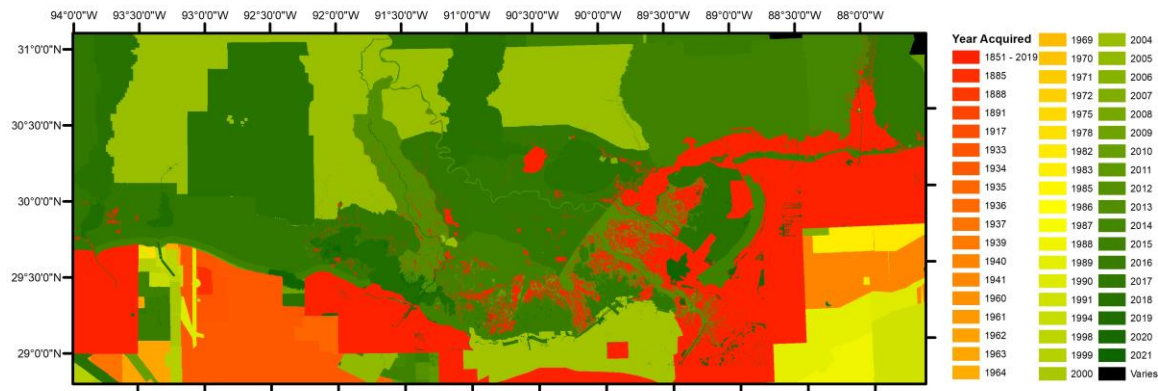


Figure 9. Year of acquisition of data used in the NGOM2 CoNED Integrated Topo/Bathymetric DEM.

INTEGRATION

The data discovery, collection and compilation efforts associated with the above-mentioned data sources were overwhelming tasks, perhaps eclipsed only by the effort required to process and integrate the resulting myriad of data sets into one, continuous surface. First, all datasets had to be reprojected into a common coordinate system, scaled into common units, and adjusted into a common vertical reference system. The NGOM2 CoNED TBDEM is provided in Universal Transverse Mercator (UTM) North American Datum (NAD) 1983, National Spatial Reference System (NSRS) 2011, Zone 15 North. The ellipsoid is Geodetic Reference System 1980 (GRS 80). The vertical datum is North American Vertical Datum of 1988 (NAVD88), Geoid 12B. NOAA's Vertical Datums Transformation (VDatum) software was used for vertical transformations. The units of the NGOM2 CoNED TBDEM are meters. Full metadata on the NGOM2 CoNED TBDEM surface is available at: <https://dx.doi.org/10.2112/SI76-008>. The following text is a brief summary of processes involved in the integration process.

The integration of topographic and bathymetric data sources involves the combination of two fundamentally different data types. Though both are quantifying the elevation of the earth surface, they are collected by different means, in different areas, and those areas must be defined and treated as distinct. Combining these disparate data sources first necessitates a determination of where they will and will not apply. Following transformation of all input datasets into common units, datums, and coordinate systems, the next step was the development of breaklines. Breaklines are features used to define where certain datasets will and will not apply. In this case, breaklines were developed to define the boundary between land and water areas thereby dictating where topographic and bathymetric data sources would apply. For the NGOM2 CoNED TBDEM, breaklines were developed for multiple data sources. In some cases, the entity or agency that collected the data had previously developed

breaklines. In other cases, breaklines had to be developed specifically for this effort. In cases in which breaklines previously existed, they were reviewed for accuracy, and revised if necessary.

Next, a list of priorities was developed to guide the selection of elevation values when multiple surveys or data sources were available in a given location. Data sources were prioritized based on project characteristics, including acquisition dates, cell size, retention of features, water surface treatment, visual inspection, and the presence of artifacts. In general, preference was given to more recent data collections, all other things being equal. All other things being equal, more accurate datasets, or those with a higher point density were prioritized over less accurate surveys.

Following this prioritization step, a geodatabase of all data sources and their priority order was created. Boundaries were created from the final set of input data based on each data sets priority. Seamlines between data sets were generalized to smooth transition boundaries between neighboring data sets. The data sets were then spatially mosaiced based on priority to create a seamless topobathymetric composite at a cell size of 1-m using a linear spatial blending (10 pixel overlapping area) technique between input source layers. Areas in which there was a gap between bathymetric and topographic data sources were interpolated in some locations. Other areas in which no bathymetric data existed were “hydro-flattened”. “Hydro-flattening is the process of creating a lidar-derived DEM in which water surfaces appear and behave as they would in traditional topographic DEMs created from photogrammetric digital terrain models (DTMs)” (Danielson et al., 2022). These hydro-flattened areas will be discussed in further detail in the Filling Bathymetry Gaps in Hydro-flattened Areas section.

FILLING BATHYMETRY GAPS IN HYDRO-FLATTENED AREAS

The NGOM2 CoNED TBDEM effort used hydro-flattening in areas in which bathymetry datasets meeting the criteria for inclusion in this effort were not available. Hydro-flattening involves the utilization of an elevation of the water surface rather than bathymetric values in water areas. As previously mentioned, bathymetry can be difficult to collect, and is not available for all waterbodies in and around coastal Louisiana. Typically, this occurs more frequently in small water bodies such as ponds. The areas in which the NGOM2 CoNED TBDEM surface includes hydro flattened values rather than bathymetric values is shown below in Figure 10. While hydro-flattening is a common technique in the absence of sufficient bathymetric data, and it is clearly stated in the metadata of the data set, those values are problematic in a modeling effort which necessitates bathymetric values for all water areas.

Therefore, for this modeling application, hydro-flattened areas had to be first identified, and replaced with bathymetric, interpolated, or assumed values to ensure proper model operation. The first step in this process was the identification of bathymetric values that were either hydro-flattened or flagged as potentially problematic to model operations. In addition to the hydro-flattened spatial data set shown in Figure 10, logical queries were run for locations identified as open water by the data set described in Section 2.2, and possessing an elevation value greater than or equal to hydrologic model output for

mean water level for 2018. These locations of hydro-flattened or flagged bathymetric data were then examined for possible alternatives including alternative bathymetric sources, interpolated data, or assumed bathymetric values.

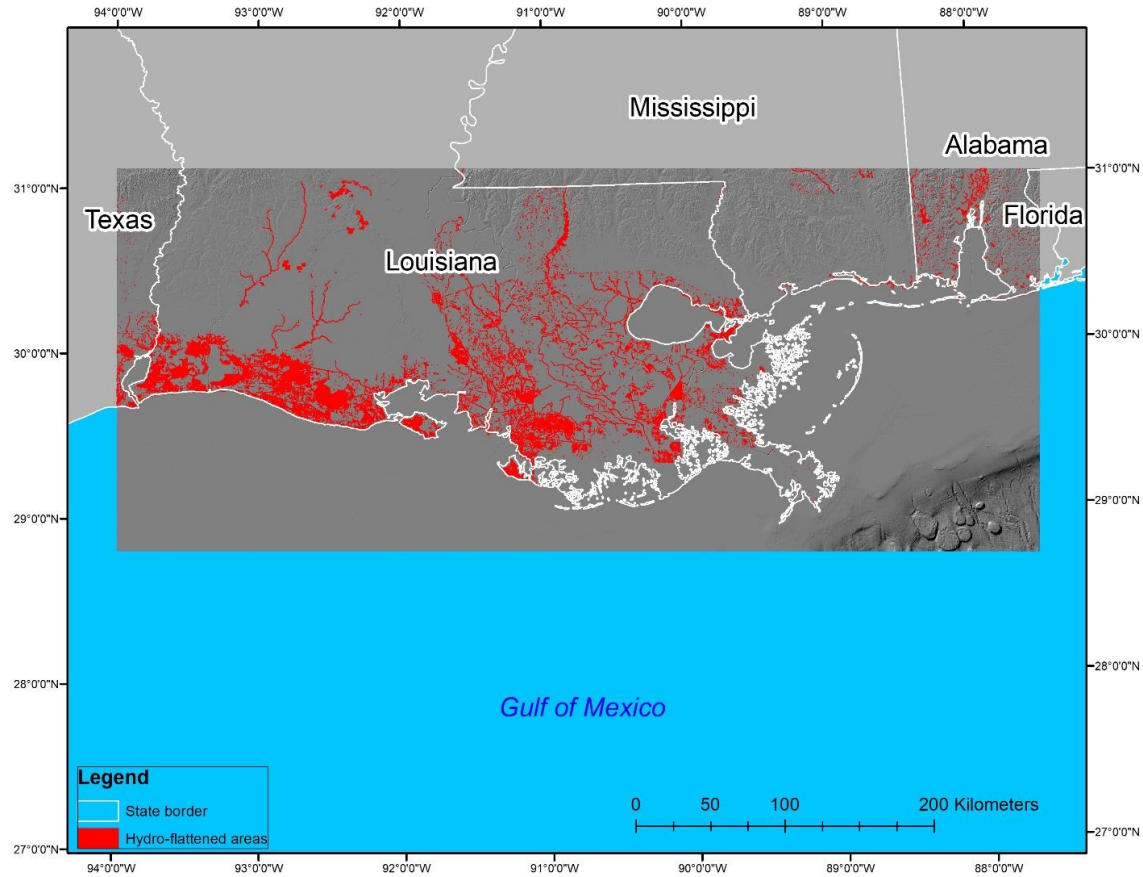


Figure 10. Hydro-flattened locations in the NGOM2 Topobathymetric Digital Elevation Model.

The primary source of alternative bathymetric values consisted of the 2017 Master Plan Baseline DEM (Couvillion, 2017). In many cases, this data is coarser resolution than was required for inclusion in the NGOM2 CoNED TBDEM. For the landscape scale modeling applications of the ICM however, that coarse resolution did not necessitate its exclusion. If a location was hydro-flattened or flagged for replacement by the previous logical query, and the 2017 surface had a logically sound bathymetric value for that location, that value was replaced with the adjusted, 2017 DEM surface value.

If no alternative bathymetric value was available for a location, however bathymetric values were present at locations in that water body sufficient to allow for interpolation across unknown locations, interpolation was used to develop values for those locations.

Finally, if no alternative bathymetric values were available and interpolation was not possible for a given location, an assumed value of 2018 mean water level minus 0.25 m was used in those locations. Typically, this only occurred in small ponds, and this assumed value assures the area will not immediately convert to land in modeling output. Rather said location would require sediment deposition in order to do so. While these assumed values are not ideal, it is a modeling assumption to prevent illogical outcomes in modeling results.

POST-PROCESSING

The NGOM2 TBDEM was created at 1-m resolution. This spatial resolution is too fine for ICM modeling applications as it would be too computationally intensive and unnecessarily detailed for the landscape level models. The surface was therefore aggregated to 10-m resolution, using the mean of all 1-m cells within a 10-m cell. For certain modeling applications, this surface was further aggregated to 30-m and or 500-m resolution as described in specific modeling reports.

2.4 INITIAL VEGETATION COMMUNITY TYPE CLASSIFICATION

While the previous two datasets describe the three-dimensional landscape, datasets defining the land use or land cover (LULC) of that location are of importance to the models as well. The land cover type, including the vegetation occupying that landscape must also be described. Many coastal processes vary depending upon the vegetation type occupying a site and as such, a dataset that describes the distribution of those classes is a necessary dataset for model initialization. The vegetation model, in particular, requires a starting or base condition. This task utilized helicopter vegetation survey data, categorized into dominant wetland vegetation types, defined by vegetation experts, to train a classification and create a 2018 Wetland Vegetation Community Type spatial data set.

WETLAND VEGETATION COMMUNITY TYPES OF INTEREST

LAVegMod, the vegetation model utilized in the ICM of the 2023 Coastal Master Plan, predicts the distribution of wetland vegetation community assemblages, and the change in those assemblages through time under varying environmental scenarios. In order to do so, it must be informed by baseline data of regarding the distribution of these community types. The community assemblages of interest were decided upon by vegetation experts involved in the creation of the LAVegMod subroutine of the ICM. The herbaceous wetland vegetation types of interest to the model are shown below in Table 2. It is important to note that although particular species codes are used to define these assemblages, these areas are not generally monospecific and homogeneous. The species listed are generally a result of what would be considered the dominant species in that location. Other species of vegetation may co-occur with that dominant species of vegetation. That something is classified in either the field data or the landcover spatial data set as a particular species, does not mean other species cannot occur in that location.

Table 2. Herbaceous wetland community types of interest

Code	Species_Code	Species Name	Common Name
1	AVGE	Avicennia germinans	black mangrove
2	CLMA10	Cladium mariscus	sawgrass
3	COES	Colocasia esculenta	elephant ear
4	DISP	Distichlis spicata	saltgrass
5	ELBA2_FLT	Eleocharis baldwinii	
6	ELCE	Eleocharis cellulosa	gulf spikerush
7	IVFR	Iva frutescens	
8	JURO	Juncus roemerianus	black needlerush
9	MOCE2	Morella cerifera	wax myrtle
10	PAHE2/PAHE2_FLT	Panicum hemitomon	maidencane
11	PAVA	Paspalum vaginatum	
12	PHAU7	Phragmites australis	roseaucane
13	POPU5	Polygonum punctatum	smartweed
14	SALA	Sagittaria sp.	bulltongue
15	SCCA11	Schoenoplectus californicus	bullwhip
16	SCAM6	Schoenoplectus americanus	three-square
17	SCRO5	Schoenoplectus robustus	coco
18	SPAL	Spartina alterniflora	oystergrass
19	SPCY	Spartina cynosuroides	hogcane
20	SPPA	Spartina patens	wiregrass
21	TYDO	Typha domingensis	southern cattail
22	ZIMI	Zizaniopsis miliacea	cutgrass

HIERARCHICAL CLASSIFICATION

Hierarchical classification methods involve splitting the landscape into distinct groups and conducting finer resolution LULC classification within those groups. For example, the data set described in the Landscape Composition section of this document can be used to first divide the landscape into land and water portions. Further classification of the land component of the landscape need not consider the water portion of the landscape.

This task is focused on classifying wetland vegetation community types however, the coastal Louisiana landscape contains other LULC types such as developed and agricultural areas. While these LULC categories are not directly modeled by the ICM, their locations in the landscape must be known to inform the model not to operate in those areas. So, similar to the dichotomous branch between land and water portions of the landscape described, the next level of hierarchical classification utilized in this methodology was to further subdivide the land portion into wetland and non-wetland components. For the purposes of this classification, non-wetland areas are going to include LULC categories such as developed, agriculture, pasture/hay, barren land, upland grassland areas, and upland forest.

There are several existing LULC products which classify these types of non-wetland LULC categories.

These include the USGS National Land Cover data set and NOAA C-CAP data. While these programs do include categories for wetlands, the wetland categories were not specific enough to fill the need of this effort. These programs generally categorize LULC approximately every four years at 30-m spatial resolution however, a 2015-2017 10-m NOAA Beta product was available at 10-m resolution, which utilized Sentinel-2 similar to the other spatial datasets in this effort (NOAA, 2022). Therefore, this 2015 to 2017 NOAA CCAP 10-m product was chosen to serve as the primary data source for non-wetland areas. An example from this NOAA CCAP data set is shown below in Table 3.

The LULC categories utilized from this data set are shown below and Table 3. Abbreviations given to these LULC categories are also described in this table which will be utilized elsewhere in this document.

Table 3. NOAA CCAP non-wetland LULC Categories

Code	Description
DHI	Developed, High Intensity
DMI	Developed, Medium Intensity
DLI	Developed, Low Intensity
DOS	Developed, Open Space
AGC	Cultivated Crops
PAS	Pasture/Hay
GRS	Grassland/Herbaceous
UDF	Upland Deciduous Forest
UEF	Upland Evergreen Forest
UMF	Upland Mixed Forest
USS	Upland Scrub/Shrub

FIELD DATA

The field data for this effort consisted of coast wide vegetation survey data from 2013 (Sasser et al., 2014). This helicopter-based survey, which occurs approximately every five to seven years, records landcover, and wetland vegetation composition (if wetlands are present) at more than 8,000 locations across coastal Louisiana. This survey recorded species composition at marsh and shrub stations throughout coastal Louisiana, which were then assigned to wetland vegetation community types using common dominants as well as species assemblages known to occur in the area. These data points were then used as training data for a remotely sensed methodology. While these data were collected in 2013, and the objective of this effort is to classify wetland vegetation community types in 2018, these data formed the best available field data for utilization as training period the temporal inconsistency among the training data set and the classification year was dealt with using a method known as change vector analysis. Satellite imagery from 2013 and 2018 was compared and survey locations in which a change was observed to have occurred in the imagery were excluded from

utilization as training or validation points.

While the survey as a whole records land cover at more than 8,000 points, approximately half of those points were recorded as water or another non-wetland LULC type. This initial step led to a total population of 3,768 points potentially available for utilization. The previously mentioned step of change vector analysis further reduced that population to 3,088 points. This dataset was further subdivided into 70% for training and 30% were held in reserve for validation. Therefore, the final training data set included 2,161 points.

An important consideration is the area over which the observers in the helicopter survey are looking when determining wetland vegetation composition. The helicopter survey involves two wetland vegetation experts looking out of each side of the helicopter over approximately a 20-m radius circle. To increase the number of sample field data points available for training, a 20-m radius buffer was run on the helicopter points and any pixels, predetermined to be wetland, within that buffer were available for selection as training data. This step increased the number of available training data locations from 2,161 points to approximately 18,000 locations which were utilized as training. The utilization of these locations will be further described in the Principal Components Analysis section of this document.

IMAGERY

The primary imagery source for this task, similar to that already discussed in the Landscape Composition Imagery section, consisted of Sentinel-2 imagery from 2018. One important difference with regard to the imagery utilized for this effort is the utilization of the entire collection, rather than a mean annual composite. In this task, the objective is to classify very specific wetland vegetation community types. While Sentinel-2 is a multispectral sensor with several spectral bands, in isolation, those bands would be insufficient to differentiate among these vegetation types. That is to say, this sensor lacks the spectral resolution to differentiate among these vegetation types on one date in isolation.

The phenology of varying vegetation types can however be exploited to increase the separability of those classes. That is to say that while two wetland vegetation types may be spectrally indistinguishable at a given time of year, those two types may have differences in their spectral characteristics at other times of year. This fact can be exploited to distinguish between those landcover categories. Therefore, while the previous two datasets utilized an annual mean composite, this task made use of both an annual mean composite and images products inform by all images throughout 2018, discussed in the following two sections.

HARMONIC ANALYSIS

Harmonic analysis was used to describe the intra-annual variability in indices such as the NDVI. This method fits a temporal series of values as a series of waves of varying wavelength on a pixel-by-pixel basis. The resulting image represents the collection of NDVI images throughout the year as a wave, described by its phase, amplitude and value. The resulting data set is visualized below in Figure 11.

This method of analysis serves not only as a means of data reduction, but also provides valuable data regarding the phenology of a location throughout a year. Differences in the waves representing two different pixels can be indicative of a multitude of parameters related to the vegetation in those locations, including species composition. The classifiers discussed later in the Classification unit in the Initial Vegetation Community Type Classification section can make use of these differences to distinguish among vegetation community types.

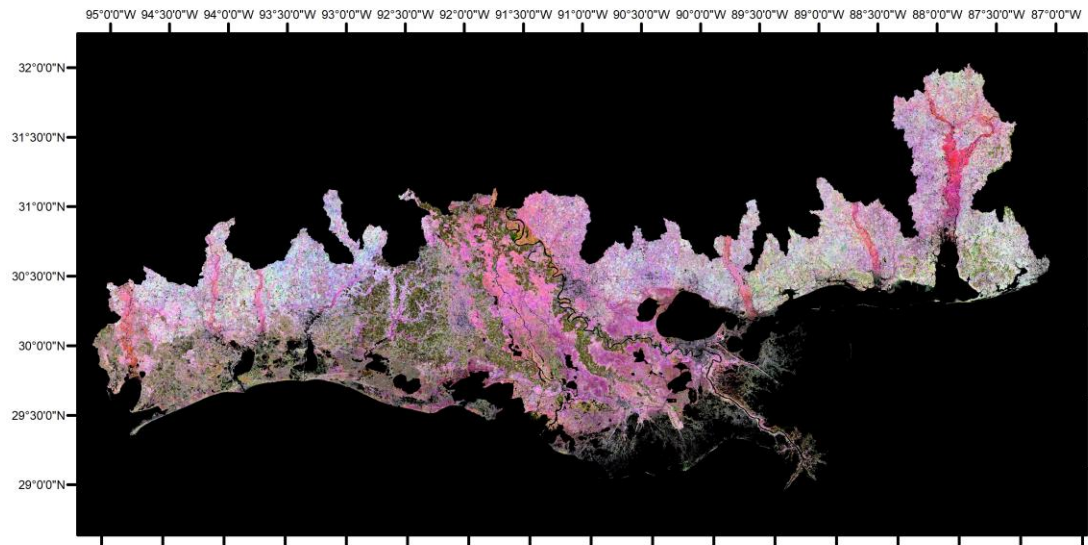


Figure 11. 2018 Sentinel-2 based NDVI harmonic image displaying phase, amplitude, and value on R,G,B.

PRINCIPAL COMPONENTS ANALYSIS

Similar to its applications with regard to statistics involving tabular data, Principal Components Analysis (PCA) can be applied to images (or a set of images) as a dimensionality reduction technique. Fundamentally it is the same in both applications. PCA transforms a set of potentially correlated values at a given pixel into a smaller number of uncorrelated variables described by principal components which are represented spatially in a raster on individual bands. An example of a PCA image for a set of images from 2018 is visualized in Figure 12 below.

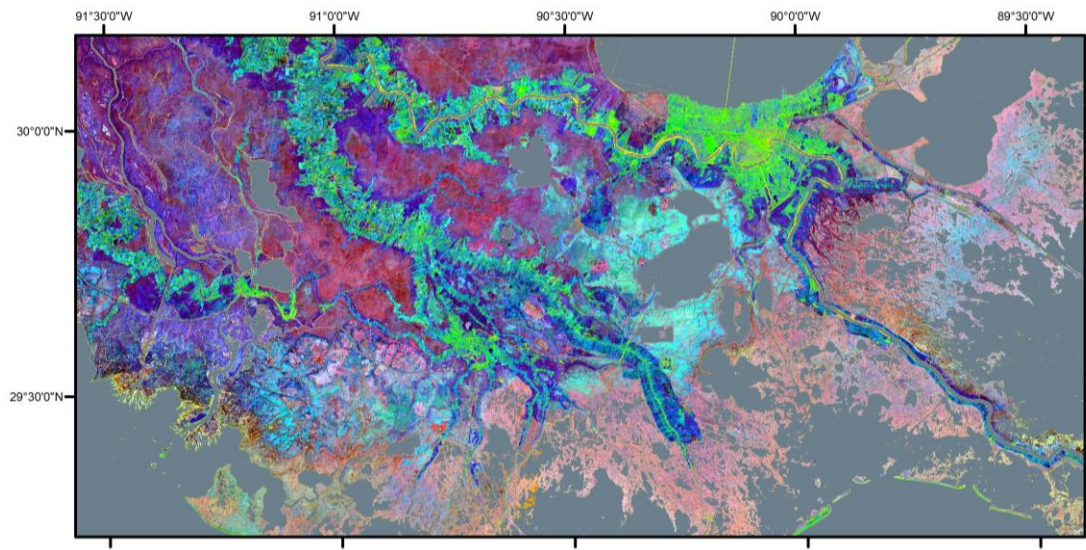


Figure 12. Example area from 2018 Sentinel-2 based PCA image.

CLASSIFICATION

The training sample from the helicopter survey described in the Field Data section above, as well as the imagery products described in the Imagery – Principal Components Analysis sections, were used in a series of classifications to categorize the herbaceous marsh portion of the landscape into the wetland vegetation types of interest. This effort utilized both Classification and Regression Trees (CART) and random forest classifiers. Multiple iterations of each classifier were run, utilizing different random samples from the approximately 18,000 possible training locations (see the Field Data section). Three iterations of CART classification and three iterations of random forest classifiers were run (each utilizing a different training sample) and the mode of the six resulting classifications at each pixel was taken as the final vegetation type classification. The results of this classification will be discussed in Section 3.3 later in this document.

ACCURACY ASSESSMENT

When previously discussing field data, it was mentioned that 30% of field data points were set aside for use in accuracy assessment. Following the various filtering of the survey data points, this left 814 data points available for accuracy assessment. These points were randomly selected, but stratified to represent a representative percentage of each vegetation type in the landscape. Following the creation of the 2018 LULC spatial data set mentioned above, these points were buffered using a 20-m radius, and the majority class was compared to the field determination. A confusion matrix, detailing this comparison was developed and will be discussed in the Wetland Vegetation Community Type Results section.

2.5 HISTORICAL EDGE EROSION RATES

Finally, a historical analysis of edge erosion rates was needed to inform the model which would reflect edge erosion in interior marshes. It is important to note that shoreline erosion on barrier islands is handled in a different sub-model. These rates are solely to inform edge erosion in interior marsh areas. Edge erosion is a process dependent upon several factors including wave energy on fine temporal scales. Reflecting this process at the spatial and temporal scales at which it occurs was determined to be too computationally intensive for landscape level models, and as such the decision was made to incorporate marsh edge erosion as a projection of historical rates.

Pertinent to the discussion of edge erosion is a decision on how “edge” is defined, and which edges are potentially subject to erosion. If “edge” or “shoreline” were defined as every transition between land and water, coastal Louisiana would contain more than 200,000 km of shoreline. This exceptionally large figure it's not however truly indicative of the edges or shorelines subject to edge erosion. Fetch is measure of the uninterrupted over water distance, over which winds can propagate waves. Previous investigations have concluded that a minimum of a 300-m fetch in at least one direction is necessary to produce the wave energy necessary to erode a marsh edge (Cortese, 2022). We therefore isolated this investigation to “edges” with at least a 300-m omnidirectional fetch.

IMAGERY

Whereas the previous two tasks made use of satellite imagery, for a process which occurs on such fine spatial scales as shoreline erosion, moderate resolution satellite imagery is typically not of a sufficient spatial resolution to measure said process. This task therefore necessitated the use of fine spatial resolution imagery. The primary source of said fine spatial scale imagery, at least historically, has been aerial imagery, typically available at 1-m resolution. One could argue that the process of shoreline erosion often occurs at sub-meter spatial scales and that would be correct, especially on fine temporal scales. Most appropriately documenting shoreline erosion would require fine-scale field measurements however, such measurements cannot be made at landscape scales. The concerns of using 1-m resolution imagery to quantify shoreline erosion are however mitigated over longer periods of observation, and in environments which experience large values of erosion. For the purposes of this landscape scale model, the shoreline erosion which occurred over a 13-year time period, as measured by 1-m aerial imagery, was determined to be sufficient for this coarse-scale application.

As part of ongoing coastal monitoring efforts through the CRMS and CWPPRA programs, aerial imagery is collected for coastal Louisiana approximately every three to four years. Aerial imagery is available for coastal Louisiana in 1998, 2005, 2008, 2012, 2015/16, and 2018. While this imagery is beneficial for certain applications in terms of spatial resolution, it is often more difficult to classify due to inconsistencies in the imagery, and often lacks the temporal resolution necessary for other applications. In this case however, it was the only data source suitable for the application.

CLASSIFICATION

For this task, an effort was conducted to classify the 2005, 2008, 2012, 2015/16, and 2018 aerial imagery into simple land and water categories. The methodology for doing so was based largely upon initial unsupervised classifications, the categories from which were recoded to land and water categories based on expert opinion. While the previous step does a relatively good job of separating land and water categories, there is no escaping the necessity for user intensive corrections. Correcting the entire, coastwide data sets would be an overwhelming, and time restrictive task. As such, this effort focused on shorelines with a greater than 300-m omnidirectional maximum fetch. By doing so, effort could be placed on accuracy in these limited locations.

The resulting categorical datasets for specific years were then matrixed to provide a data set informative of change throughout those time periods. An example of this change matrix is shown below in Figure 13below.

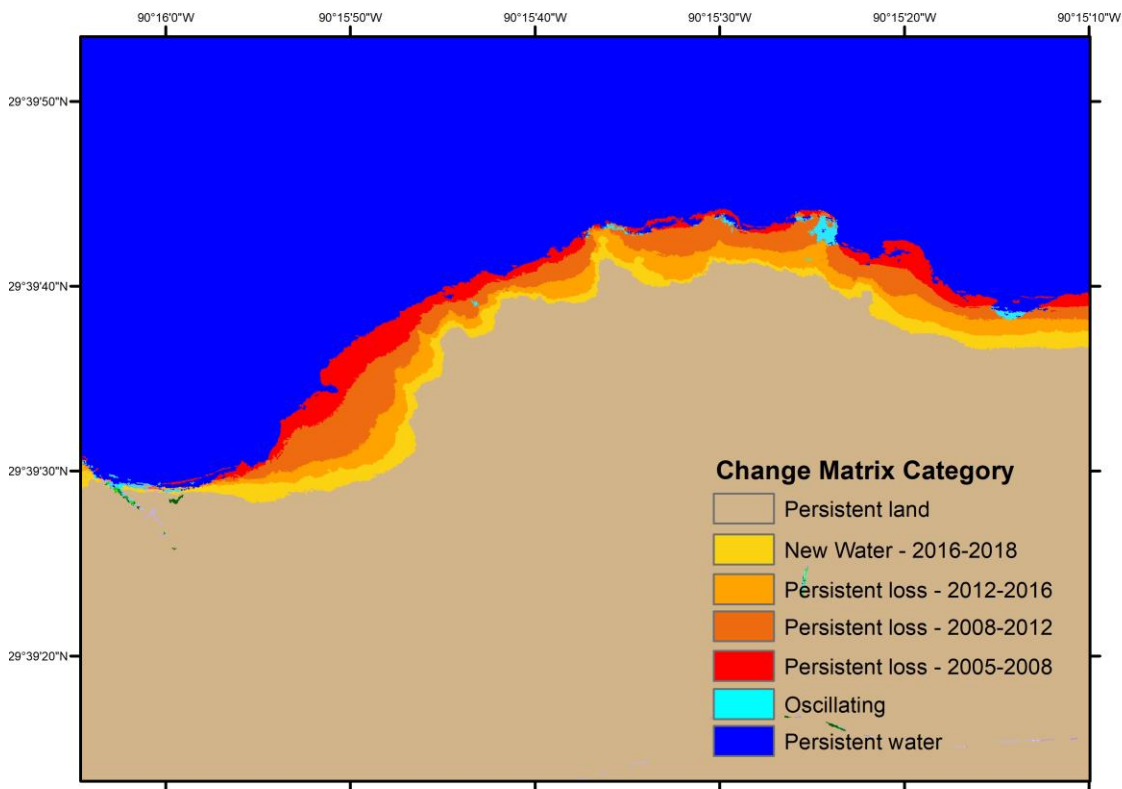


Figure 13. An example area of the land area change matrix – 2005, 2008, 2012, 2015/16, and 2018.

The above data set categorizes changes from land to water categories in each specific time interval. The data set was created with the intended purpose of using this spatial data to measure erosion rates. While the erosion rate at specific or randomly sampled points could be manually measured from this dataset, there was a desire to quantify erosion rates at all locations with at least a 300-m omnidirectional fetch. Doing so on this fine resolution spatial data would require hundreds of millions of calculations. We therefore sought an automated, though computationally intensive method of calculating these rates.

EUCLIDEAN DISTANCE AND DIRECTION

Euclidean distance is a method by which the distance between each pixel, and the closest source pixel can be calculated throughout a raster data set. As there is directionality to shoreline erosion, Euclidean distance is not the typical means of measuring shoreline erosion. If the predominant direction of erosion were known, the distance would be measured in that direction. In a simple Euclidean distance calculation, directionality is not enforced, but rather the distance is calculated in a direction that varies based on the closest available source pixel. In this case, the predominant direction of erosion was not always known, and fortunately, erosion typically occurs in a direction often perpendicular to the shoreline.

For this application, the pixels on the landward side of the 2005 shoreline were defined as the pixels from which to calculate distance, and the closest available pixel along with 2018 shoreline was defined as the destination pixels. An example visualization of these Euclidean distance calculations is shown below in Figure 14. In this figure, Euclidean distance calculations are shown in the area which has changed between 2005 and 2018. Areas which did not change are shown in black.

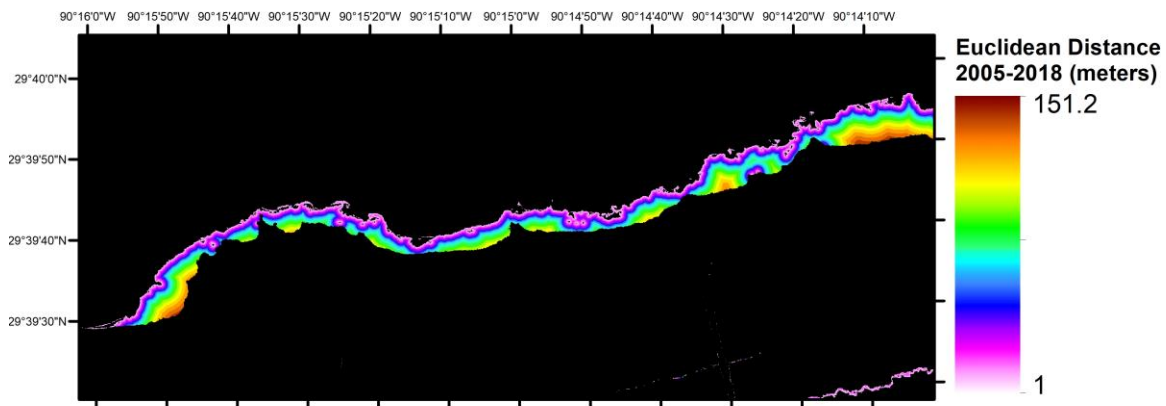


Figure 14. An example area of the Euclidean distance calculation.

After performing a Euclidean distance calculation, a neighborhood function was run to isolate only the maximum value within a 3 x 3 neighborhood along the 2018 shoreline. The results of said step will be

discussed later in the Marsh Edge Erosion Rate Results section.

3.0 RESULTS

The wetland change analyses which have resulted from this effort have revealed a complex and dynamic landscape, with patterns of wetland change which vary through both space and time. The processes and drivers of coastal wetland change vary in both space and time, and as such, it is not surprising that the observed patterns of wetland change also vary.

3.1 LANDSCAPE COMPOSITION RESULTS

The initial landscape composition data set for 2018 created by this effort forms both the initialization data for several models of the ICM, as well as an important baseline for comparison with regard to modeling results. The data set created as part of this effort is a 2018 annual mean fractional estimate of Land, FAV, SAV, and Water for every 10-m pixel in the domain. The resulting data set is shown below in Figure 15

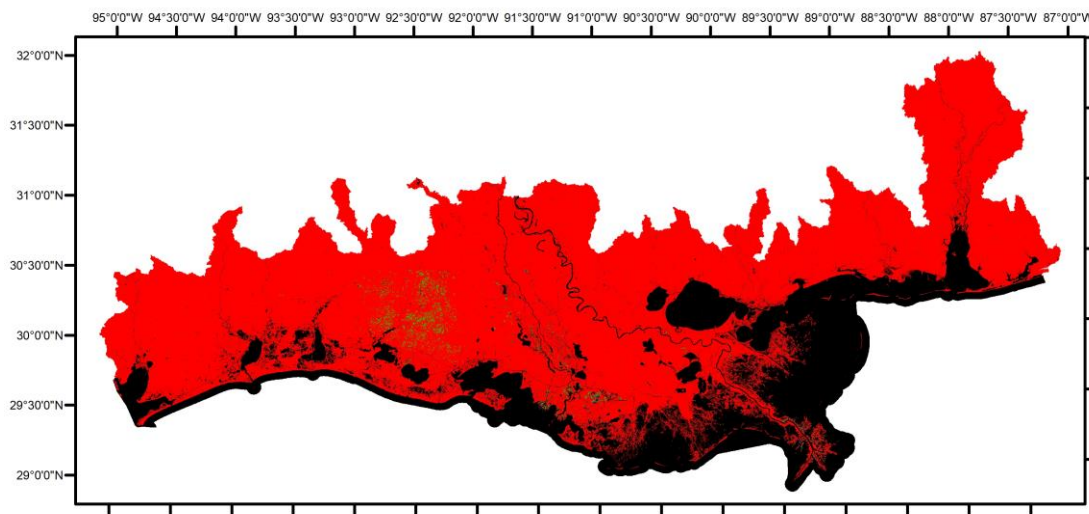


Figure 15. Landscape Composition (fractional land is showing in red, fractional FAV in green, fractional SAV in blue, and fractional water in black).

While the above data set seems relatively simplistic, it forms the first and most important dichotomous branch for several hierarchical classifications. These classifications will be further discussed in the Marsh Edge Erosion Rate Results section. This data set also forms the initial condition for several processes within the ICM, and an important baseline for comparison model results.

3.2 DIGITAL ELEVATION MODEL – INTEGRATED TOPO/ BATHYMETRIC DATA

The surface resulting from this effort constitutes the most appropriate compilation of the best available topography and bathymetry data for use in the 2023 Coastal Master Plan effort. An overall visualization of the final surface is shown in Figure 16 below. While Figure 16 gives an overall impression of the data set, the finer detail in the data set cannot be observed at this scale. Consequently, visuals on a 0.5° x 0.5° grid are available in Appendix A.

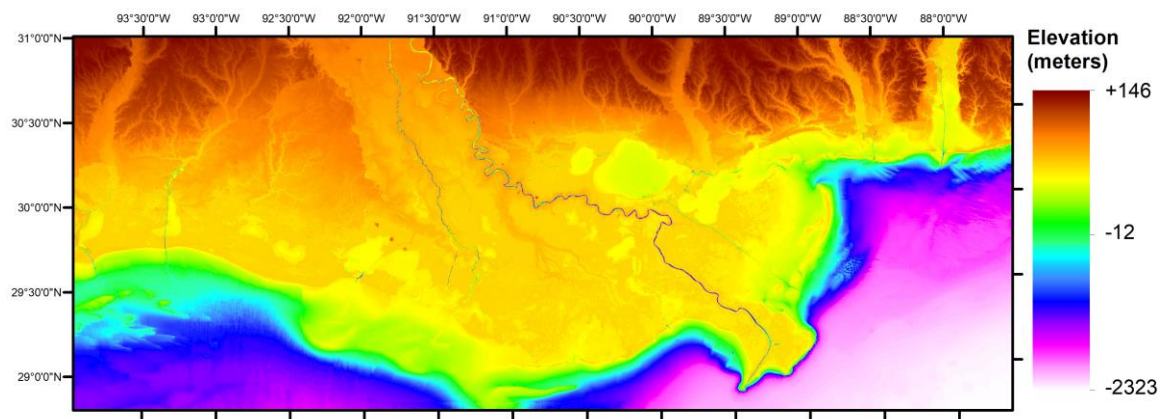


Figure 16. DEM.

The vertical accuracy of the NGOM2 CoNED TBDEM was assessed using multiple datasets. The first assessment used 4,510 Real-Time Kinematic (RTK) Global Positioning System (GPS) control points compiled by Dr. Scott Hagen of Louisiana State University (LSU). These points consisted of survey efforts in five locations: 1: Big Branch, 2: Grand Bay, 3: Maurepas, 4: Pascagoula, 5: Pearl River. These points are more indicative of wetland areas within the NGOM 2 TBDEM surface. The root mean square error (RMSE) of the TBDEM surface versus these LSU control points was 0.271 m.

The second assessment used 276 National Oceanic and Atmospheric Administration (NOAA) National Geodetic Survey (NGS) Global Positioning System (GPS) on Benchmarks (GPSONBM) control points distributed mostly throughout upland or developed areas of the NGOM 2 TBDEM surface. The RMSE of the TBDEM surface versus these GPSONBM control points was 0.236 m.

The third assessment used 2,568 RTK GPS points from the Coastwide Reference Monitoring System (CRMS). In this case, multiple elevations are taken at a given CRMS station. These elevations are taken within a 2-m x 2-m plot, and the elevations are intended to be reflective of the average value of the 2-m x 2-m plot. As such, for the purposes of this assessment, multiple elevations for a given plot were averaged and that value was used as the control point for comparison. The average of the NGOM 2 TBDEM surfaced was used within this same plot for comparison. Any CRMS elevation points with

notes that justified their exclusion, such as a note indicating the elevation was taken on top of vegetative material, were excluded from the analysis. The remaining CRMS points were distributed throughout, and therefore more indicative of, coastal herbaceous wetland areas of Louisiana. The RMSE of the TBDEM surface versus these CRMS control points was 0.262 m.

Overall, RMSE over the land and nearshore area is 0.267 m versus a combined 7,354 LSU, GPSONBM, and CRMS control points distributed throughout the NGOM 2 study area. It is important to note that the control points used for this vertical accuracy assessment represent land elevations rather than bathymetric values. As such this vertical accuracy assessment is only reflective of the vertical accuracy of the land component in the data set. There is not sufficient data to accurately quantify the vertical accuracy of the bathymetric portion of this data set. Please refer to the bathymetric data sources for measures of vertical accuracy and uncertainty of the input source data when available.

3.3 WETLAND VEGETATION COMMUNITY TYPE RESULTS

The 2018 baseline LULC data set resulting from this effort constitute possibly the most complete and specific land cover classification ever created for wetlands in this region. An overall visualization of the final data set is shown in Figure 17 below. Abbreviations in the legend of Figure 17 are defined in Table 2 and Table 3 in previous sections. While Figure 17 gives an overall impression of the data set, the finer detail in the data set cannot be observed at this scale. Consequently, visuals on a 0.5° x 0.5° grid are available in Appendix B.

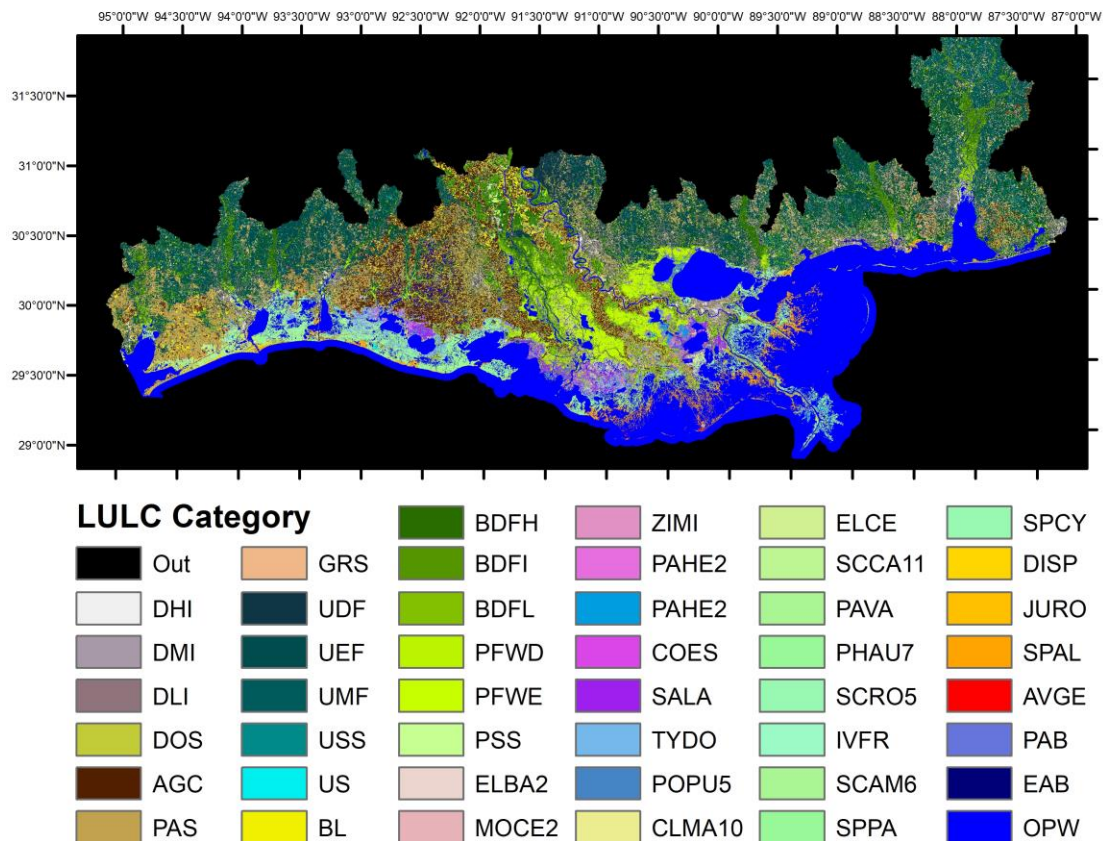


Figure 17. 2018 LULC Classification.

Remotely sensed classifications are commonly assessed on the basis of an accuracy assessment. Accuracy assessments are a quantitative analysis used to judge the accuracy of a classification at known points, in this case, helicopter survey points, which were not used as training, but were rather held in reserve for accuracy assessment. A random but stratified 30% sample was taken for accuracy assessment and the classification results were compared to the reference helicopter points. The results of that comparison are shown in the confusion matrix in Table 5 below. In this table, correct classification results are shown in the diagonal line of cells denoted in green. These cells list the number of points at which the classifier labeled a particular vegetation type, and the helicopter survey data confirmed that the vegetation type was indeed present at that location. All other cells in the confusion matrix represent an inaccuracy. This representation enables assessment of how often the classifier is right and wrong, but more importantly, it identifies the classes that it tends to label incorrectly, and what it mistakes them for. The greatest value of the confusion matrix is providing information on where the confusion is occurring among classes.

Table 4 also lists both a producer's and user's accuracy. These two types of accuracy result from the

two types of misclassification errors in remotely sensed classifications; errors of omission, and errors of commission. Errors of commission reflect the inclusion of a vegetation type in a location in which it should not have been included and are represented by user's accuracy. Conversely, errors of omission reflect the omission of a vegetation type in a location in which it should have been included and are represented by the producer's accuracy. Overall, the classification achieved an accuracy of 81.45%, which is generally considered to be exceptional for remotely sensed classifications, particularly when so many classes are included. Finally, the kappa statistic measures the probability that the results differ significantly from what would be expected by random chance. The kappa statistic ranges from -1 to 1, though negative values are only theoretically possible. The kappa value generally ranges from 0 to 1, with values closer to 1 representing increased significance of a deviation from a random assignment. The overall kappa statistic attained in the classification was 0.785 (Table 4), which again, is generally considered exceptional in a classification with this many classes. It is also important to note that this classification was hierarchical in approach, meaning earlier classifications of land and water for instance were first used to define the land area upon which the vegetation classification would take place. Any errors in that dataset are not reflected in these accuracy results, and therefore, these values may be slightly inflated. Refer to metadata of the NOAA C-CAP product for accuracy information regarding non-wetland categories (NOAA, 2022).

Table 4. Confusion Matrix – Herbaceous Wetland Types - 2018

		Classified Data																							
	AVGE	CLMA10	COES	DISP	ELBA2_FLT	ELCE	IVFR	JURO	MOCE2	PAHE2/FLT	PAVA	PHAU7	POPUS	SALA	SCAA11	SCAM6	SCRO5	SPAL	SPCY	SPPA	TYDO	ZIMI	Total	User Accuracy	
Reference Data	AVGE	4	0	0	0	0	0	0	0	0	0	0	0	0	0	0	0	0	1	0	0	0	0	5	80.00%
	CLMA10	0	6	0	0	0	0	0	0	0	0	0	0	0	0	0	0	0	1	0	4	2	2	15	40.00%
	COES	0	0	4	0	0	0	0	0	0	0	0	1	0	0	0	0	0	0	0	0	0	0	5	80.00%
	DISP	0	0	0	22	0	0	1	0	0	0	0	0	0	0	0	0	0	1	0	3	0	0	27	81.48%
	ELBA2_FLT	0	0	0	0	8	8	0	0	0	4	0	1	1	0	0	0	0	0	0	1	1	24	33.33%	
	ELCE	0	0	0	0	0	14	0	0	0	0	0	0	0	0	0	0	0	0	0	0	0	0	14	100.00%
	IVFR	0	0	0	0	0	0	5	0	0	0	0	0	0	0	0	0	0	0	0	0	0	0	5	100.00%
	JURO	0	0	0	1	0	0	0	16	0	0	0	0	0	0	0	0	0	0	0	2	0	0	19	84.21%
	MOCE2	0	0	0	0	0	5	1	0	2	2	0	0	0	1	0	0	0	0	0	1	0	0	12	16.67%
	PAHE2/FLT	0	0	0	0	0	2	0	0	0	54	0	0	0	0	0	0	0	0	0	0	1	0	57	94.74%
	PAVA	0	0	0	0	0	0	0	0	0	1	4	0	0	0	0	0	0	0	0	2	0	0	7	57.14%
	PHAU7	0	0	0	0	0	0	0	0	0	0	0	42	0	0	0	0	0	1	0	5	1	0	49	85.71%
	POPUS	0	0	0	0	0	1	0	0	0	1	0	0	6	0	0	0	0	0	0	0	2	0	10	60.00%
	SALA	0	0	0	0	0	8	0	0	0	1	0	0	0	47	0	0	0	0	0	5	1	0	62	75.81%
	SCAA11	0	1	0	0	0	0	0	0	0	0	1	0	0	0	11	0	0	0	0	2	2	0	17	64.71%
	SCAM6	0	0	0	0	0	1	0	1	0	1	0	0	0	0	1	35	1	1	1	14	0	0	56	62.50%
	SCRO5	0	0	0	0	0	0	0	0	0	0	0	0	0	0	0	0	2	0	0	1	0	0	3	66.67%
	SPAL	0	0	0	0	0	0	0	1	0	0	0	0	0	0	0	0	0	129	0	28	0	0	158	81.65%
	SPCY	0	0	0	0	0	0	1	0	0	0	0	0	0	0	0	0	0	0	10	2	0	0	13	76.92%
	SPPA	0	0	0	1	0	0	0	0	0	0	0	0	0	0	0	0	0	5	0	192	0	0	198	96.97%
	TYDO	0	0	0	0	0	1	0	0	0	0	0	0	0	0	0	0	0	0	0	6	44	0	51	86.27%
	ZIMI	0	0	0	0	0	1	0	0	0	0	0	0	0	0	0	0	0	0	0	0	0	6	7	85.71%
	Total	4	7	4	24	8	41	8	18	2	64	5	42	8	49	12	35	3	139	11	267	54	9	663	Total Correct
Producer Accuracy		100.00%	85.71%	100.00%	91.67%	100.00%	34.15%	62.50%	88.89%	100.00%	84.38%	80.00%	100.00%	75.00%	95.92%	91.67%	100.00%	66.67%	92.81%	90.91%	71.91%	81.48%	66.67%	Total	814
																							Overall Accuracy	81.45%	
																							Kappa Statistic	0.785044	

3.4 MARSH EDGE EROSION RATE RESULTS

The model results constitute the most complete assessment of shoreline erosion for all land-water transitions with a greater than 300-m omnidirectional maximum fetch.

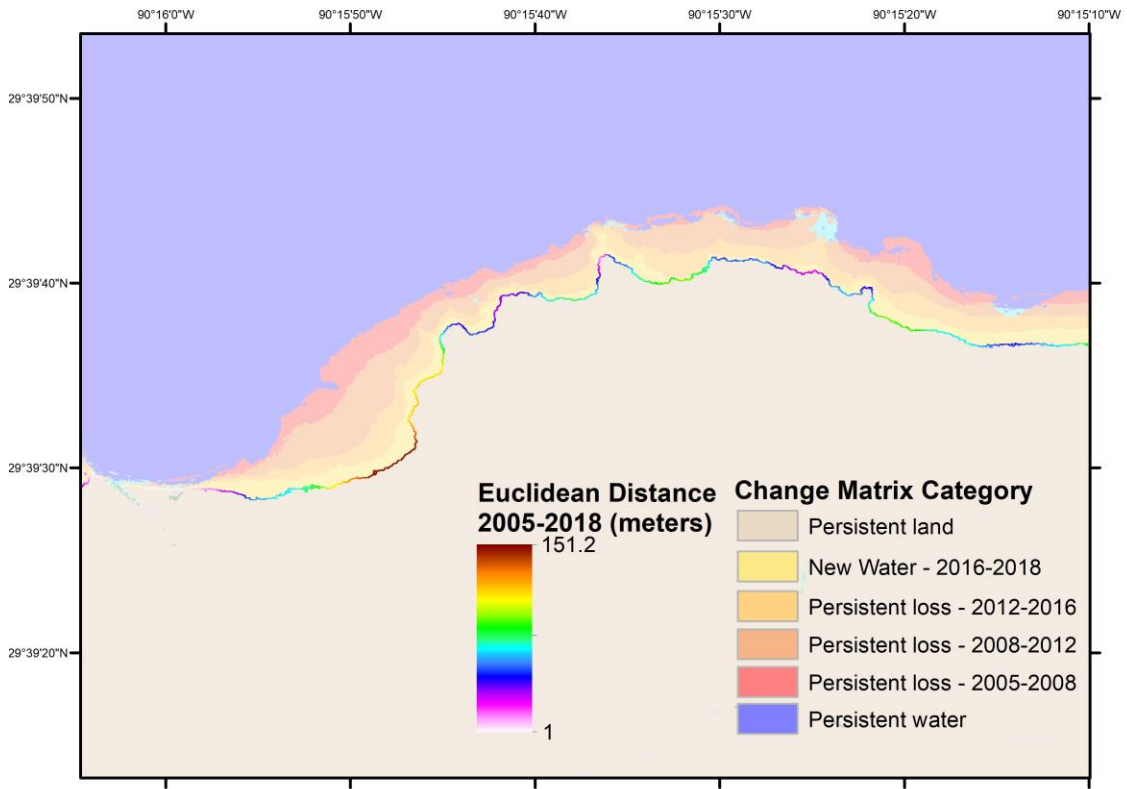


Figure 18. Marsh Edge Erosion Rates – 1-m resolution. Values along the 2018 shoreline represent the Euclidean Distance (m) from the 2005 shoreline to the 2018 shoreline.

The shoreline erosion results were created at 1-m resolution, but this resolution was too fine for incorporation into the ICM and as such, model results were aggregated to 100-m, 250-m, and 500-m resolutions. An example of these generalized datasets can be observed in Figure 19 below.

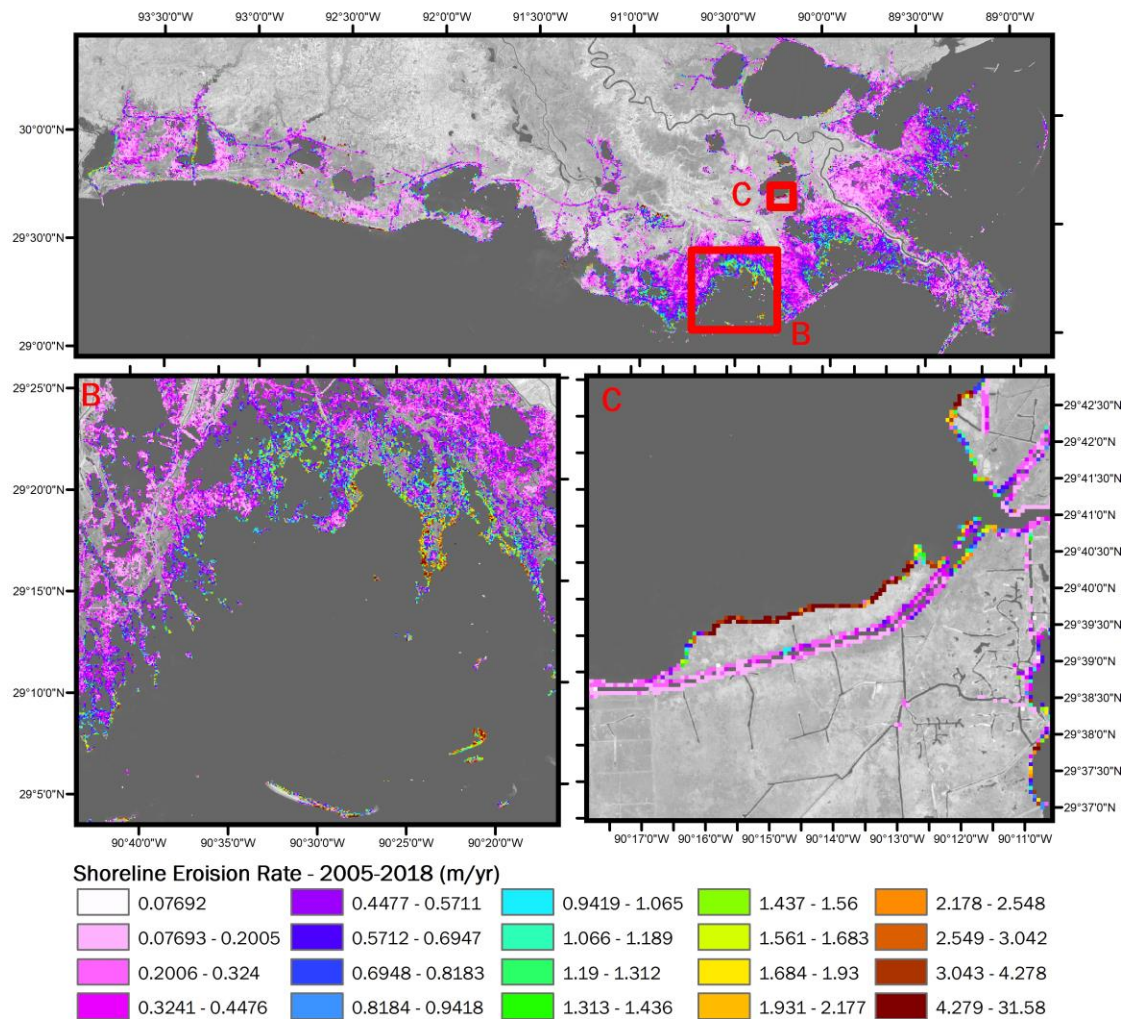


Figure 19. Generalized (100-m) marsh edge erosion rates.

4.0 DISCUSSION

Input data is the backbone of any modeling effort. A model can have every formula representing each process correct, but if the starting point is incorrect, so too will be the results. The primary objective of the ICM models is to reflect the coastal Louisiana landscape and the processes influencing it. The data created by this effort informed the ICM, both with regard to the landscape and those processes.

While no dataset is ever completely accurate, the data created as part of this effort represent the best data available for the 2023 Coastal Master Plan modeling. Not only are the datasets created by this effort more accurate, they provide increased spatial and categorical resolution, never before available in such a modeling effort.

One of the most important data sets, the integrated topographic and bathymetric DEM, benefited from extensive efforts to collect new elevation information, at improved spatial resolutions and utilizing new methods to decrease error, thereby decreasing uncertainty. Topographic, Lidar-based data comprises the majority of the newly available data compiled into this data set. Additionally, more is known regarding the vertical accuracy of the topographic portion of this data set. Future efforts should focus on collecting bathymetric data, as well as field data upon which accuracy of that bathymetric data can be assessed, to further improve this data set.

Another data set created as part of this effort which forms a huge leap forward in spatial datasets describing coastal Louisiana is the 2018 Coastal Wetland Vegetation Type LULC data set. Possibly with the exception of National Wetlands Inventory (NWI) data, which can be more descriptive in some respects but less descriptive in others, this data set likely constitutes the most specific land cover data set available for the region. While wetland categories are often described by a dominant species, users of this data set are cautioned that other species of wetland vegetation may be present at these locations. The listed species is only used as a label, typically based off of a species which often constitutes the dominant species in these wetland areas.

Finally, this effort created a data set which constitutes the most complete assessment of recent edge erosion ever created for coastal Louisiana. This data set was used to drive edge erosion as a process in the ICM. Details on how this data set informed that process are available in (Attachment C8: 2023 Modeling Wetland Vegetation and Morphology: ICM-LAVegMod and ICM-Morph). While this data set was generalized to drive model processes, the original resolution data set is a valuable descriptor of adoration and may be further utilized to describe this important process in the future analyses.

5.0 REFERENCES

- CoNED TOPOBATHY Data for Entity ID: TBDEMNGOM00034. (2015). U.S. Geological Survey (USGS), Earth Resources Observation System (EROS) Center. Sioux Falls, SD USA. Retrieved from https://lta.cr.usgs.gov/coned_tbdem.
- Cortese, L., & Fagherazzi, S. (2022). Fetch and distance from the bay control accretion and erosion patterns in Terrebonne marshes (Louisiana, USA). *Earth Surface Processes and Landforms*, 47(6), 1455-1465.
- Couvillion, B. R., Beck, H. J., Dugas, J., Garber, A., & Mouton, K., 2018, Coastwide Reference Monitoring System (CRMS) 2016 land-water classifications: U.S. Geological Survey data release, <https://doi.org/10.5066/P90RE64M>.
- Couvillion, B. R., Beck, H. J., Dugas, J., Garber, A., & Mouton, K., 2018b, Coastwide Reference Monitoring System (CRMS) 2015 land-water classifications: U.S. Geological Survey data release, <https://doi.org/10.5066/F7930RDX>.
- Couvillion, B. (2017). 2017 Coastal Master Plan Modeling: Appendix C3-27: Landscape Data. Version Final. (pp. 1-84). Baton Rouge, Louisiana: Coastal Protection and Restoration Authority.
- Couvillion, B. R., Barras, J. A., Steyer, G.D., Sleavin, W., Fischer, M., Beck, H., Trahan, N., Griffin, B., & Heckman, D. (2011). Land area change in coastal Louisiana from 1932 to 2010: U.S. Geological Survey Scientific Investigations Map 3164, scale 1:265,000 (p.12). Pamphlet.
- Cunningham, R., Gisclair, D., & Craig, J. (2002). The Louisiana Statewide LIDAR Project. Retrieved on June 28, 2015. From http://atlas.lsu.edu/central/la_LIDAR_project.pdf. Homer, C., Huang, C., Yang, L., Wylie, B.K., and Coan, M. (2004). Development of a 2001 National Land-Cover Database for the United States. Retrieved from <http://digitalcommons.unl.edu/usgsstaffpub/620>.
- Danielson, J. J., Tyler, D. J., Cushing, W.M., Barras, J. A., Poppenga, S.K. Beverly, S.D., & Shogib, R., 2022, Topobathymetric Model of the Northern Gulf of Mexico, 1885 to 2021: U.S. Geological Survey data release, <https://doi.org/10.5066/P99JULDN>.
- National Oceanic and Atmospheric Administration, Office for Coastal Management, 2022: 2015-2017 C-CAP Derived 10 meter Land Cover - BETA, <https://www.fisheries.noaa.gov/inport/item/57099>.
- Sasser, C. E., Gosselink, J. G., Swenson, E. M., & Evers, D. E. (1995). Hydrologic, vegetation, and substrate characteristics of floating marshes in sediment-rich wetlands of the Mississippi river delta plain, Louisiana, USA. *Wetlands Ecology and Management*, 3(3) (pp. 171-187).
- Sasser, C. E., Visser, J. M., Mouton, E., Linscombe, J., & Hartley, S. B. (2014). Vegetation types in

- coastal Louisiana in 2013: U.S. Geological Survey Scientific Investigations Map 3290, 1 sheet, scale 1:550,000. Retrieved from <http://dx.doi.org/10.3133/sim3290>. U.S. Fish and Wildlife Service (USFWS). (1988). National Wetlands Inventory website. U.S. Department of the Interior, Fish and Wildlife Service, Washington, D.C. Retrieved from <http://www.fws.gov/wetlands/>.
- Xu, H. (2006). Modification of normalized difference water index (NDWI) to enhance open water features in remotely sensed imagery. *International Journal of Remote Sensing* 27 (14): 3025-3033

APPENDIX A: DIGITAL ELEVATION MODEL GRIDDED VISUALIZATIONS

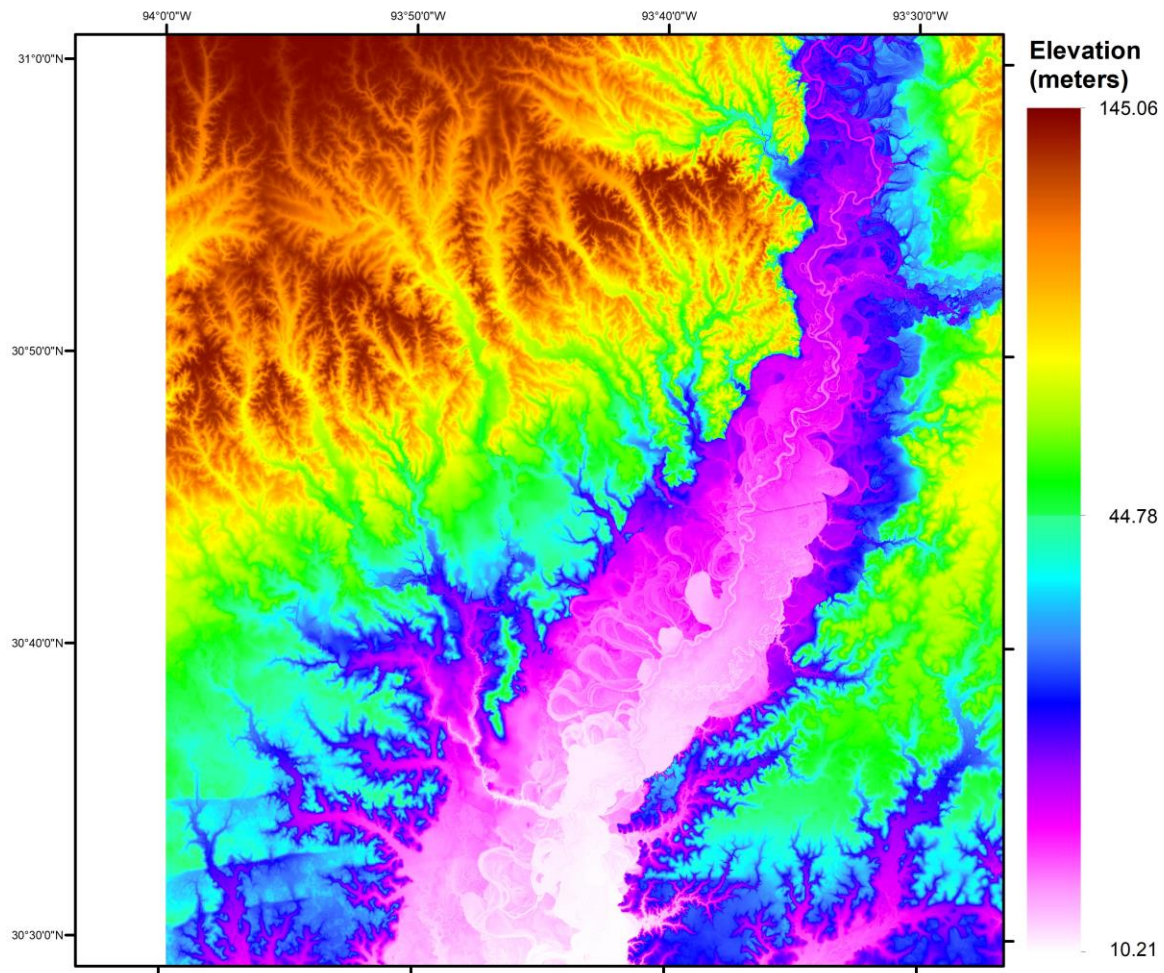


Figure A1. DEM Visualization of a 0.5° x 0.5° cell from approximately 30.5°N to 31°N and 94°W to 93.5°W.

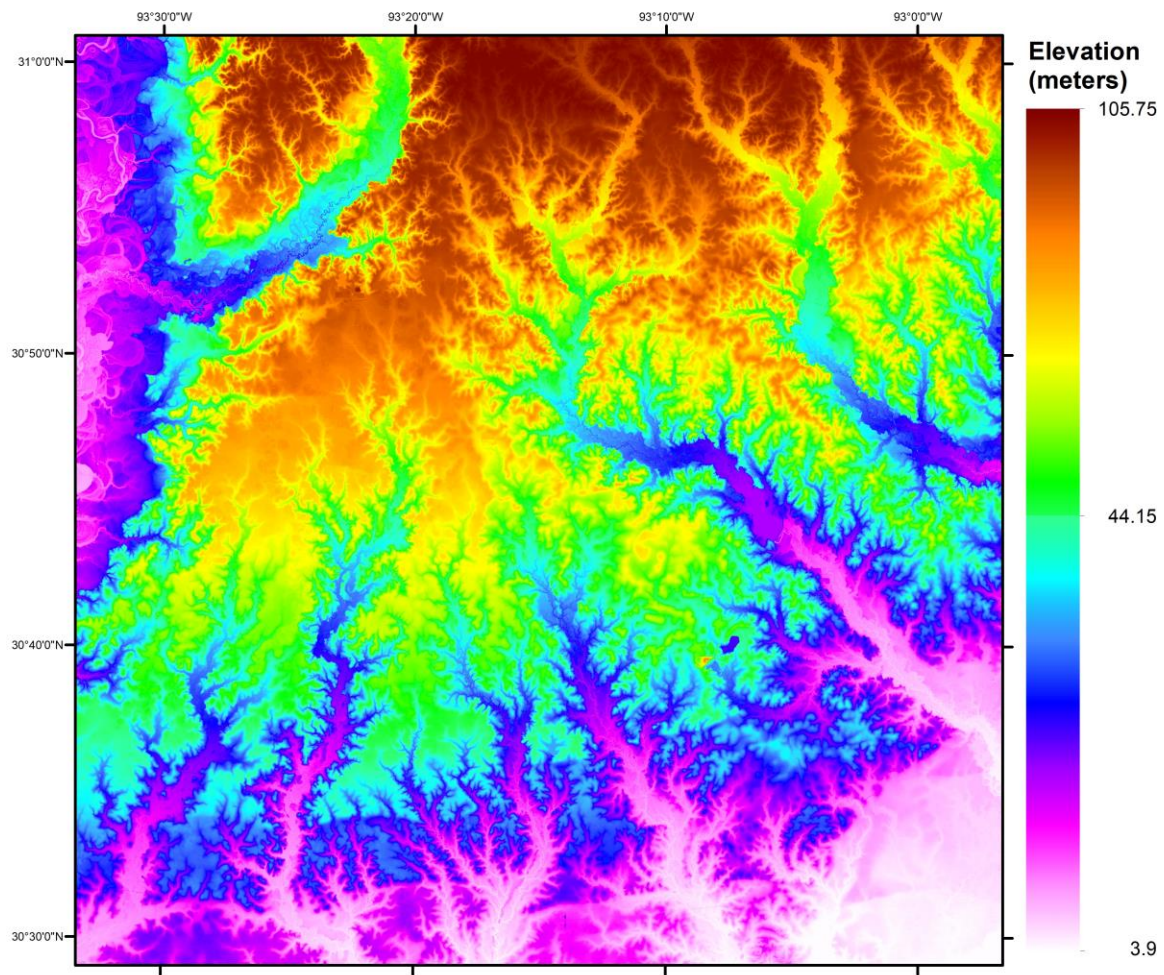


Figure A2. DEM Visualization of a 0.5° x 0.5° cell from approximately 30.5°N to 31°N and 93.5°W to 93°W.

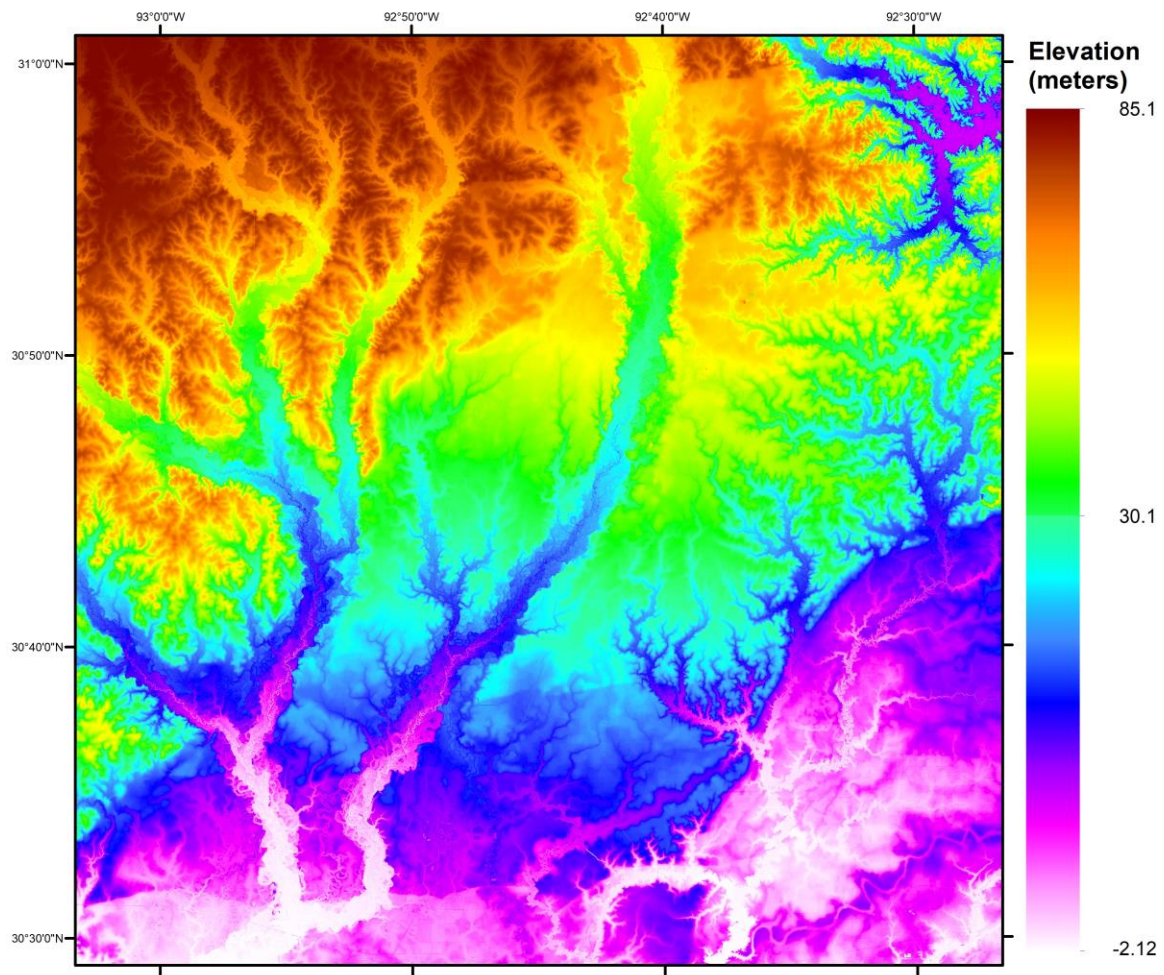


Figure A3. DEM Visualization of a 0.5° x 0.5° cell from approximately 30.5°N to 31°N and 93°W to 92.5°W.

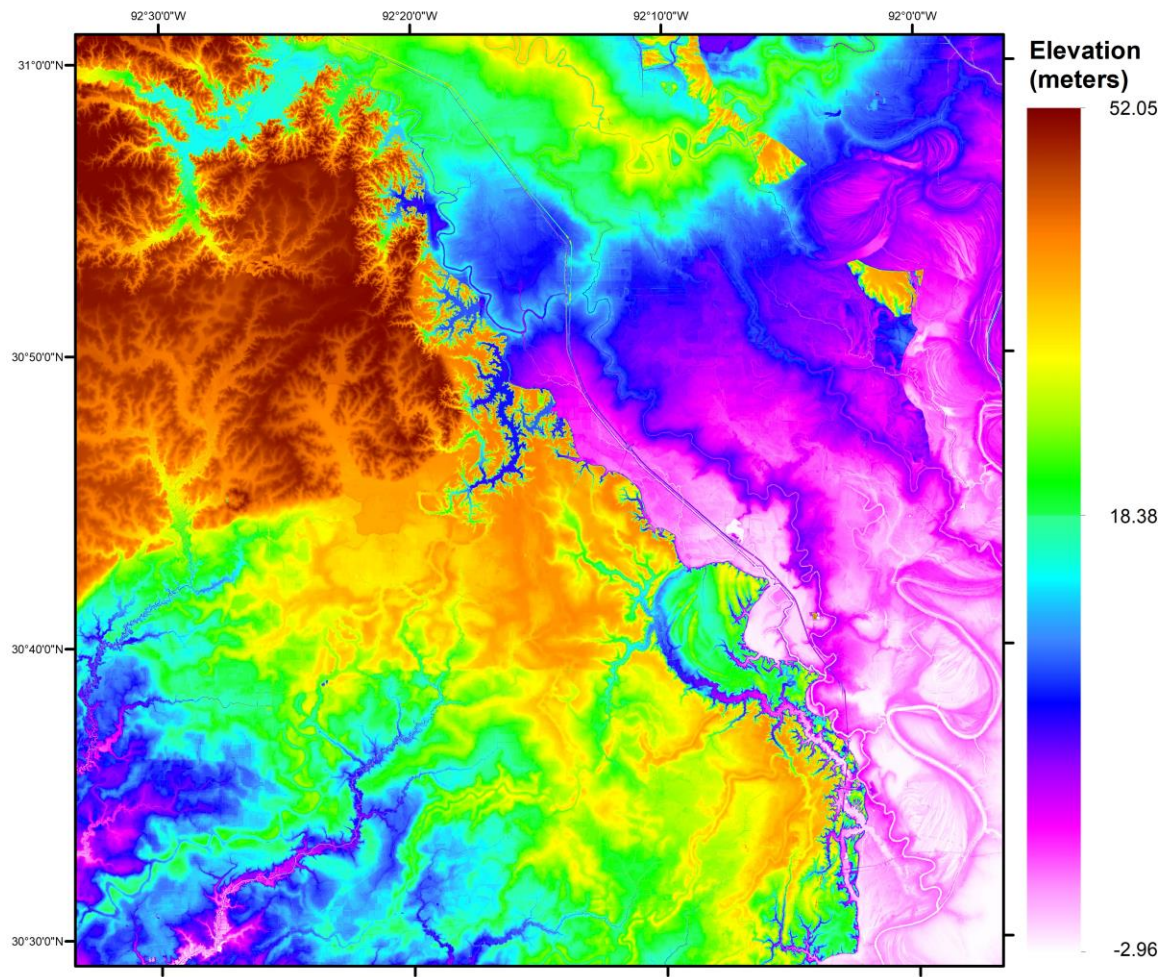


Figure A4. DEM Visualization of a 0.5° x 0.5° cell from approximately 30.5°N to 31°N and 92.5°W to 92°W.

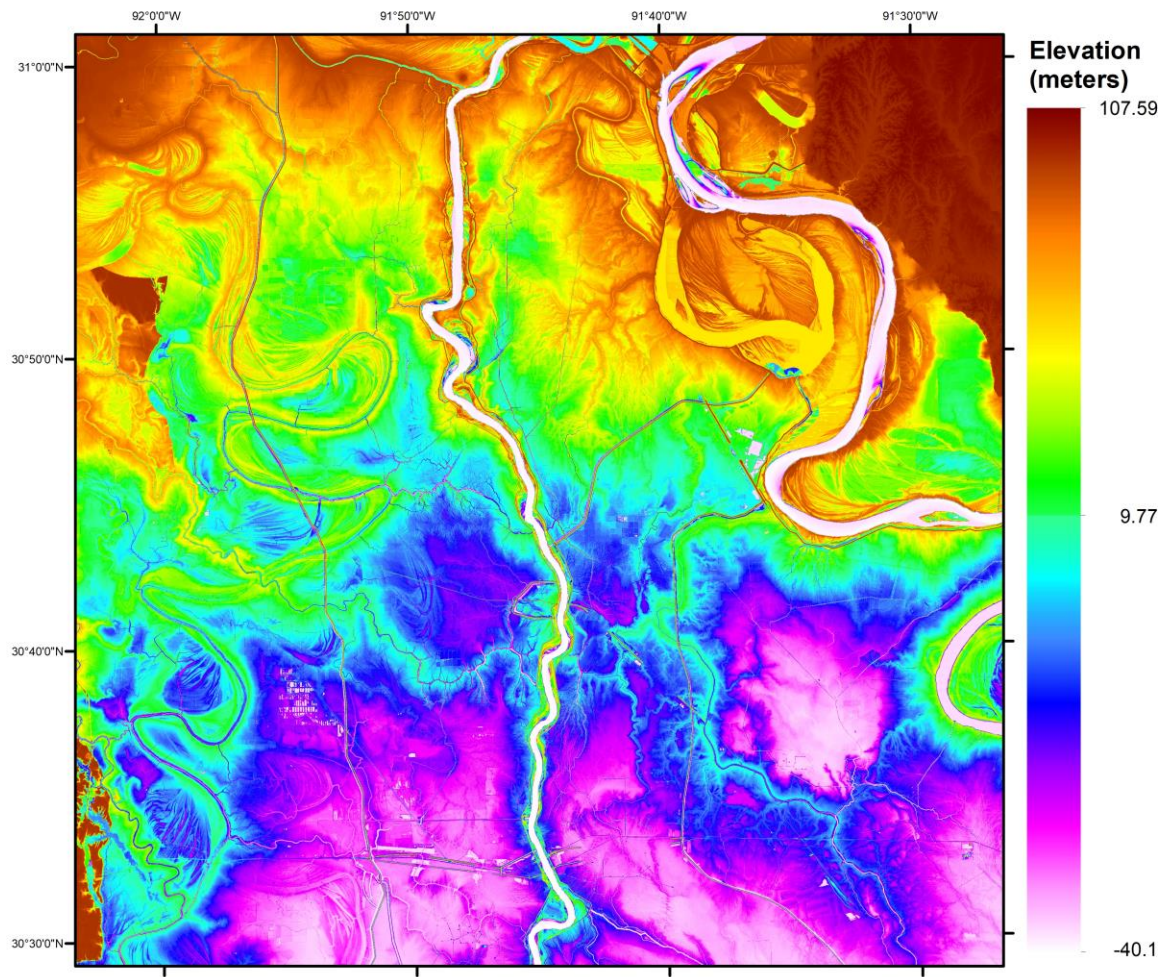


Figure A5. DEM Visualization of a 0.5° x 0.5° cell from approximately 30.5°N to 31°N and 92°W to 91.5°W.

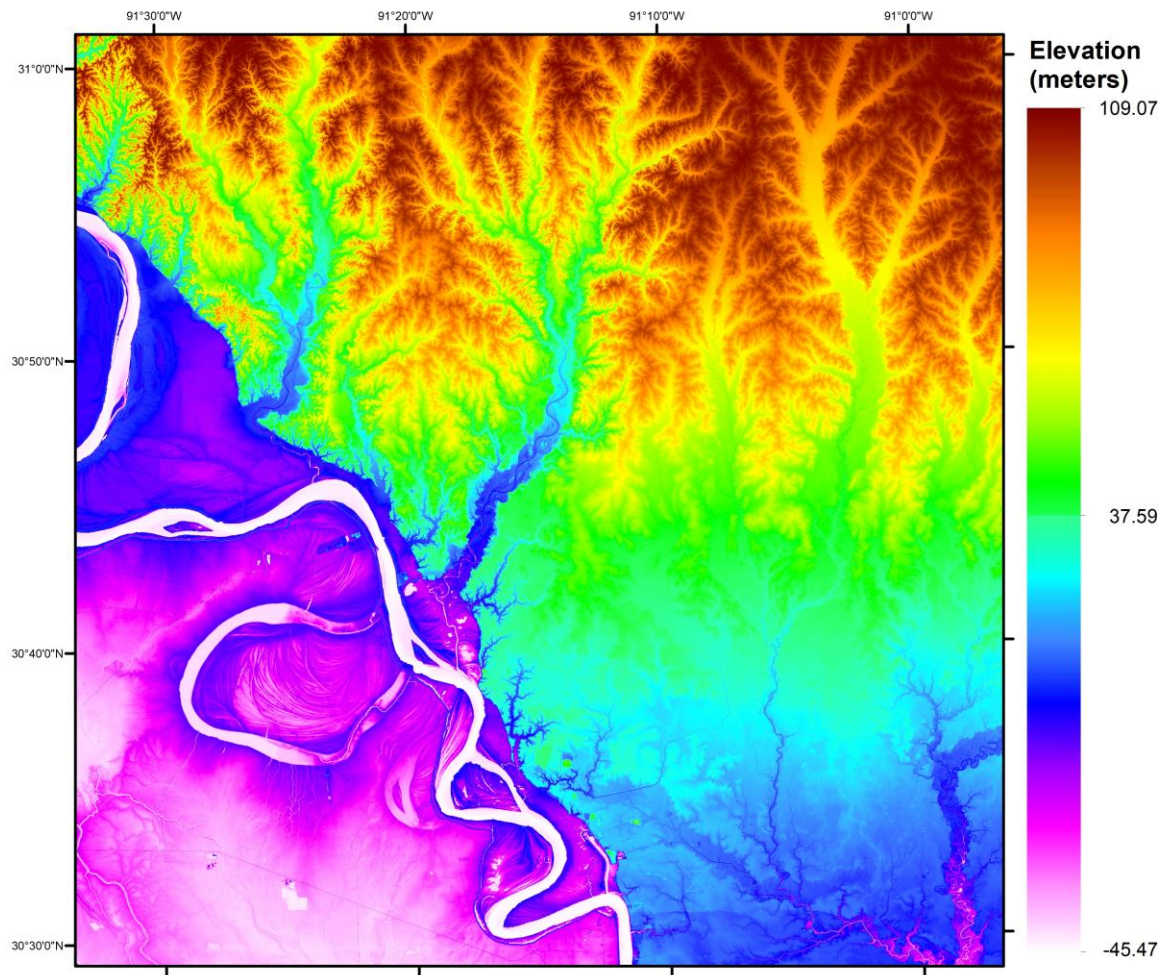


Figure A6. DEM Visualization of a 0.5° x 0.5° cell from approximately 30.5°N to 31°N and 91.5°W to 91°W.

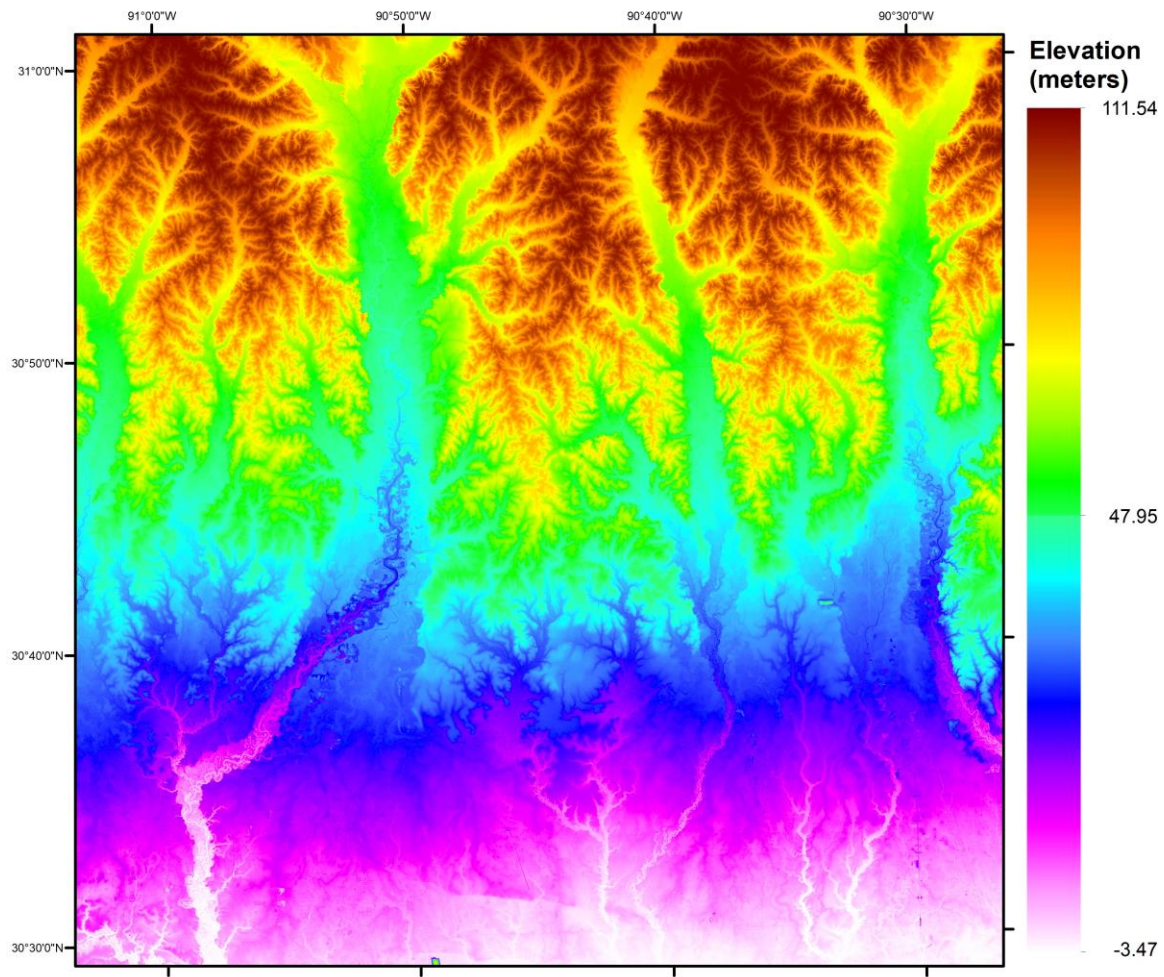


Figure A7. DEM Visualization of a 0.5° x 0.5° cell from approximately 30.5°N to 31°N and 91°W to 90.5°W.

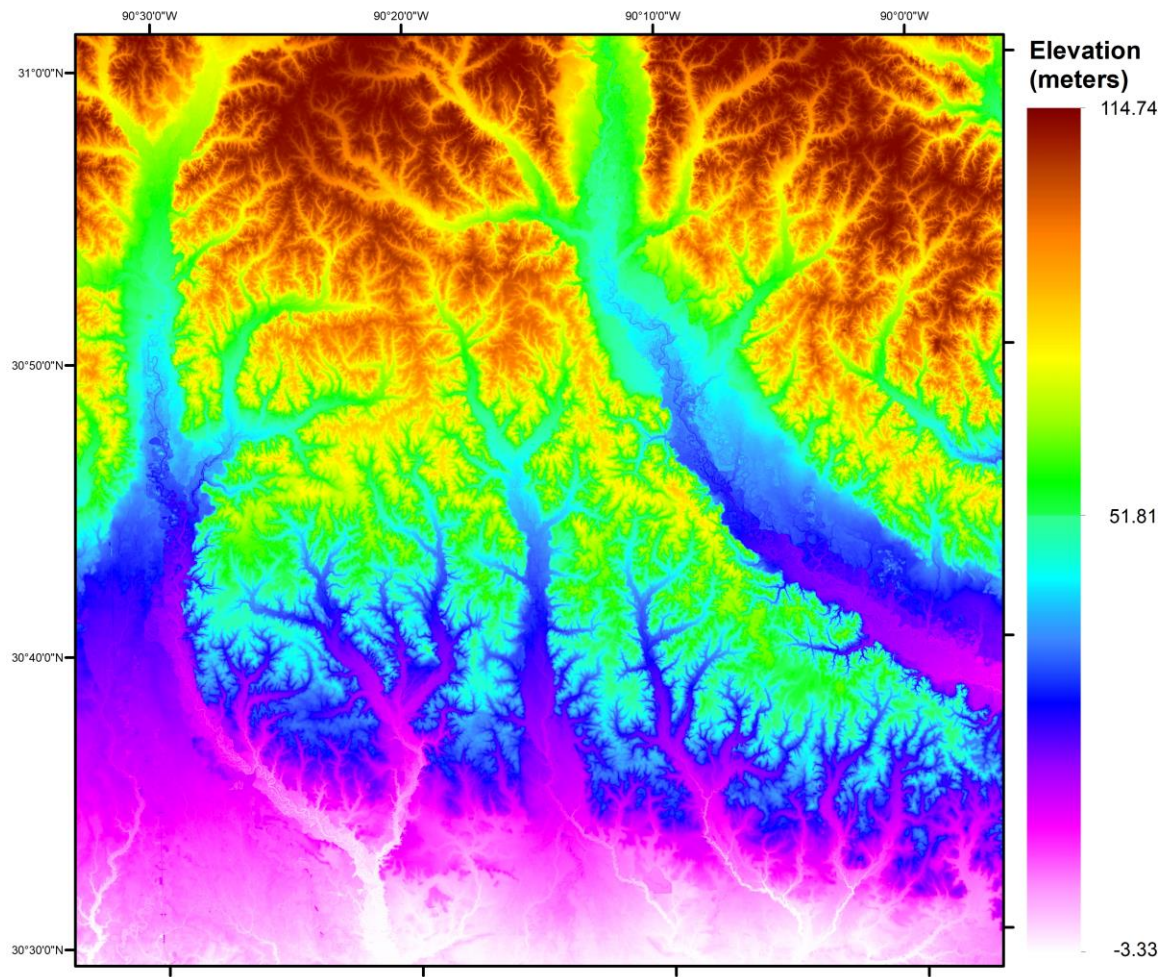


Figure A8. DEM Visualization of a 0.5° x 0.5° cell from approximately 30.5°N to 31°N and 90.5°W to 90°W.

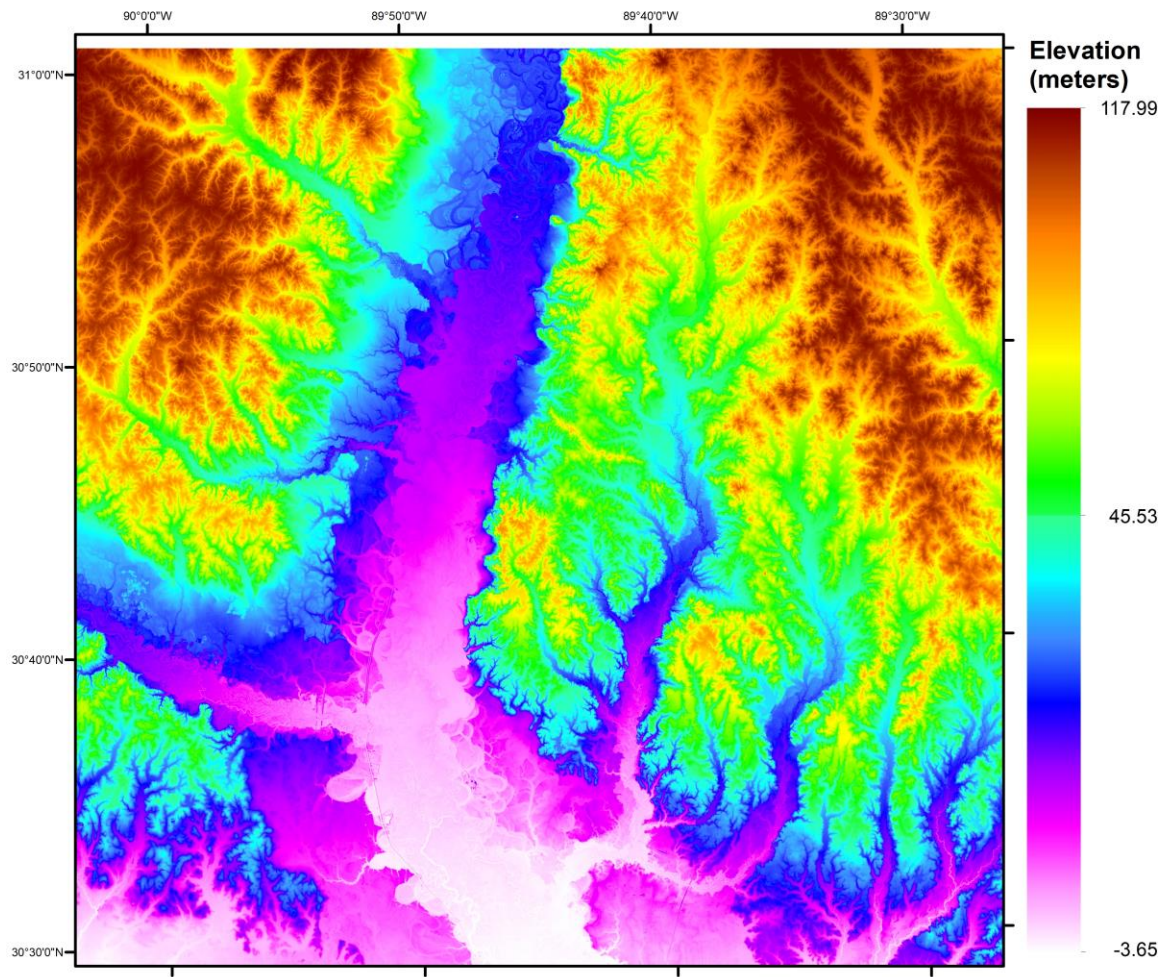


Figure A9. DEM visualization of a 0.5° x 0.5° cell from approximately 30.5°N to 31°N and 90°W to 89.5°W.

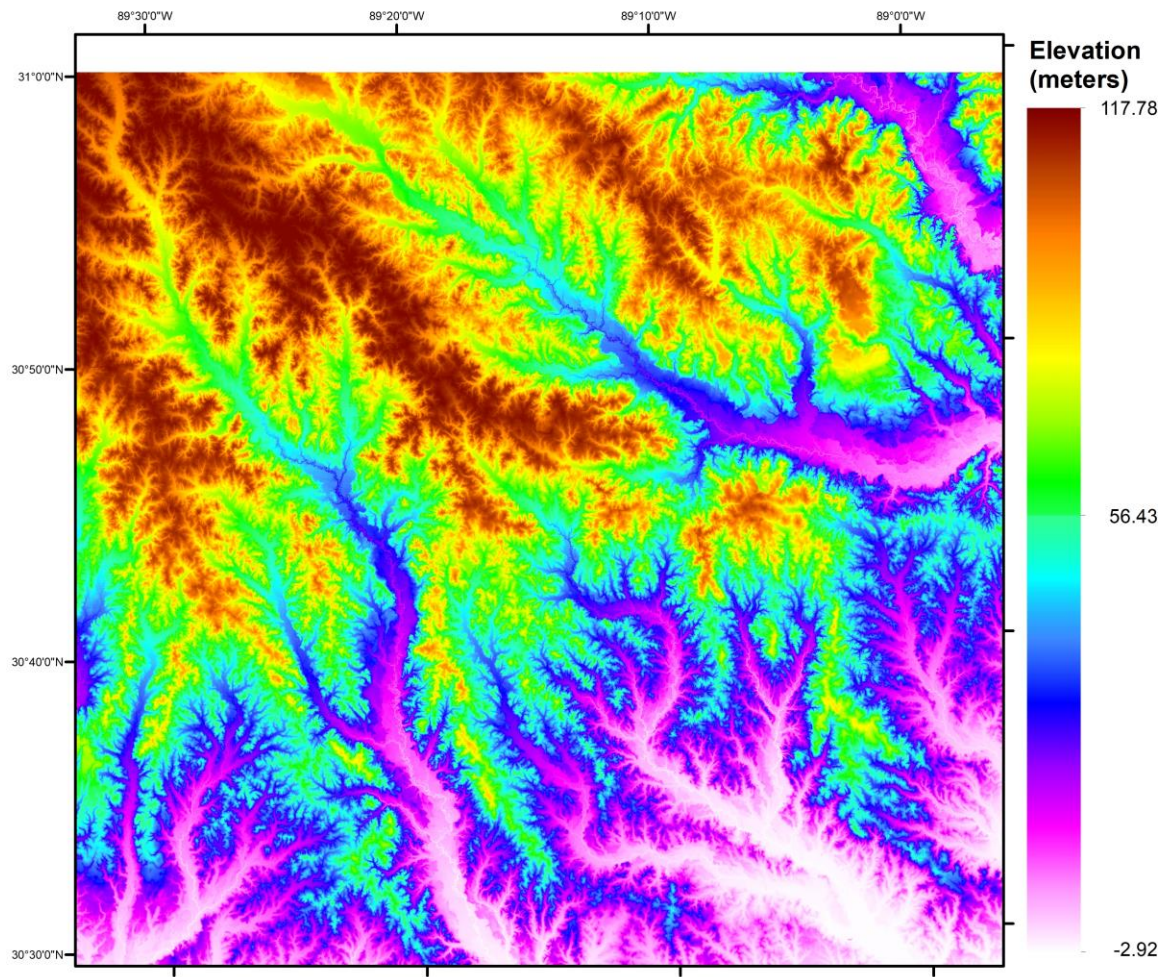


Figure A10. DEM visualization of a 0.5° x 0.5° cell from approximately 30.5°N to 31°N and 89.5°W to 89°W.

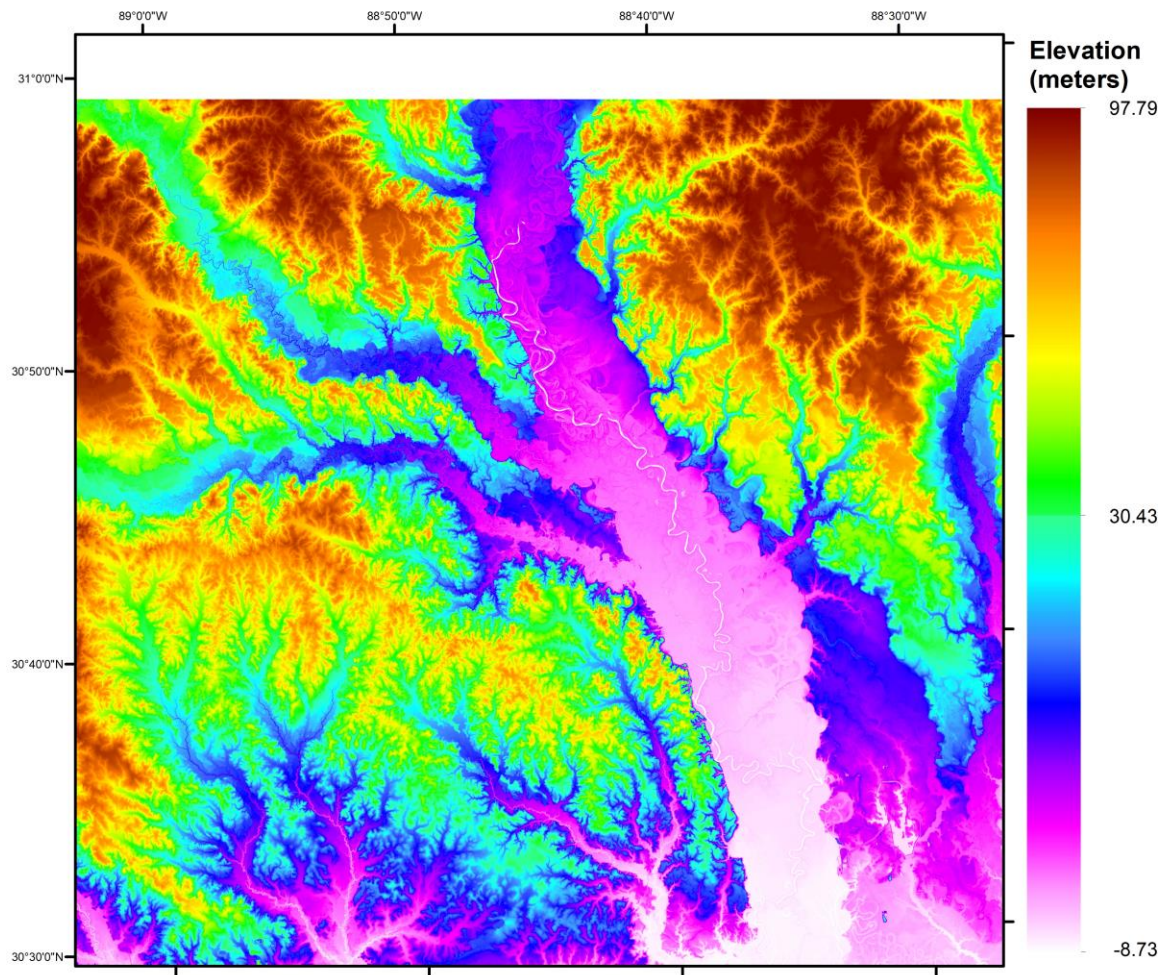


Figure A11. DEM visualization of a 0.5° x 0.5° cell from approximately 30.5°N to 31°N and 89°W to 88.5°W.

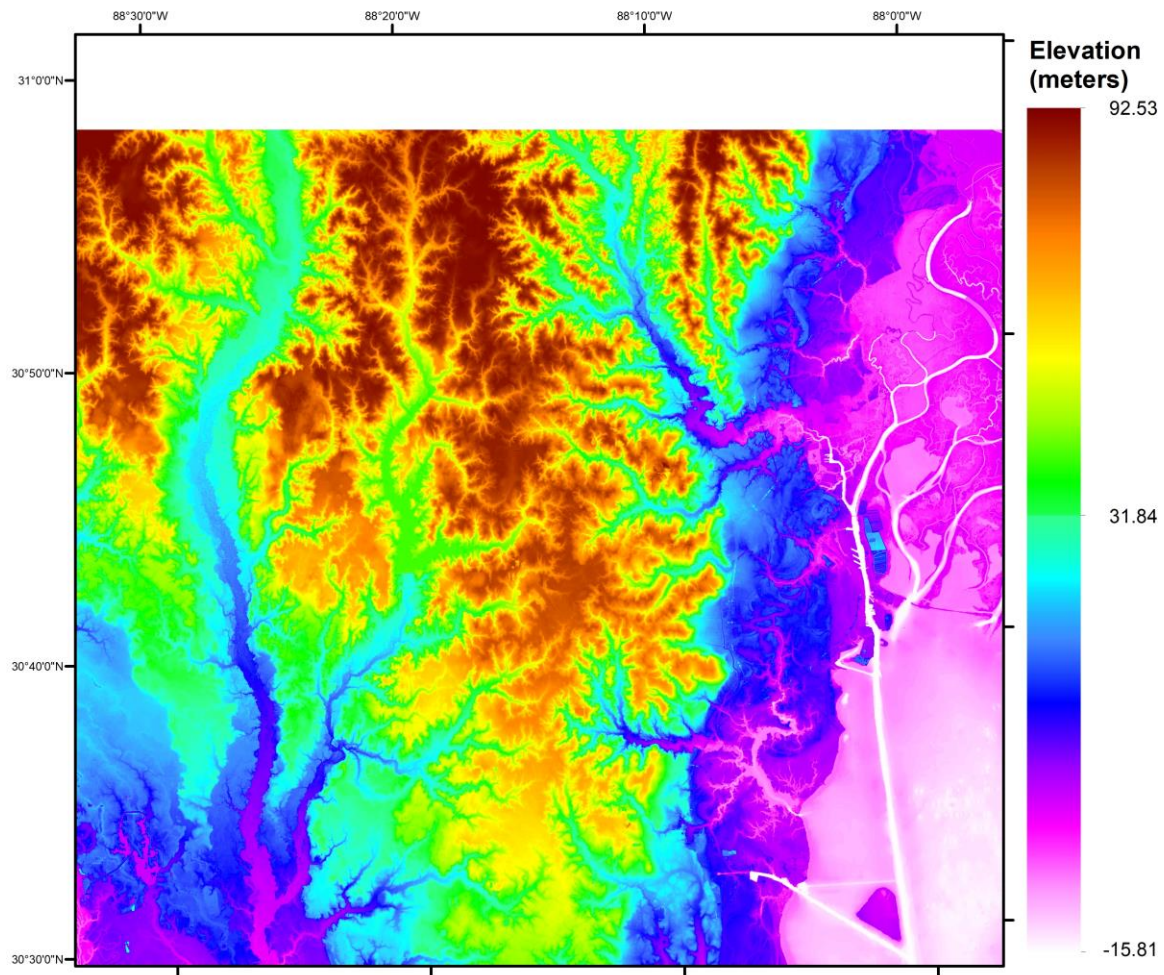


Figure A12. DEM visualization of a 0.5° x 0.5° cell from approximately 30.5°N to 31°N and 88.5°W to 88°W.

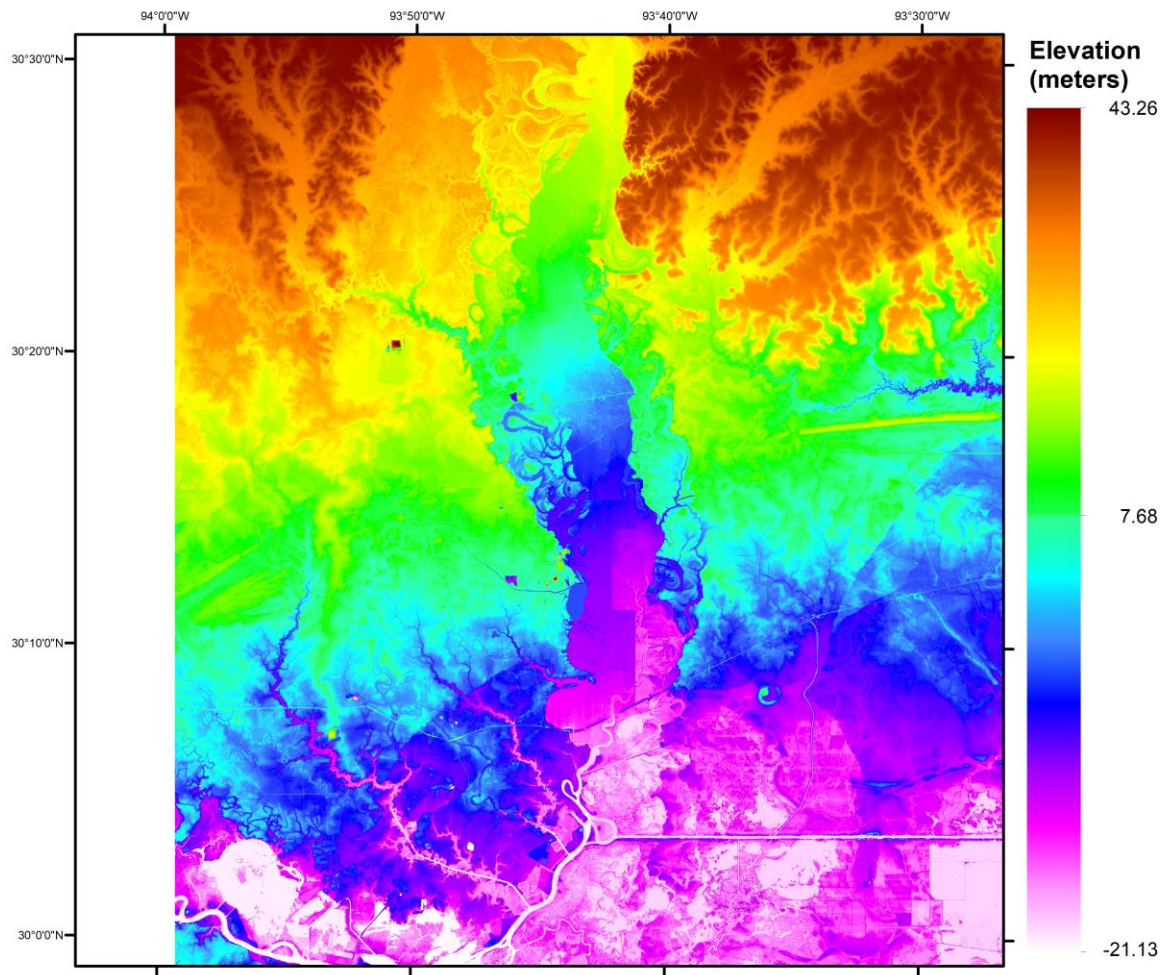


Figure A13. DEM visualization of a 0.5° x 0.5° cell from approximately 30°N to 30.5°N and 94°W to 93.5°W.

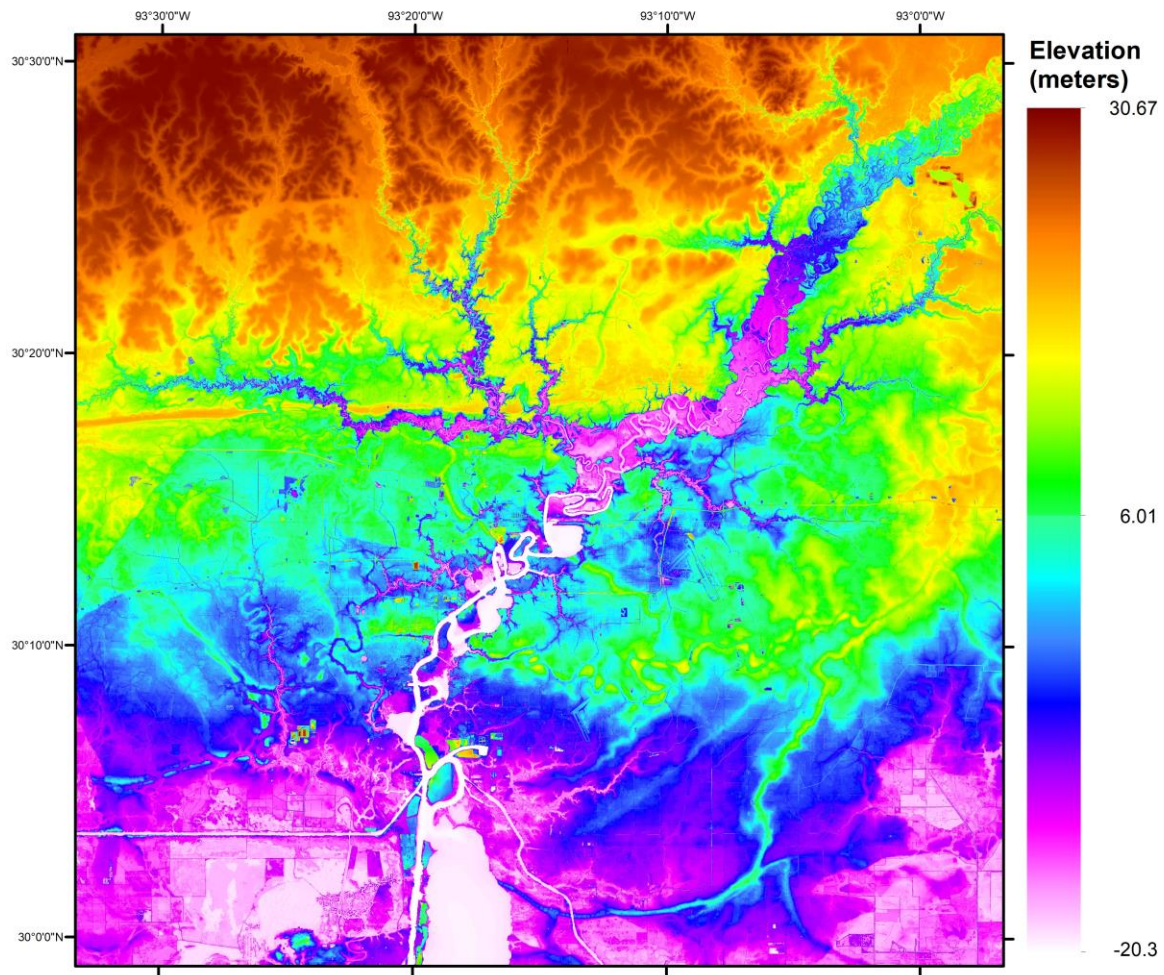


Figure A14. DEM visualization of a 0.5° x 0.5° cell from approximately 30°N to 30.5°N and 93.5°W to 93°W.

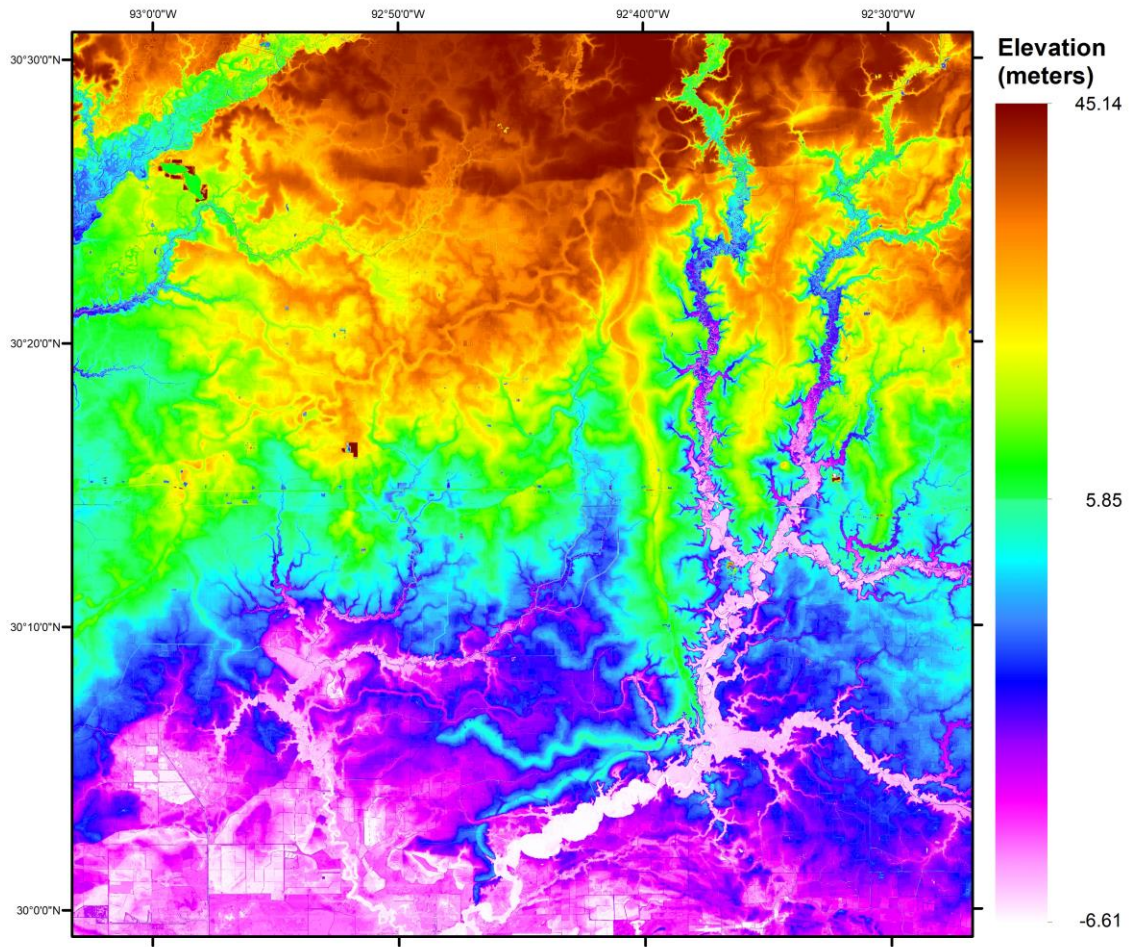


Figure A15. DEM visualization of a 0.5° x 0.5° cell from approximately 30°N to 30.5°N and 93°W to 92.5°W.

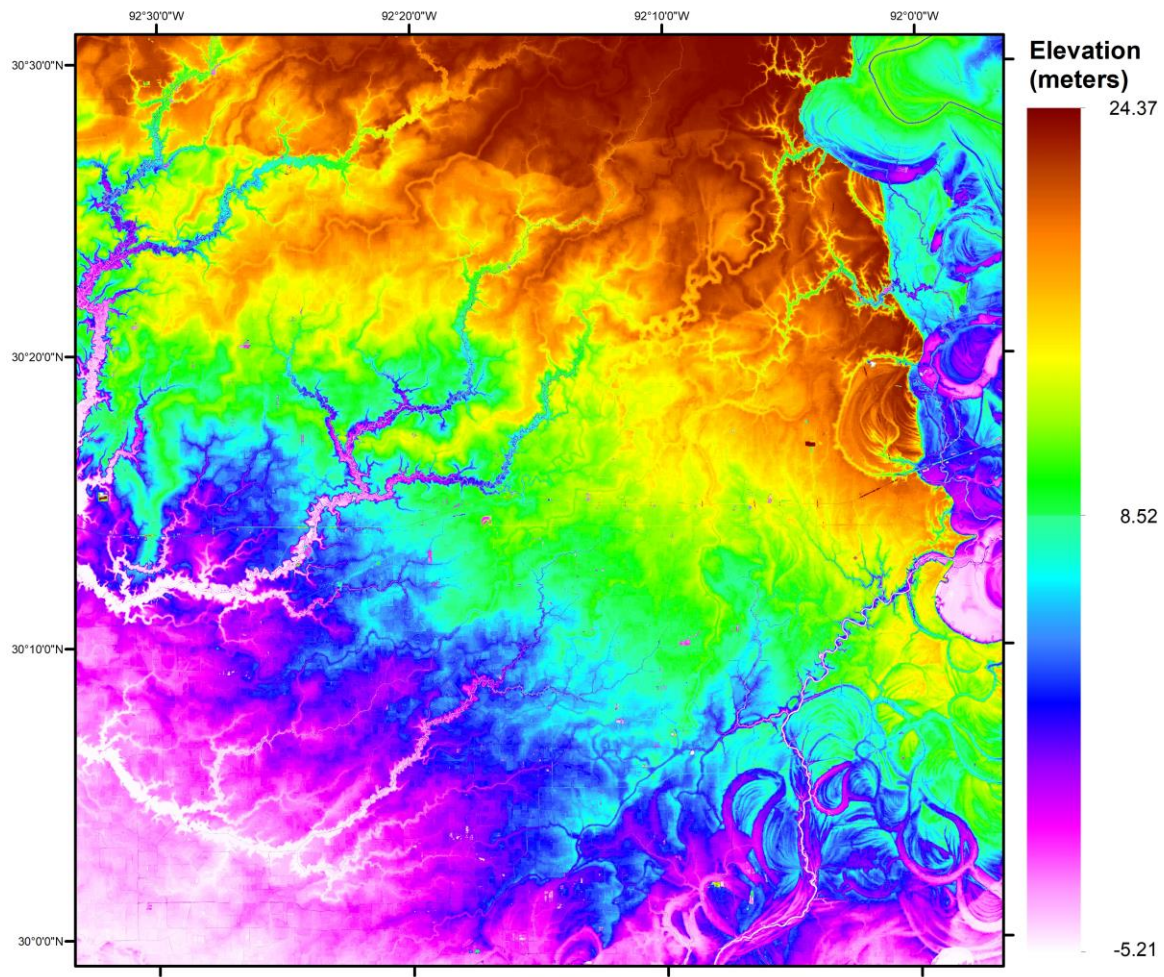


Figure A16. DEM visualization of a 0.5° x 0.5° cell from approximately 30°N to 30.5°N and 92.5°W to 92°W.

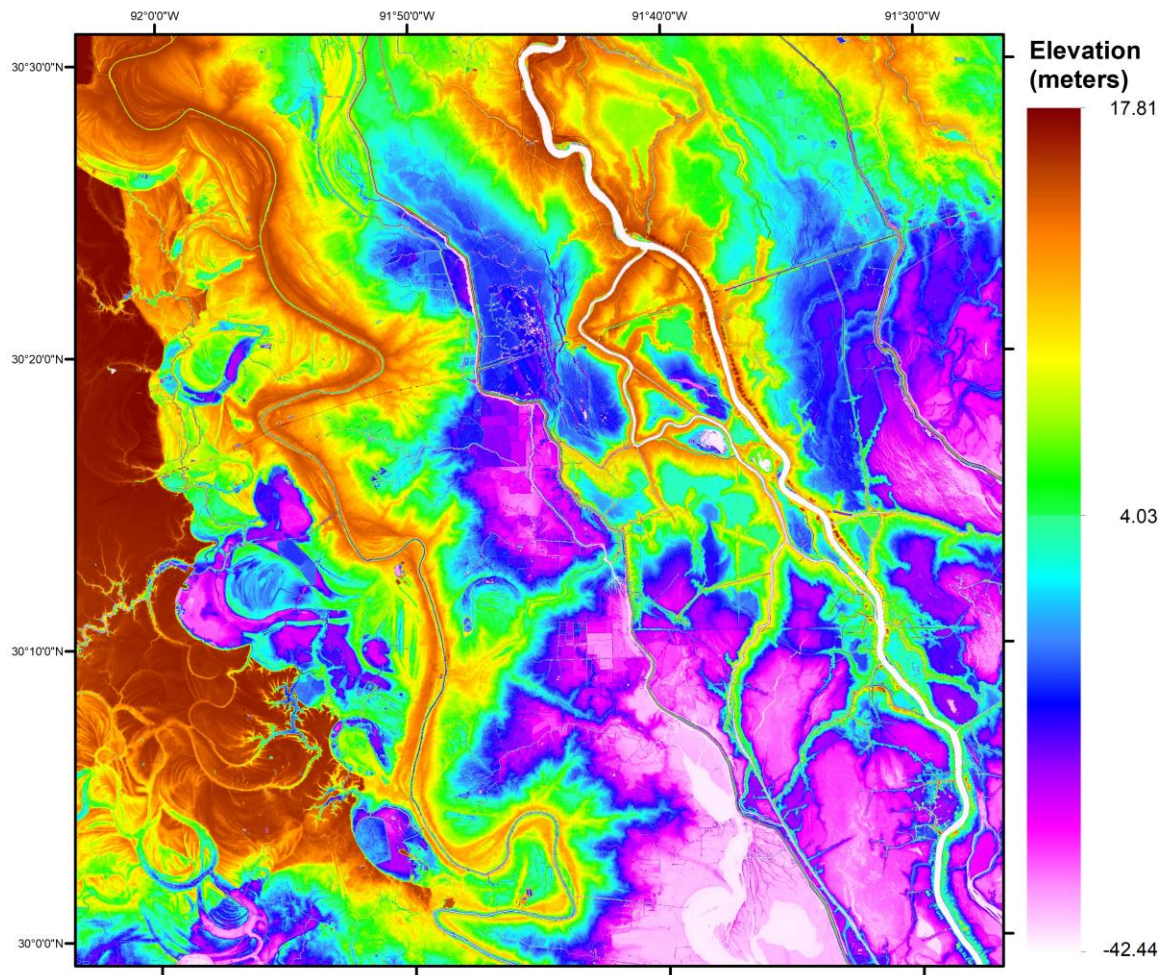


Figure A17. DEM visualization of a 0.5° x 0.5° cell from approximately 30°N to 30.5°N and 92°W to 91.5°W.

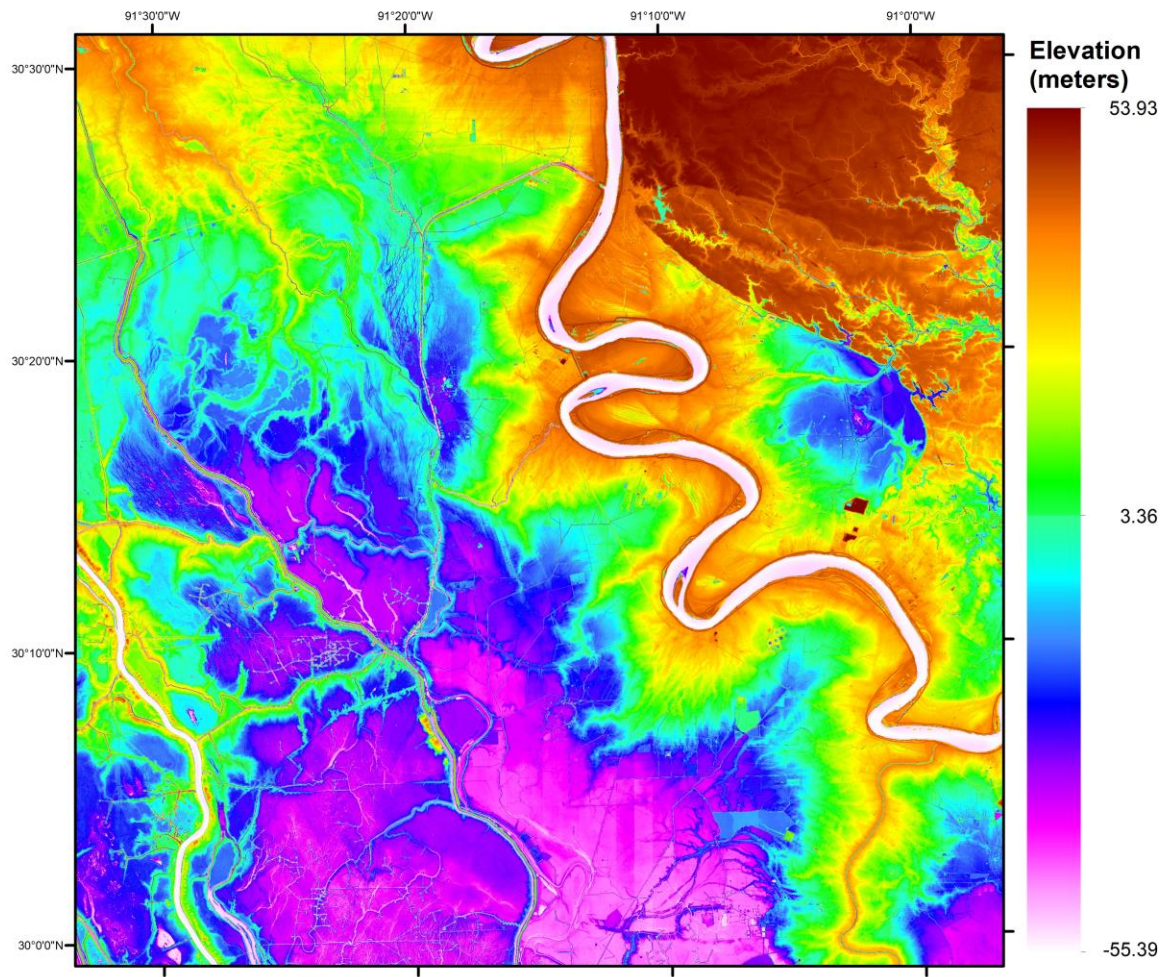


Figure A18. DEM visualization of a 0.5° x 0.5° cell from approximately 30°N to 30.5°N and 91.5°W to 91°W.

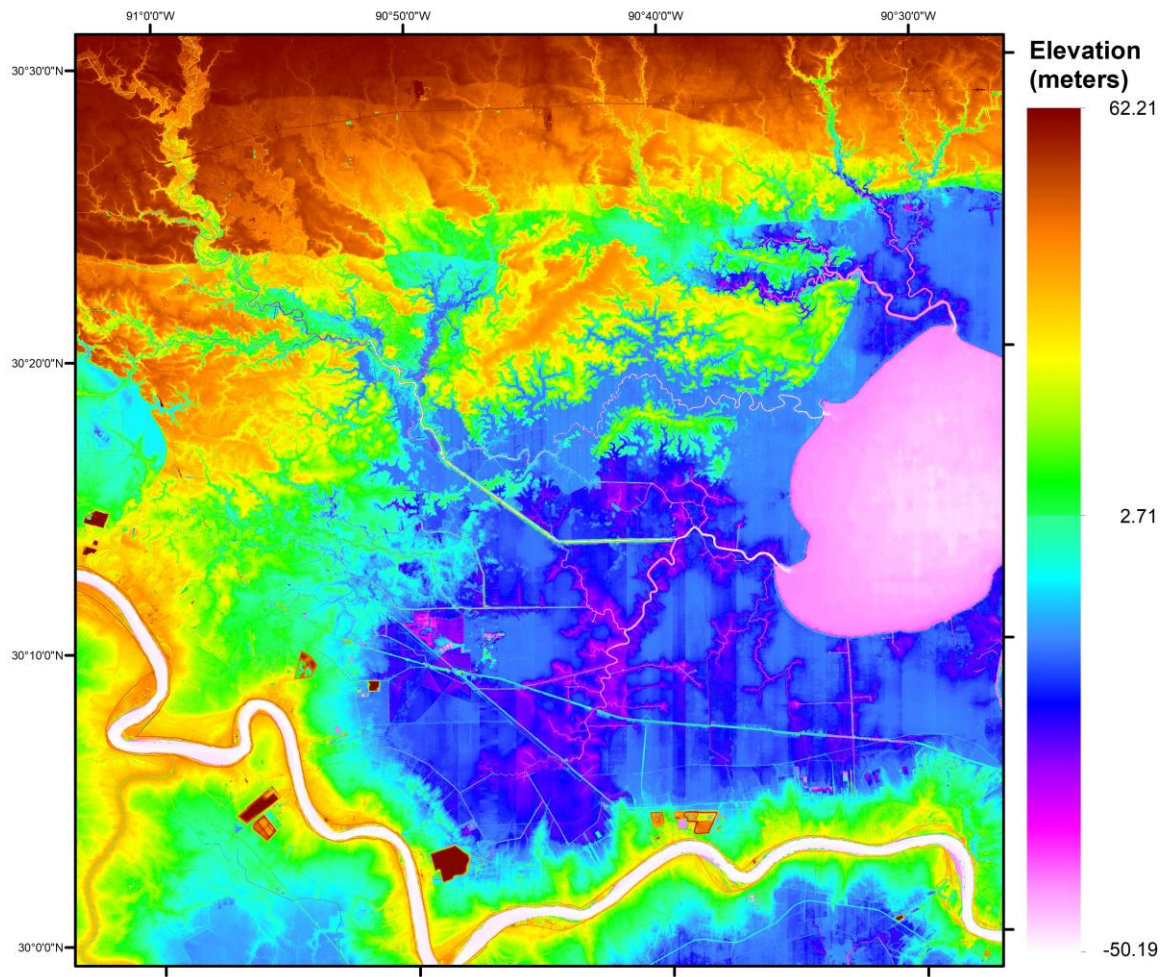


Figure A19. DEM visualization of a 0.5° x 0.5° cell from approximately 30°N to 30.5°N and 91°W to 90.5°W.

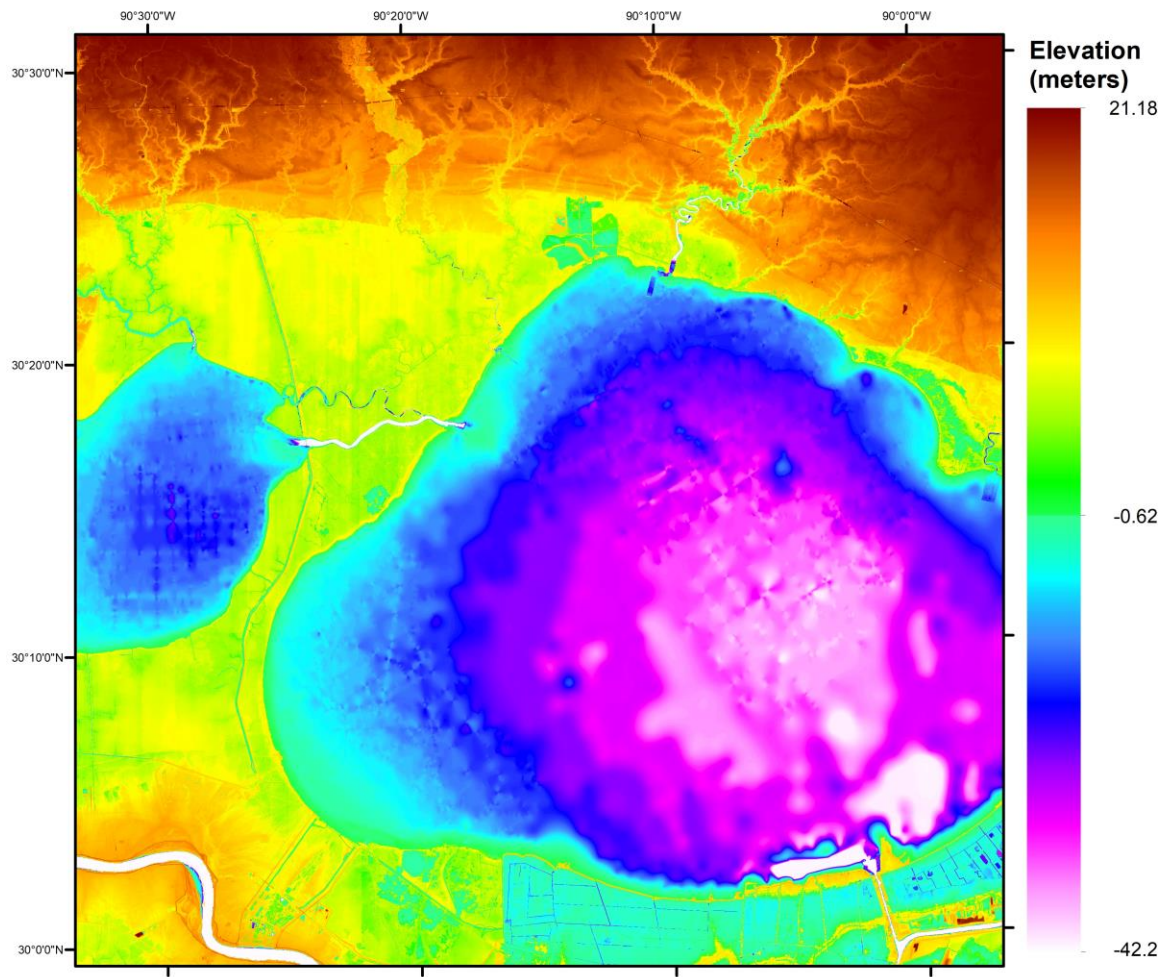


Figure A20. DEM visualization of a 0.5° x 0.5° cell from approximately 30°N to 30.5°N and 90.5°W to 90°W.

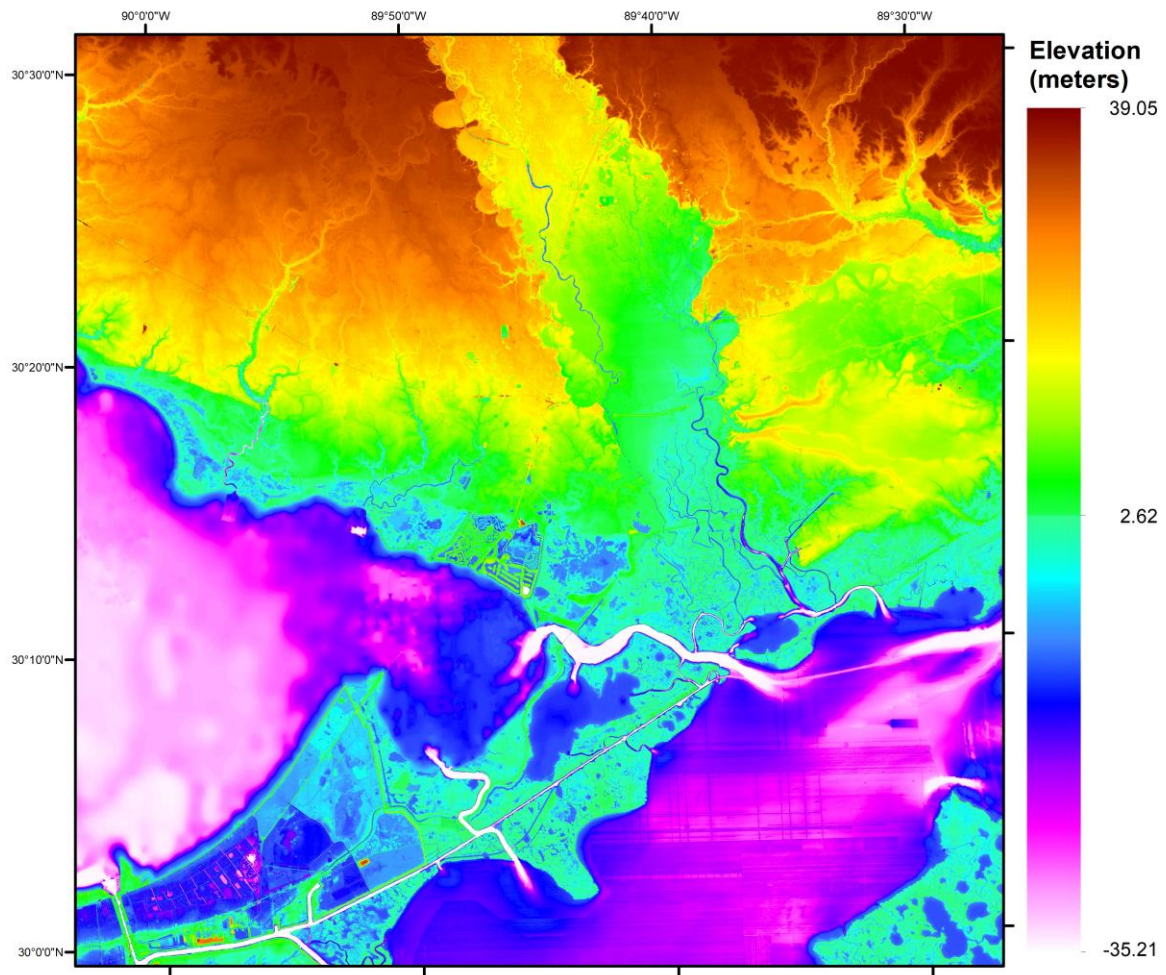


Figure A21. DEM visualization of a 0.5° x 0.5° cell from approximately 30°N to 30.5°N and 90°W to 89.5°W.

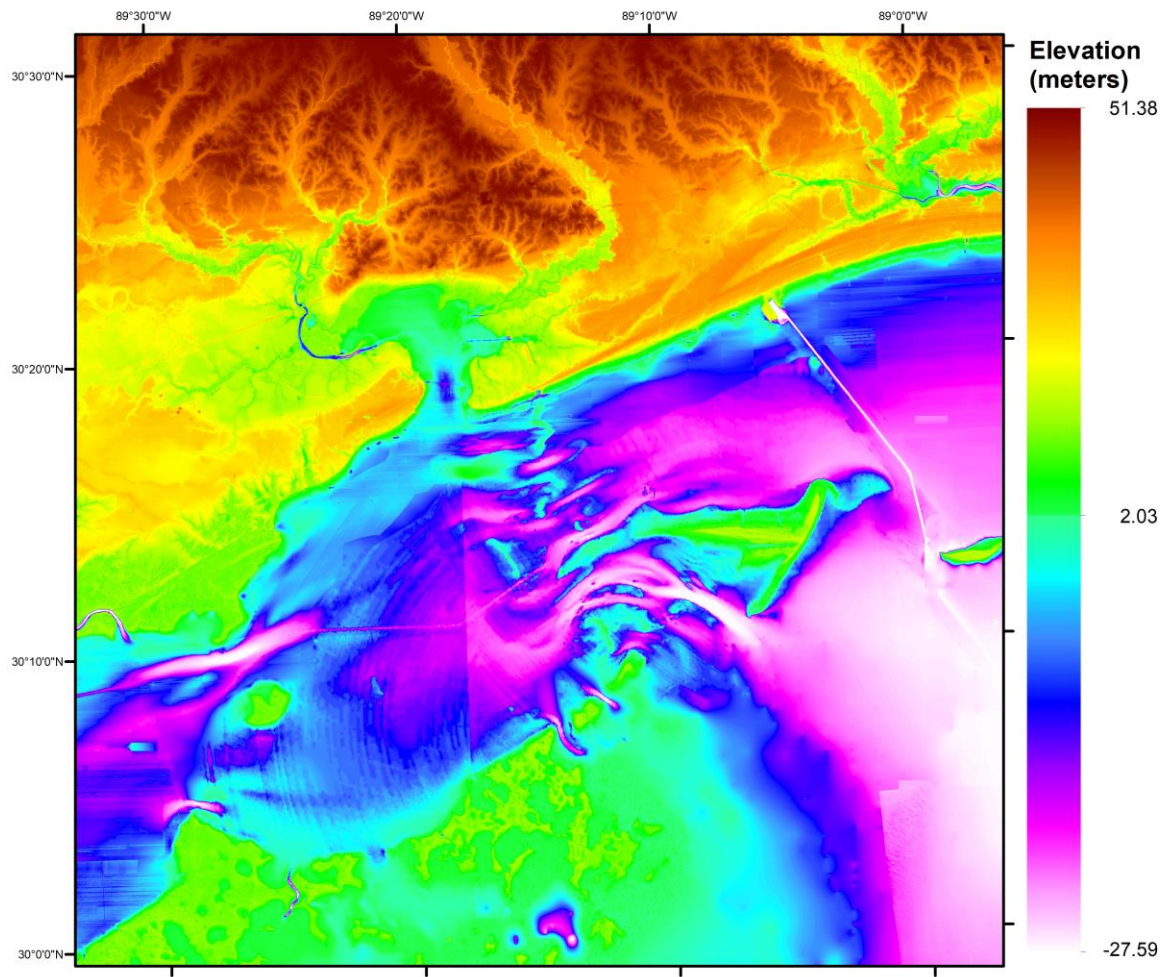


Figure A22. DEM visualization of a 0.5° x 0.5° cell from approximately 30°N to 30.5°N and 89.5°W to 89°W.

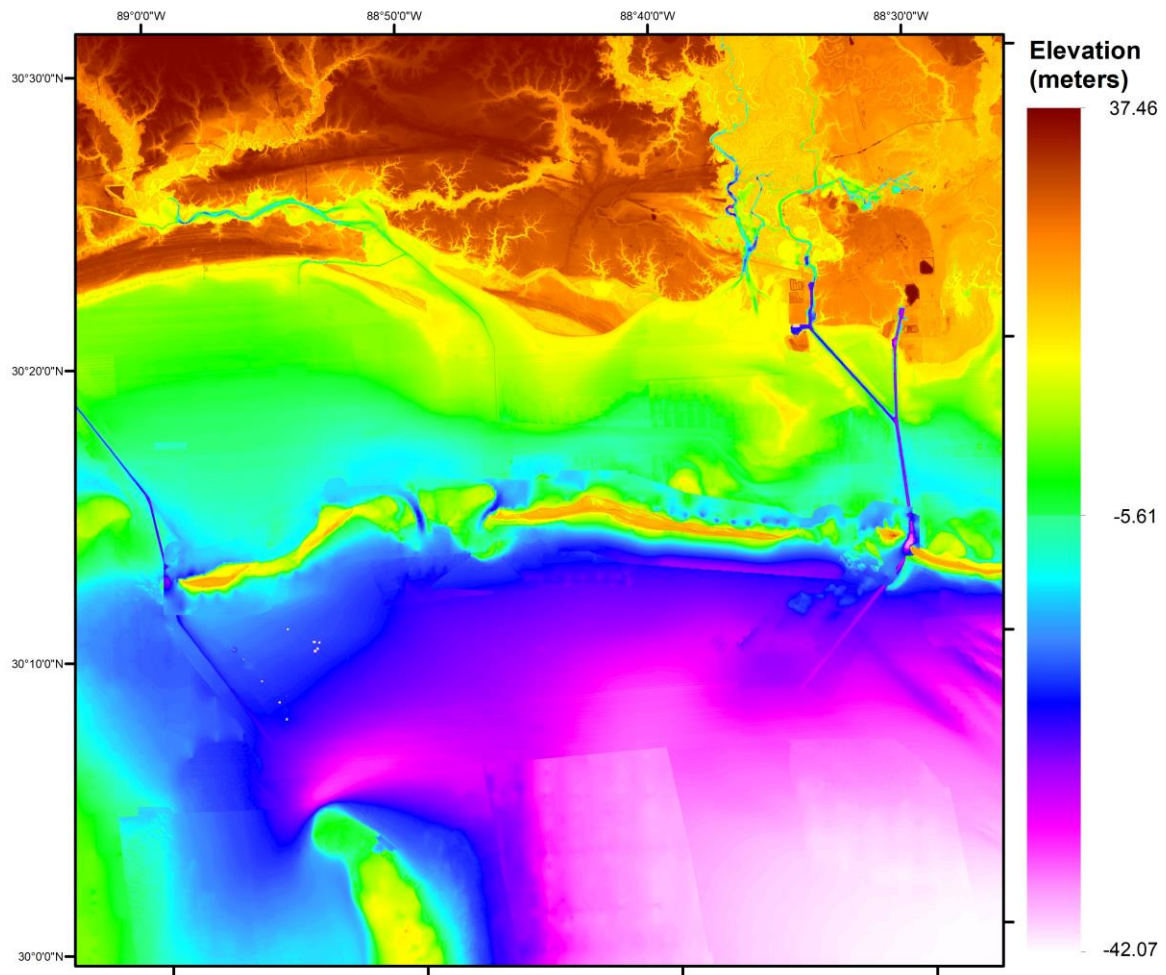


Figure A23. DEM visualization of a 0.5° x 0.5° cell from approximately 30°N to 30.5°N and 89°W to 88.5°W.

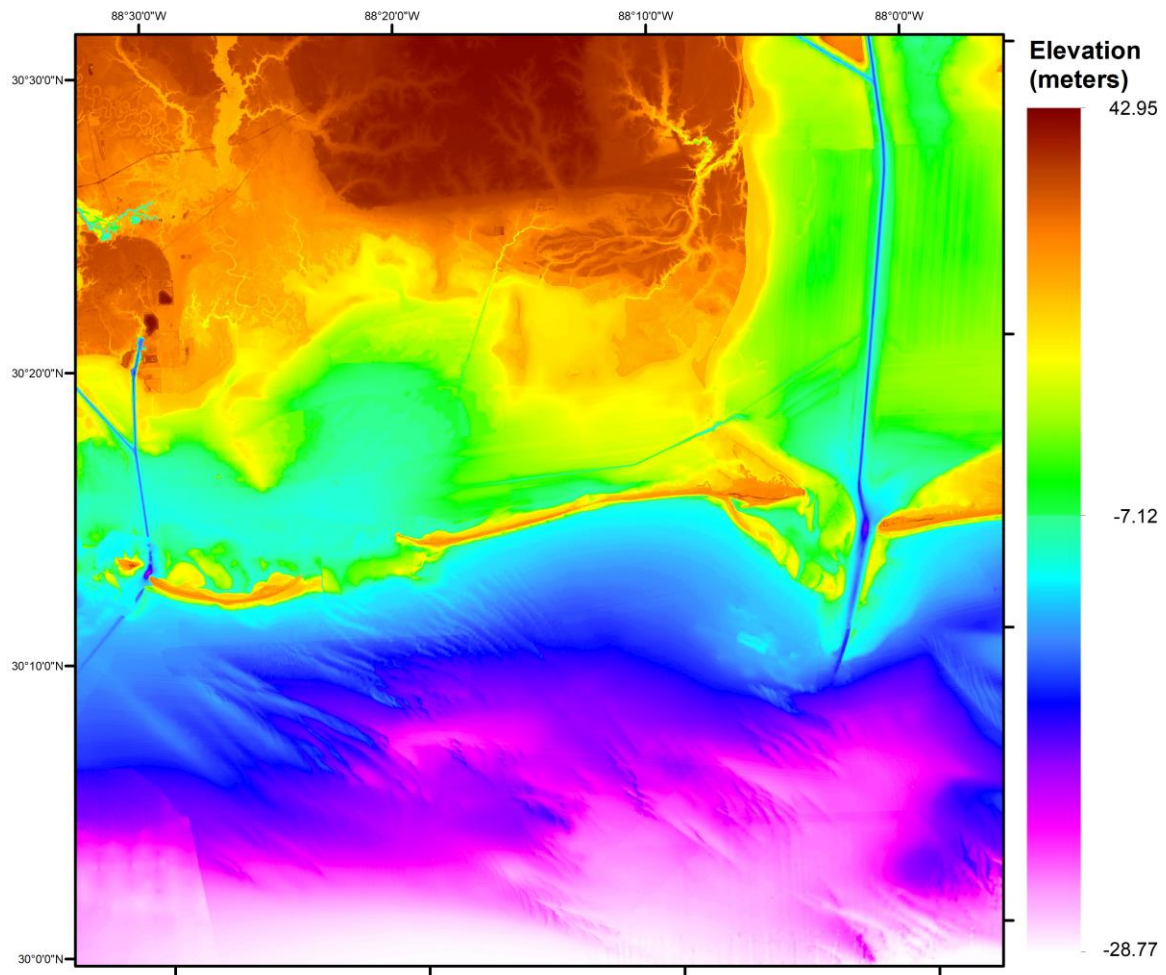


Figure A24. DEM visualization of a 0.5° x 0.5° cell from approximately 30°N to 30.5°N and 88.5°W to 88°W.

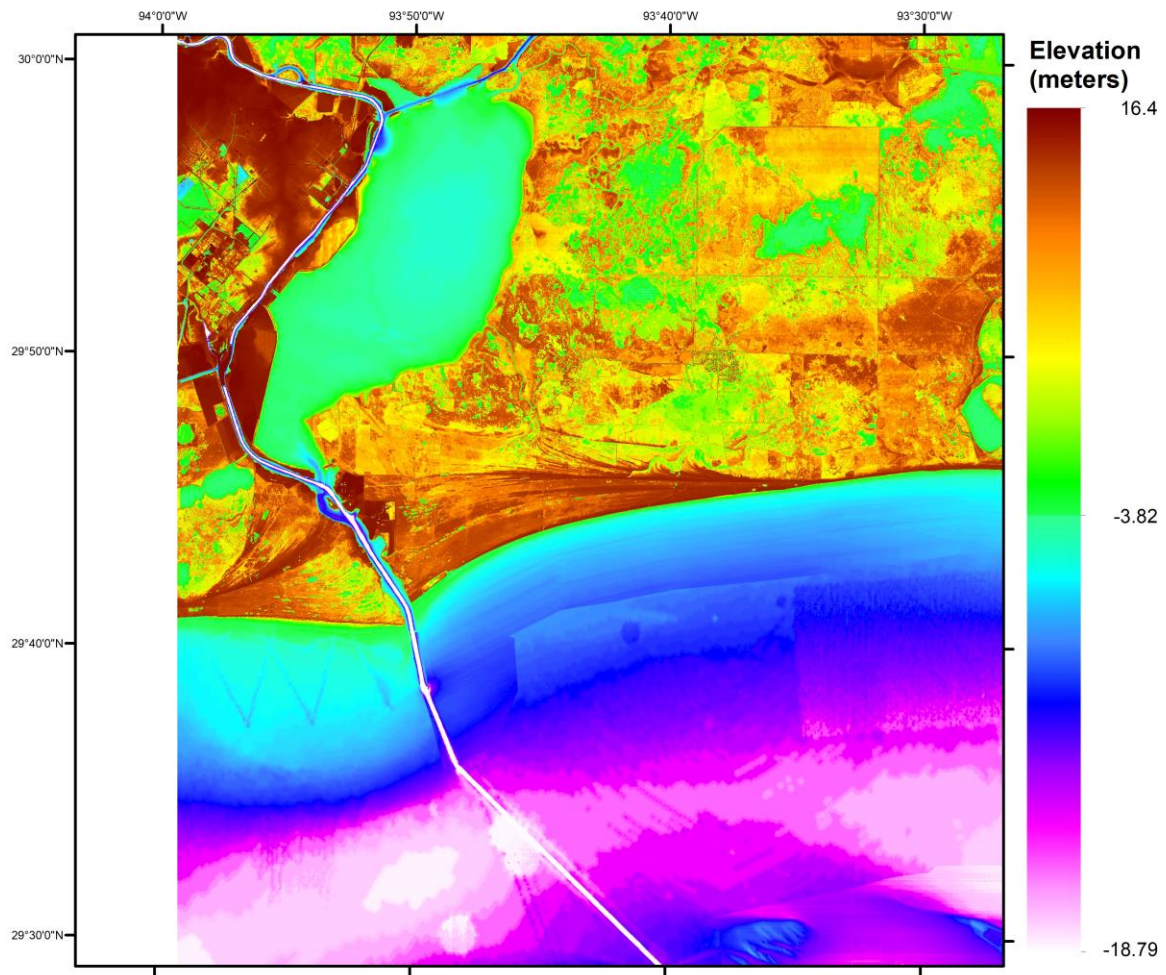


Figure A25. DEM visualization of a 0.5° x 0.5° cell from approximately 29.5°N to 30°N and 94°W to 93.5°W.

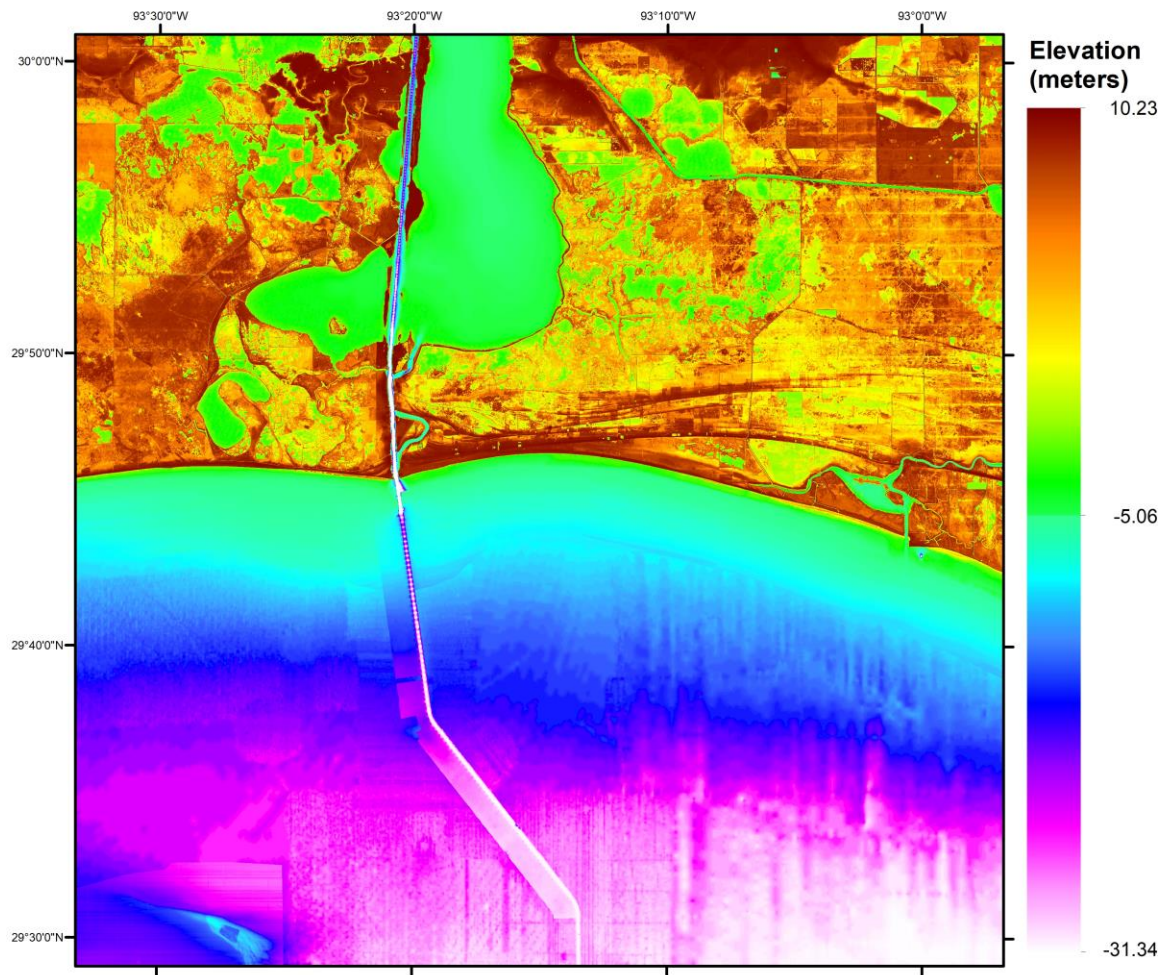


Figure A26. DEM visualization of a 0.5° x 0.5° cell from approximately 29.5°N to 30°N and 93.5°W to 93°W.

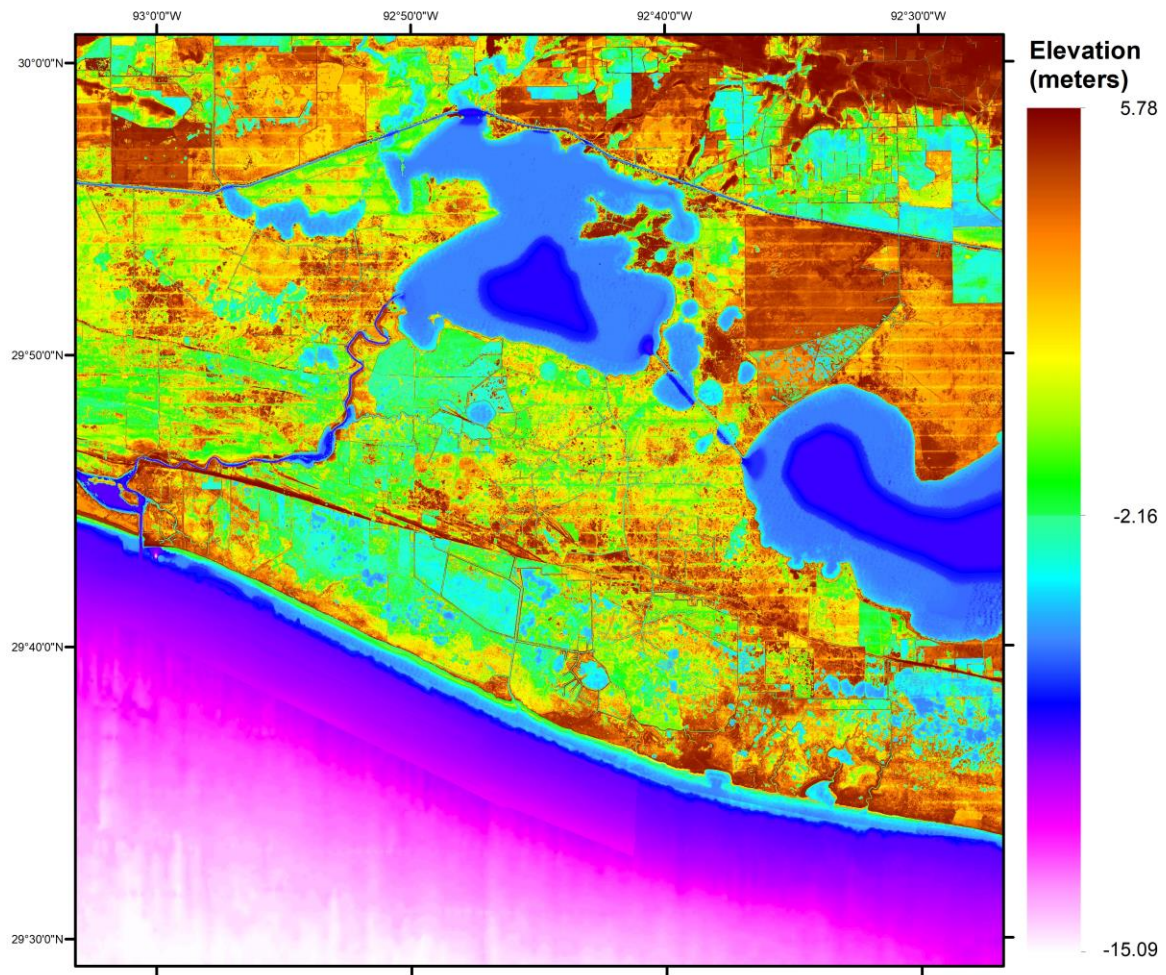


Figure A27. DEM visualization of a 0.5° x 0.5° cell from approximately 29.5°N to 30°N and 93°W to 92.5°W.

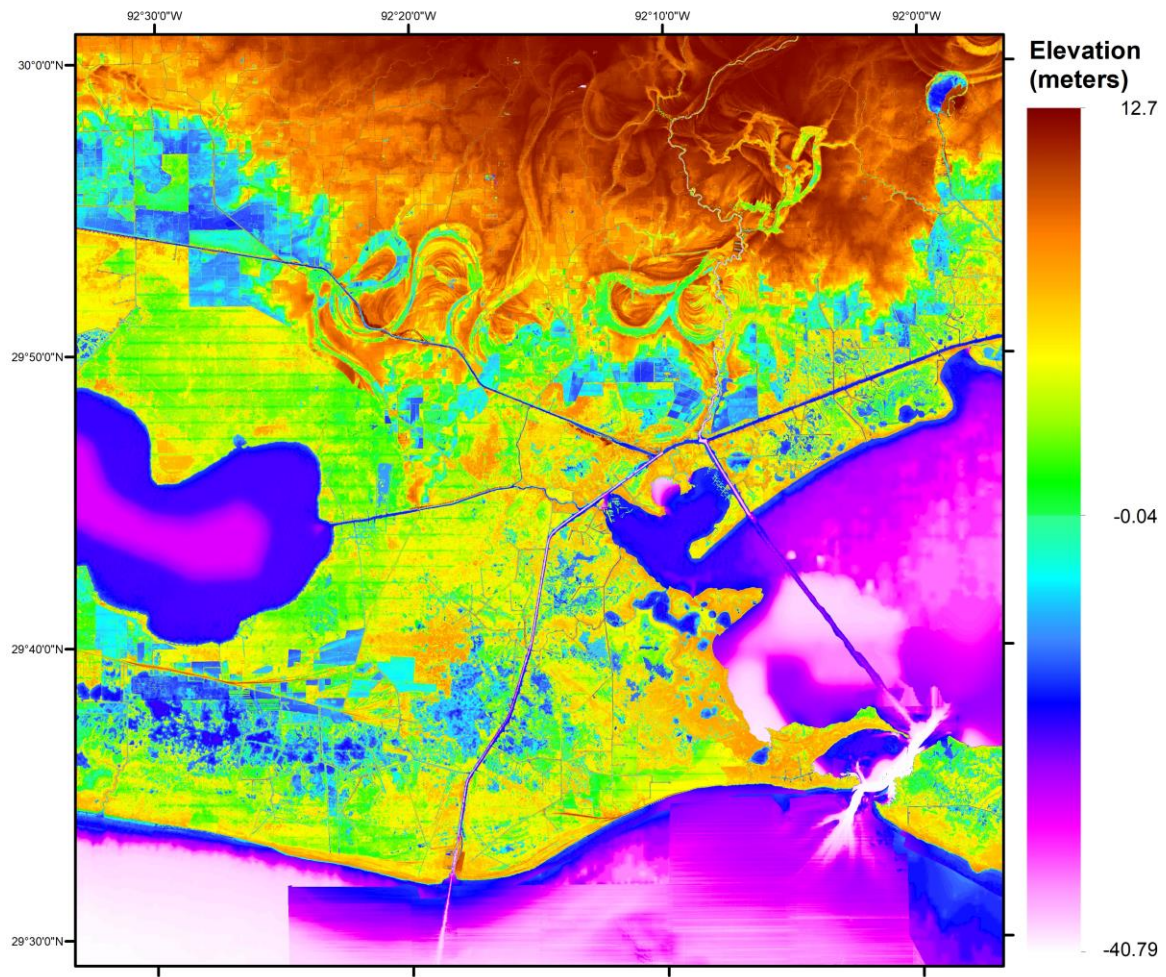


Figure A28. DEM visualization of a 0.5° x 0.5° cell from approximately 29.5°N to 30°N and 92.5°W to 92°W.

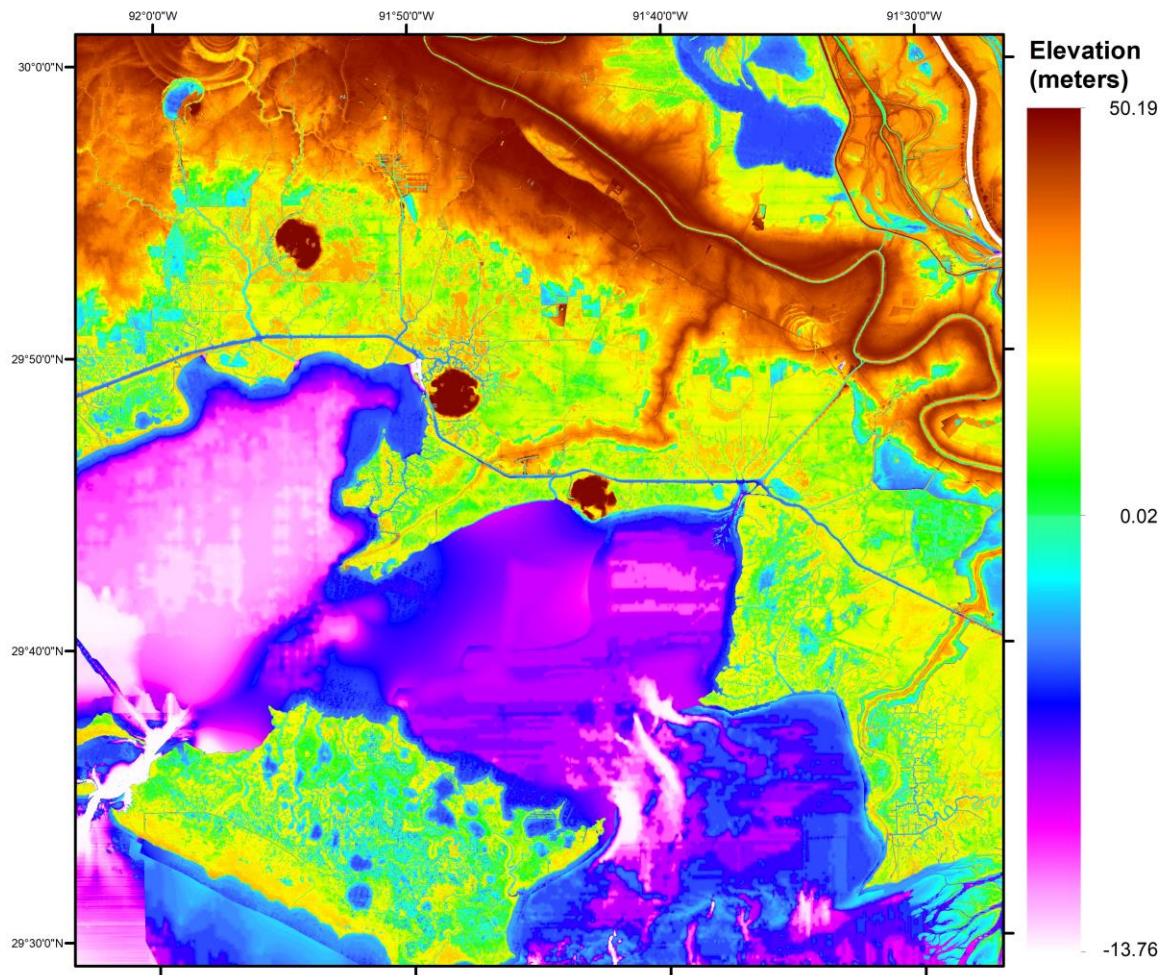


Figure A29. DEM visualization of a 0.5° x 0.5° cell from approximately 29.5°N to 30°N and 92°W to 91.5°W.

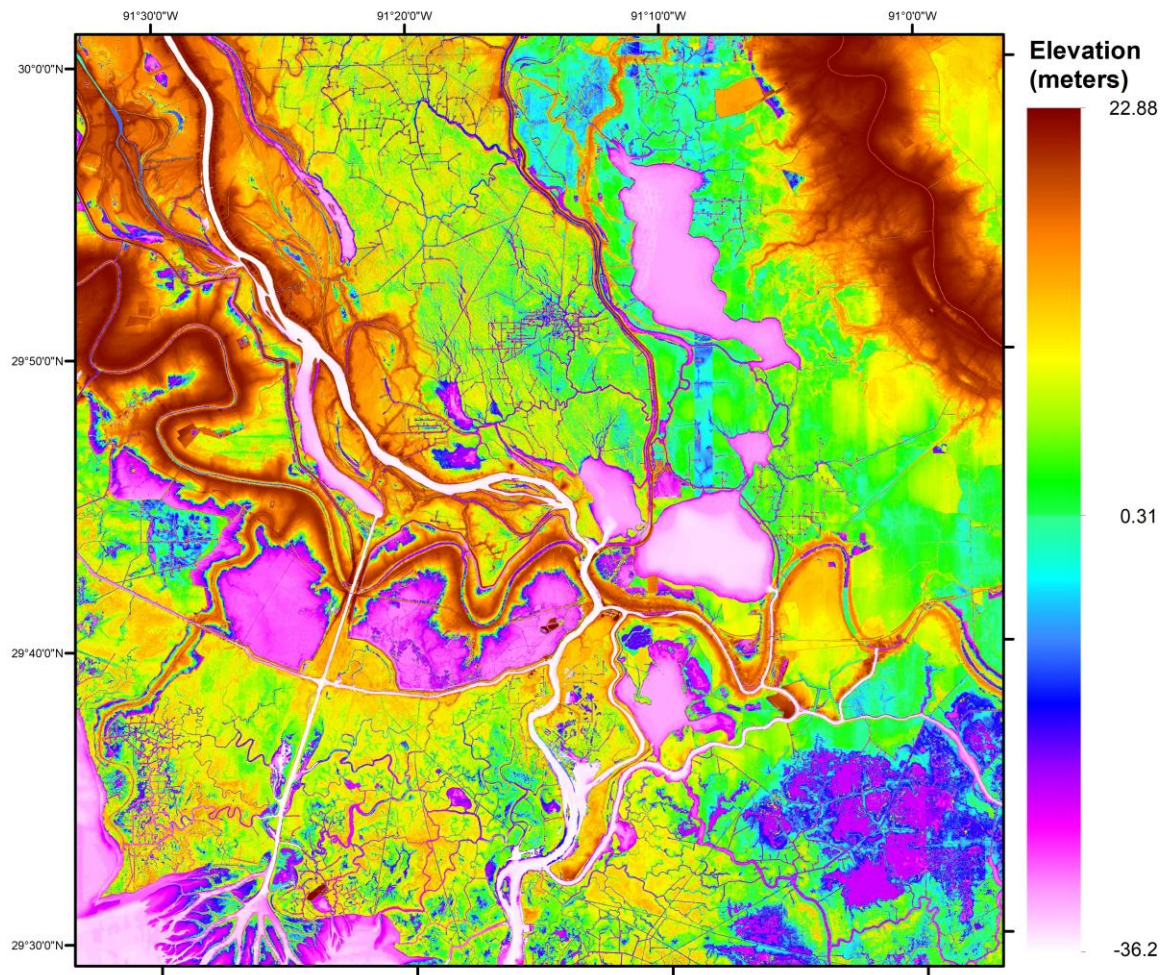


Figure A30. DEM visualization of a 0.5° x 0.5° cell from approximately 29.5°N to 30°N and 91.5°W to 91°W.

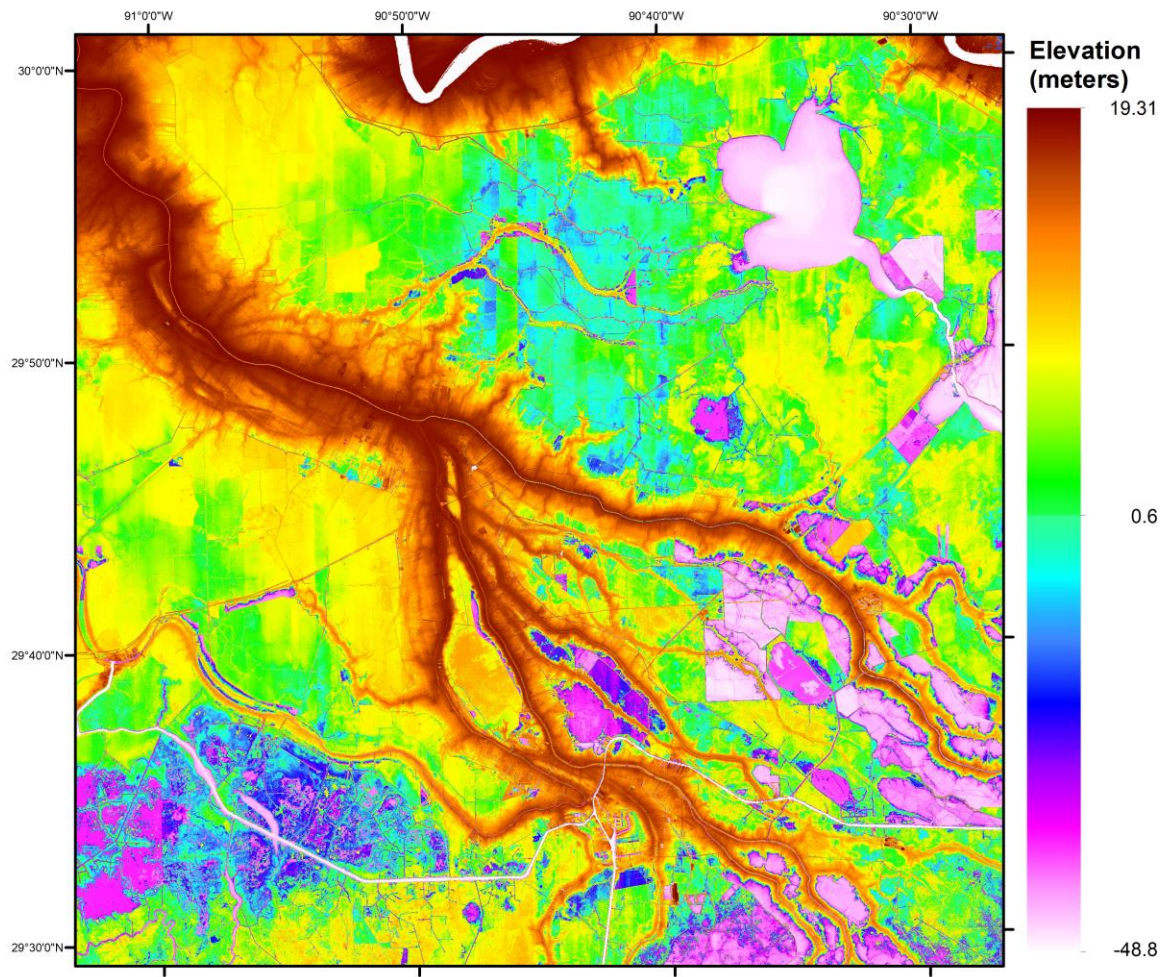


Figure A31. DEM visualization of a 0.5° x 0.5° cell from approximately 29.5°N to 30°N and 91°W to 90.5°W.

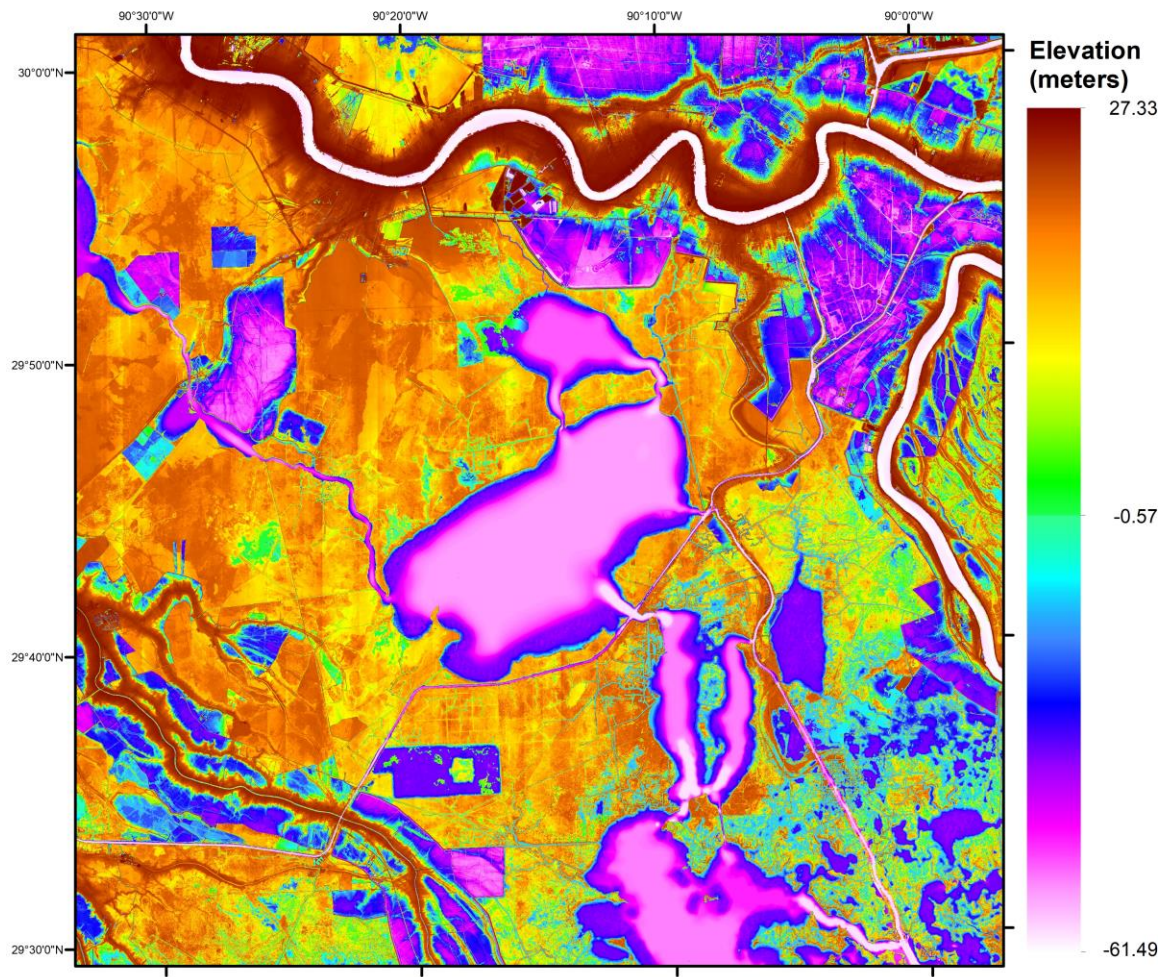


Figure A32. DEM visualization of a 0.5° x 0.5° cell from approximately 29.5°N to 30°N and 90.5°W to 90°W.

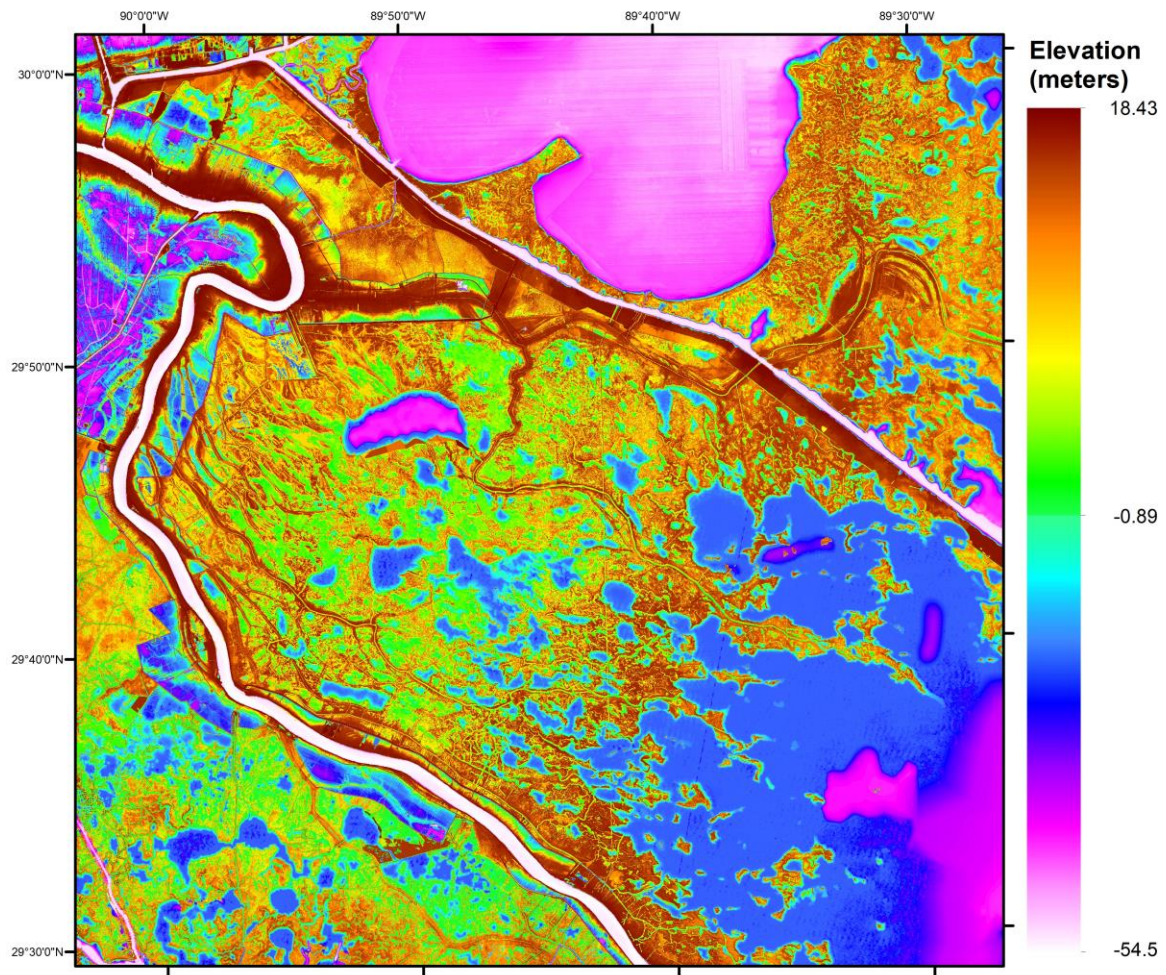


Figure A33. DEM visualization of a 0.5° x 0.5° cell from approximately 29.5°N to 30°N and 90°W to 89.5°W.

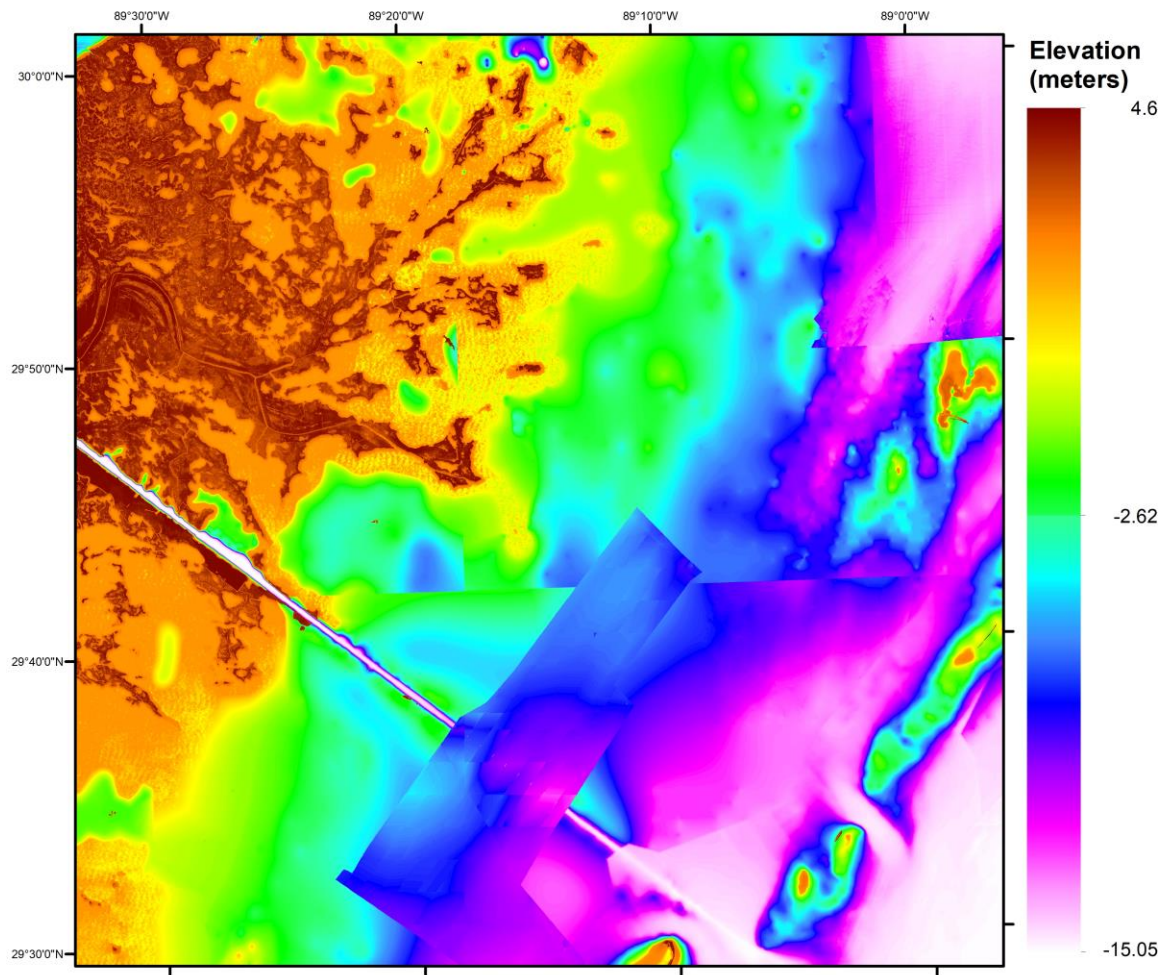


Figure A34. DEM visualization of a 0.5° x 0.5° cell from approximately 29.5°N to 30°N and 89.5°W to 89°W.

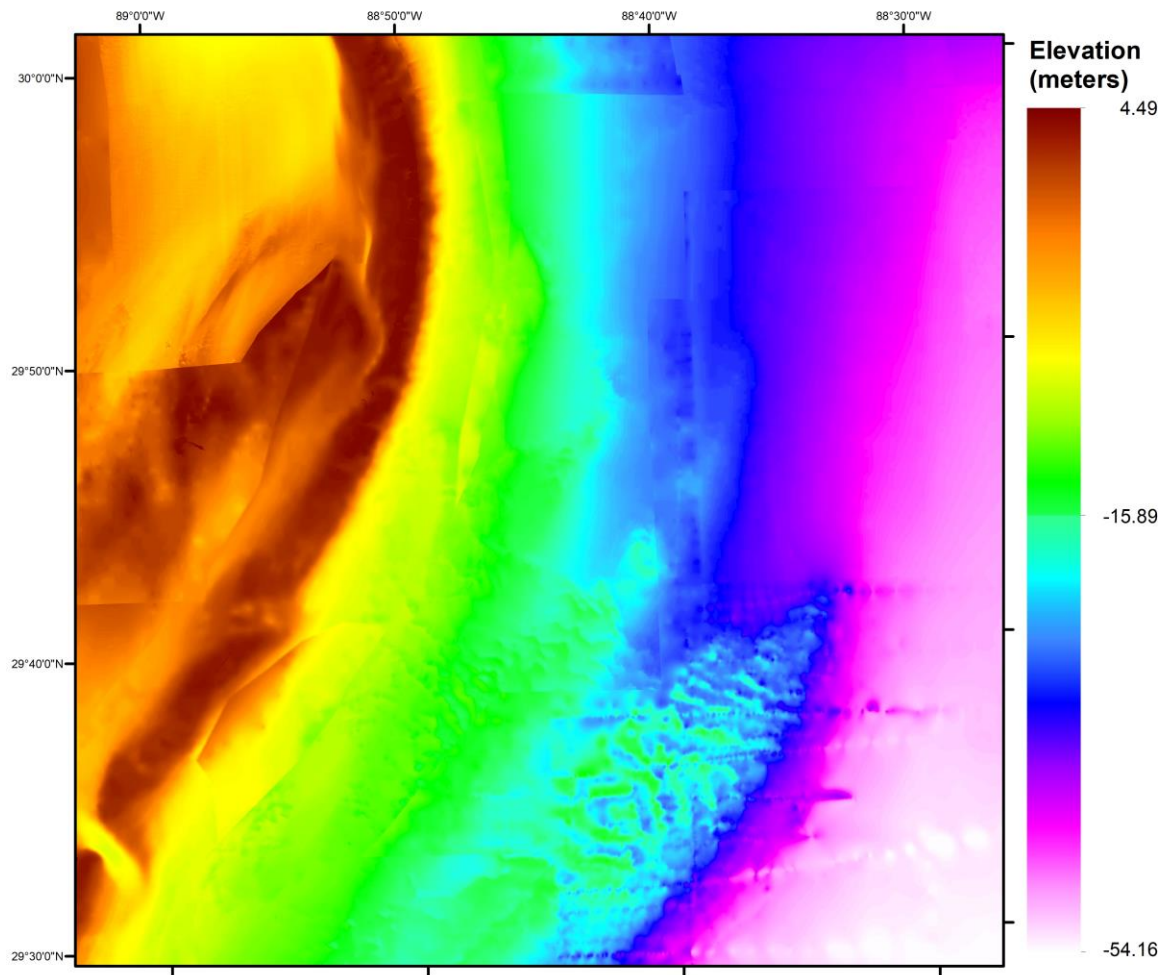


Figure A35. DEM visualization of a 0.5° x 0.5° cell from approximately 29.5°N to 30°N and 89°W to 88.5°W.

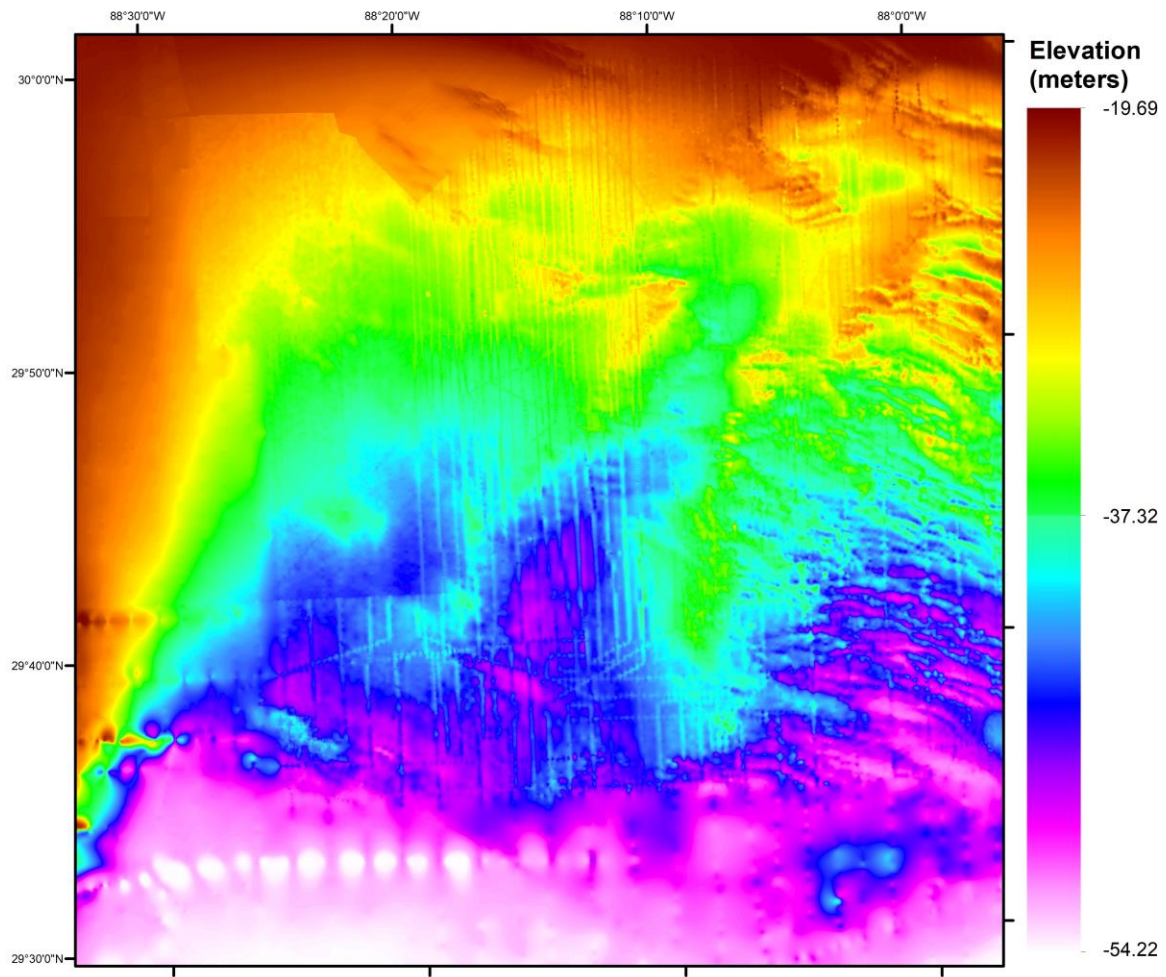


Figure A36. DEM visualization of a 0.5° x 0.5° cell from approximately 29.5°N to 30°N and 88.5°W to 88°W.

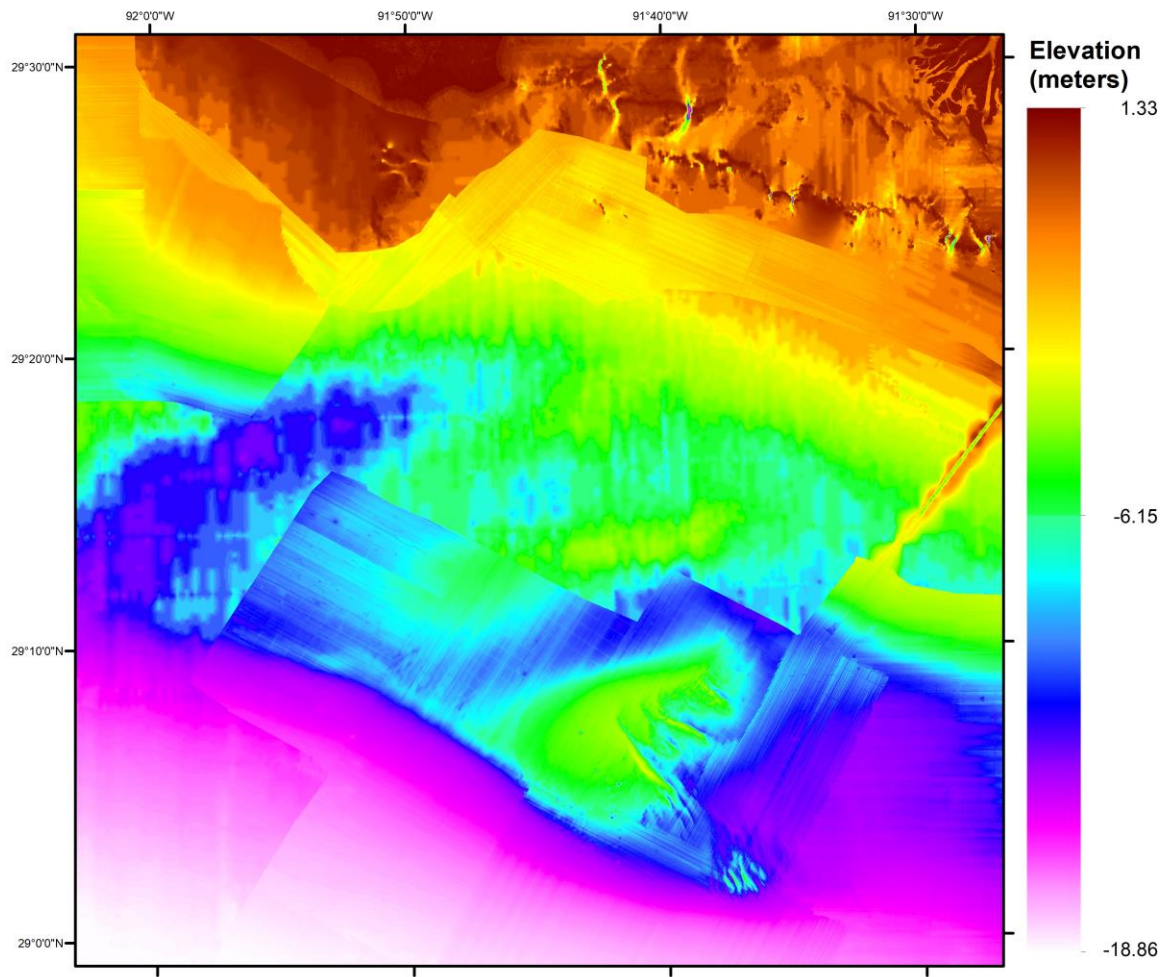


Figure A37. DEM visualization of a 0.5° x 0.5° cell from approximately 29°N to 29.5°N and 92°W to 91.5°W.

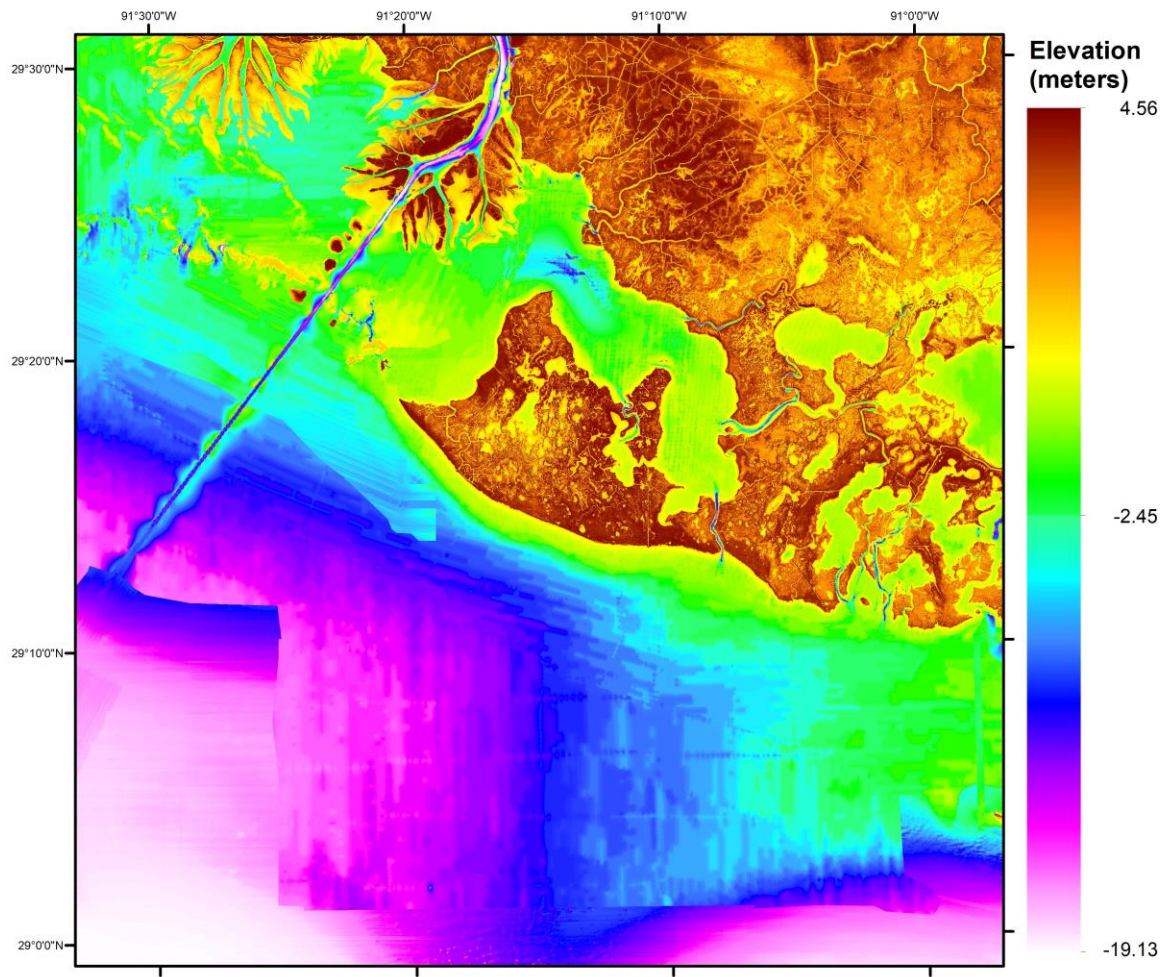


Figure A38. DEM visualization of a 0.5° x 0.5° cell from approximately 29°N to 29.5°N and 91.5°W to 91°W.

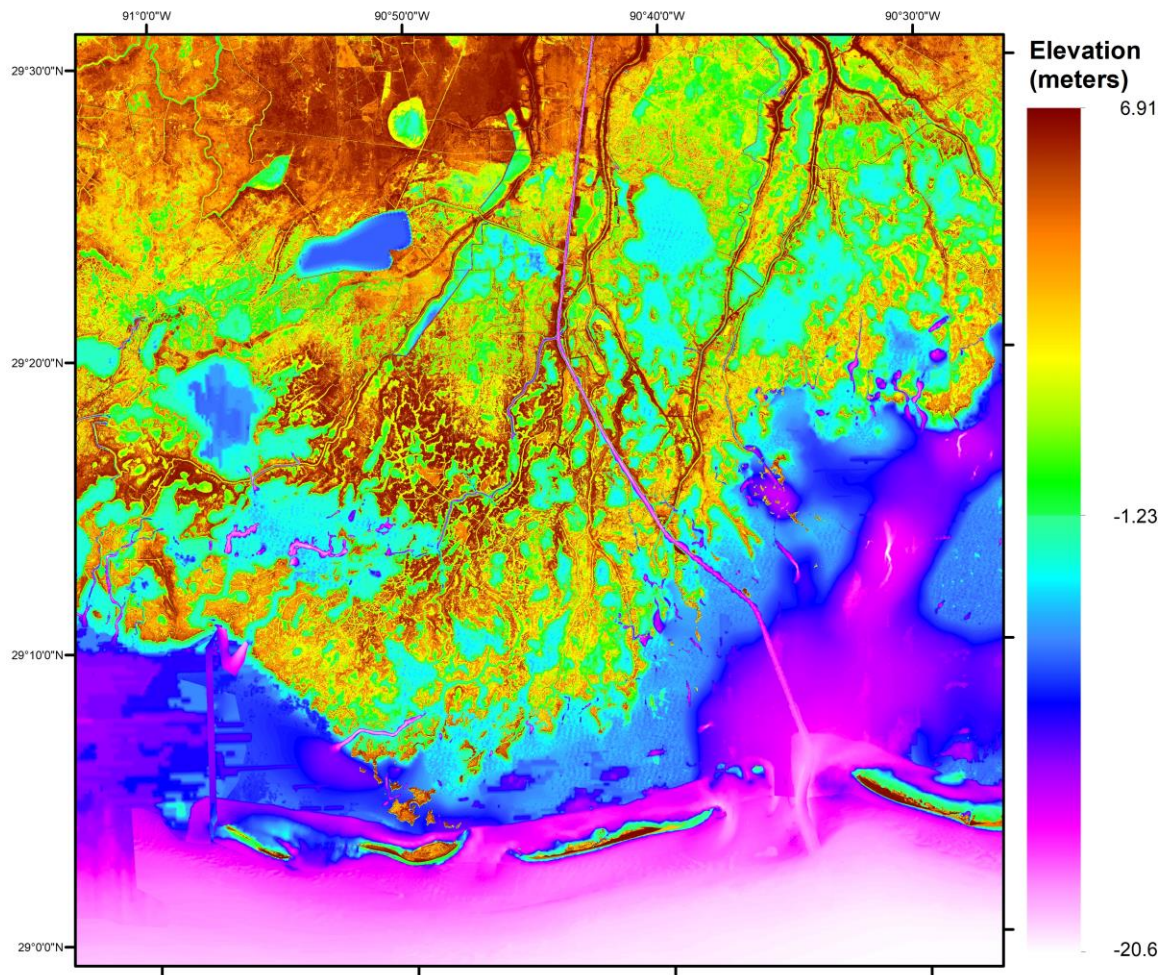


Figure A39. DEM visualization of a 0.5° x 0.5° cell from approximately 29°N to 29.5°N and 91°W to 90.5°W.

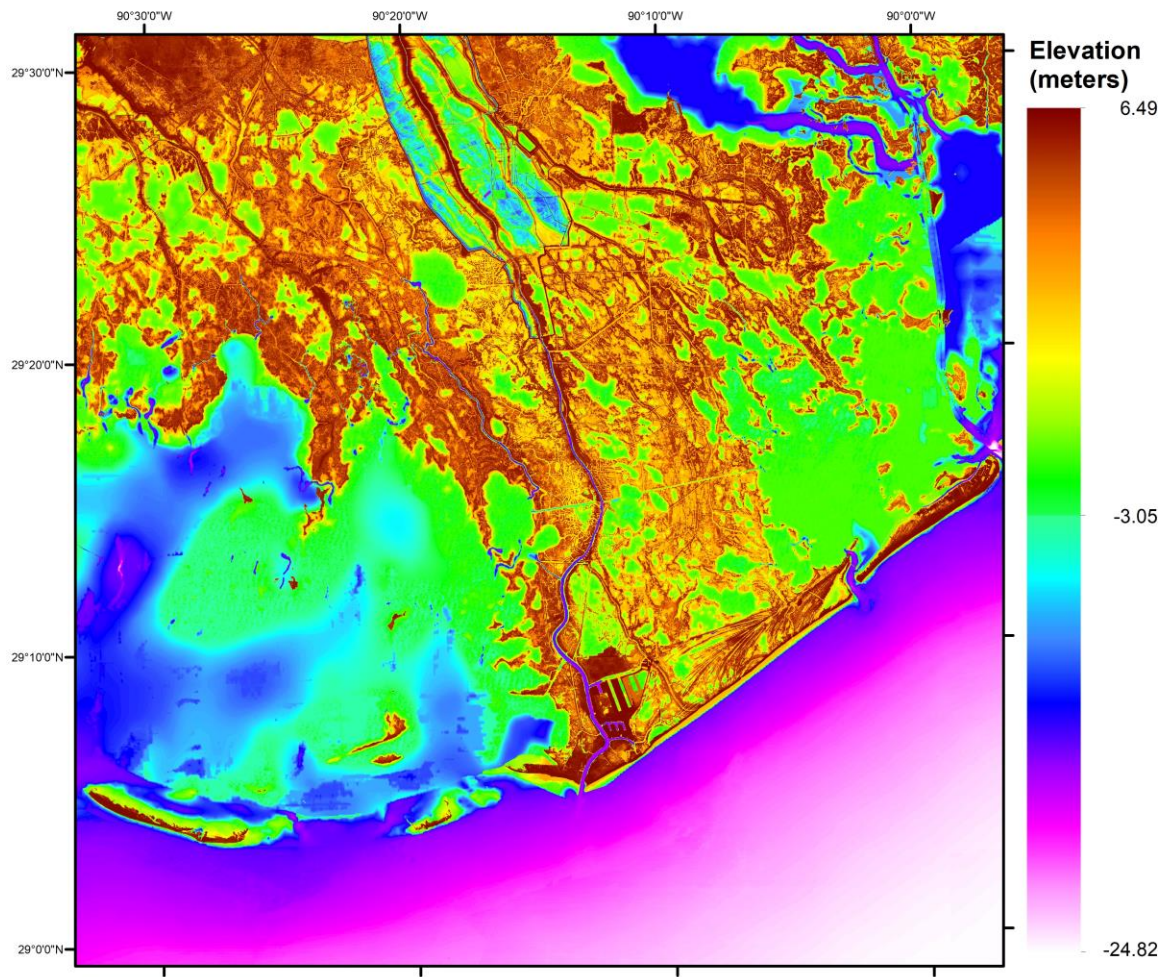


Figure A40. DEM visualization of a 0.5° x 0.5° cell from approximately 29°N to 29.5°N and 90.5°W to 90°W.

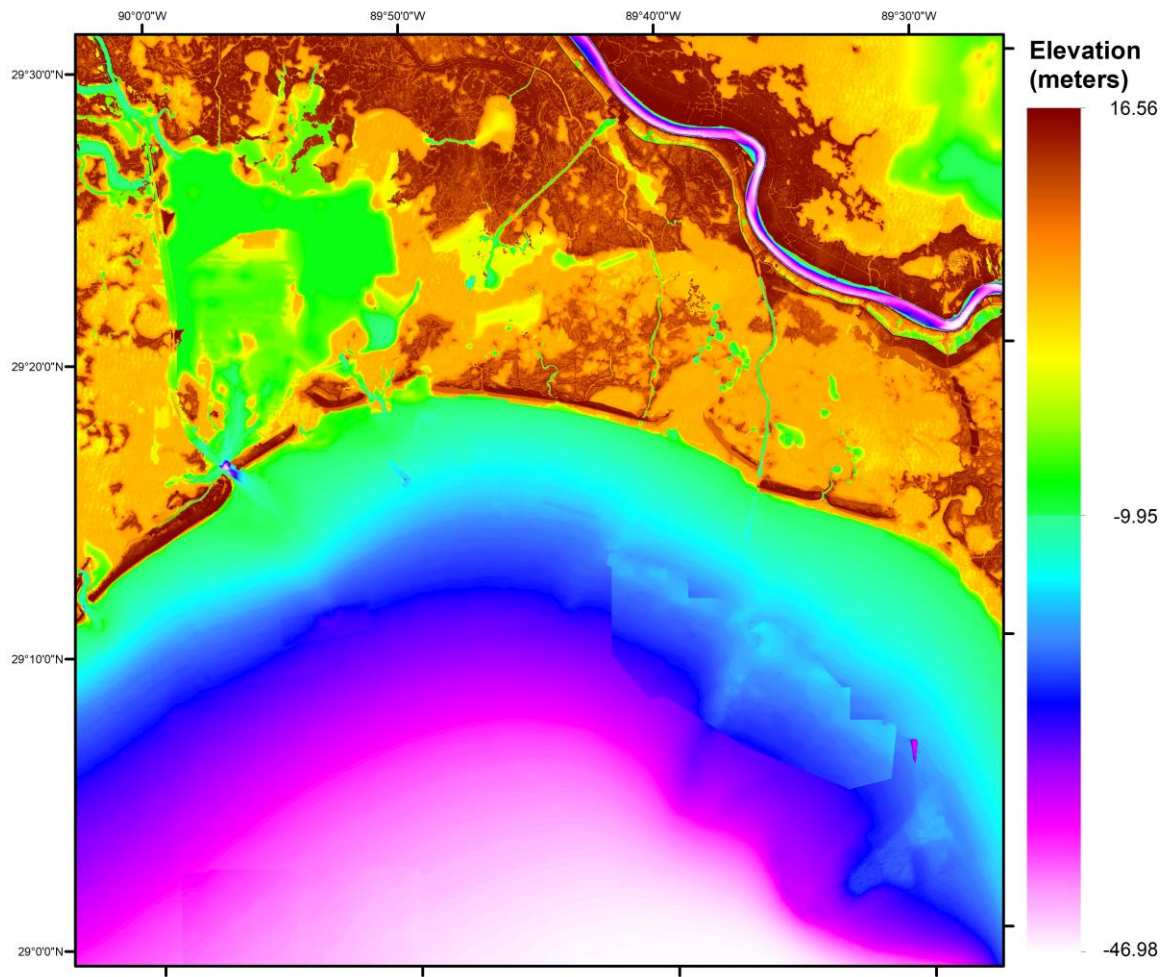


Figure A41. DEM visualization of a 0.5° x 0.5° cell from approximately 29°N to 29.5°N and 90°W to 89.5°W.

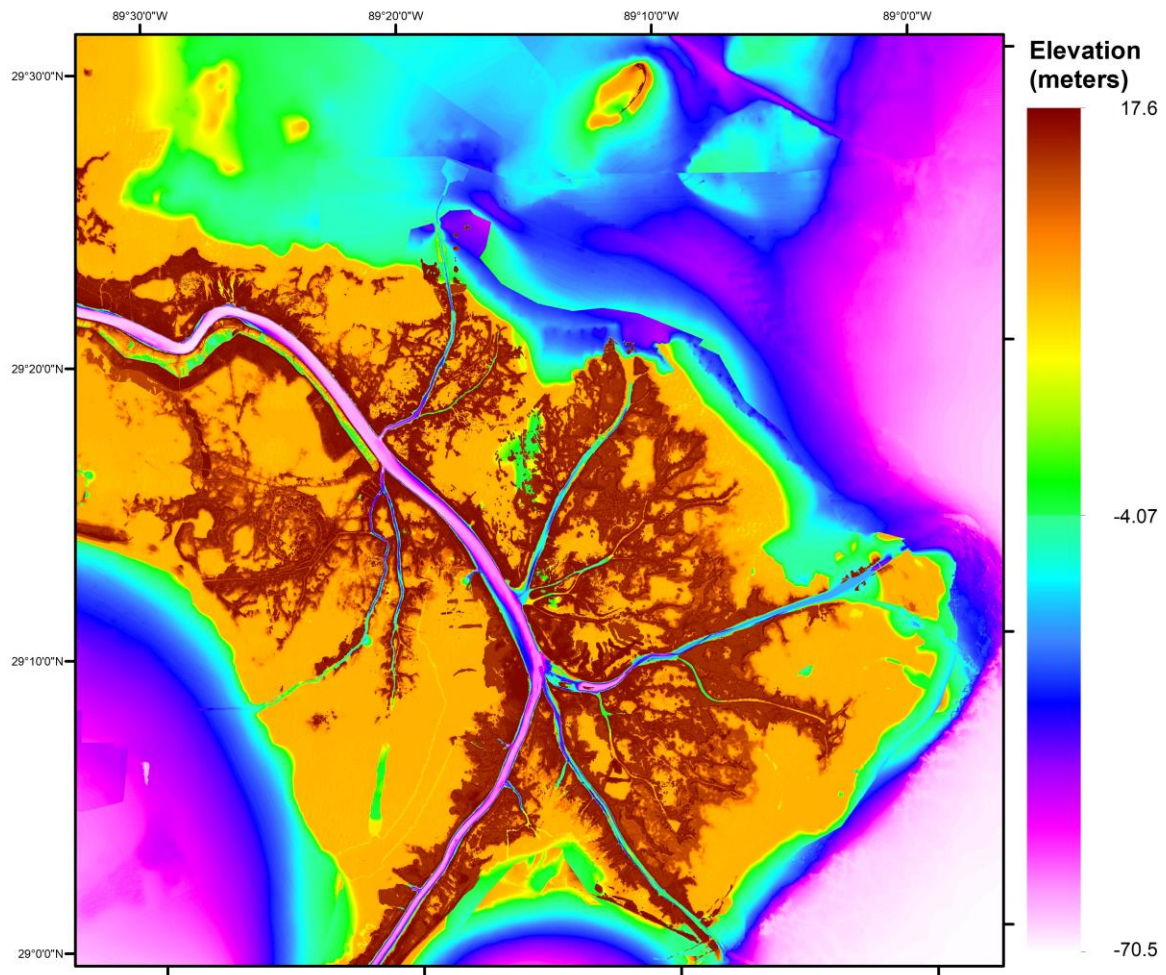


Figure A42. DEM visualization of a 0.5° x 0.5° cell from approximately 29°N to 29.5°N and 89.5°W to 89°W.

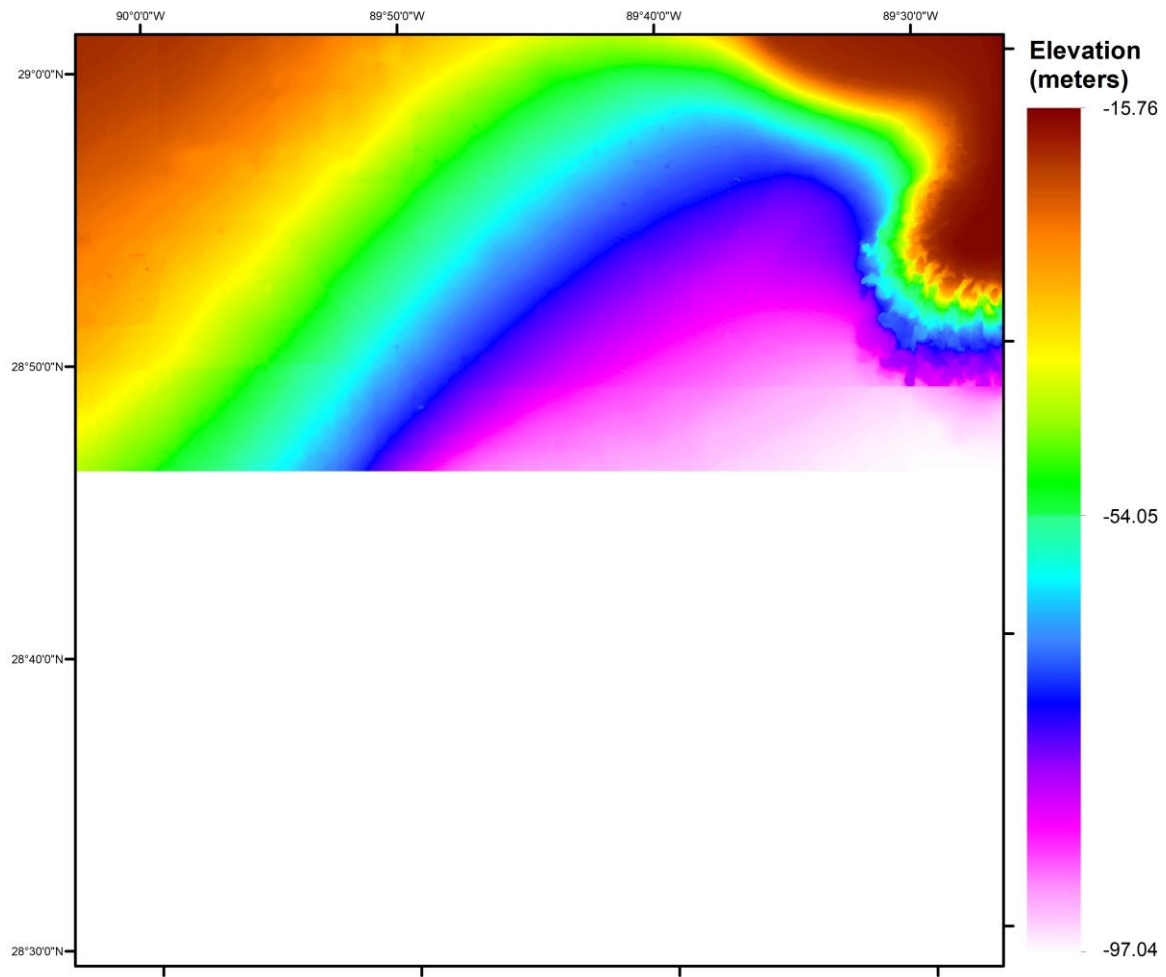


Figure A43. DEM visualization of a 0.5° x 0.5° cell from approximately 28.5°N to 29°N and 90°W to 89.5°W.

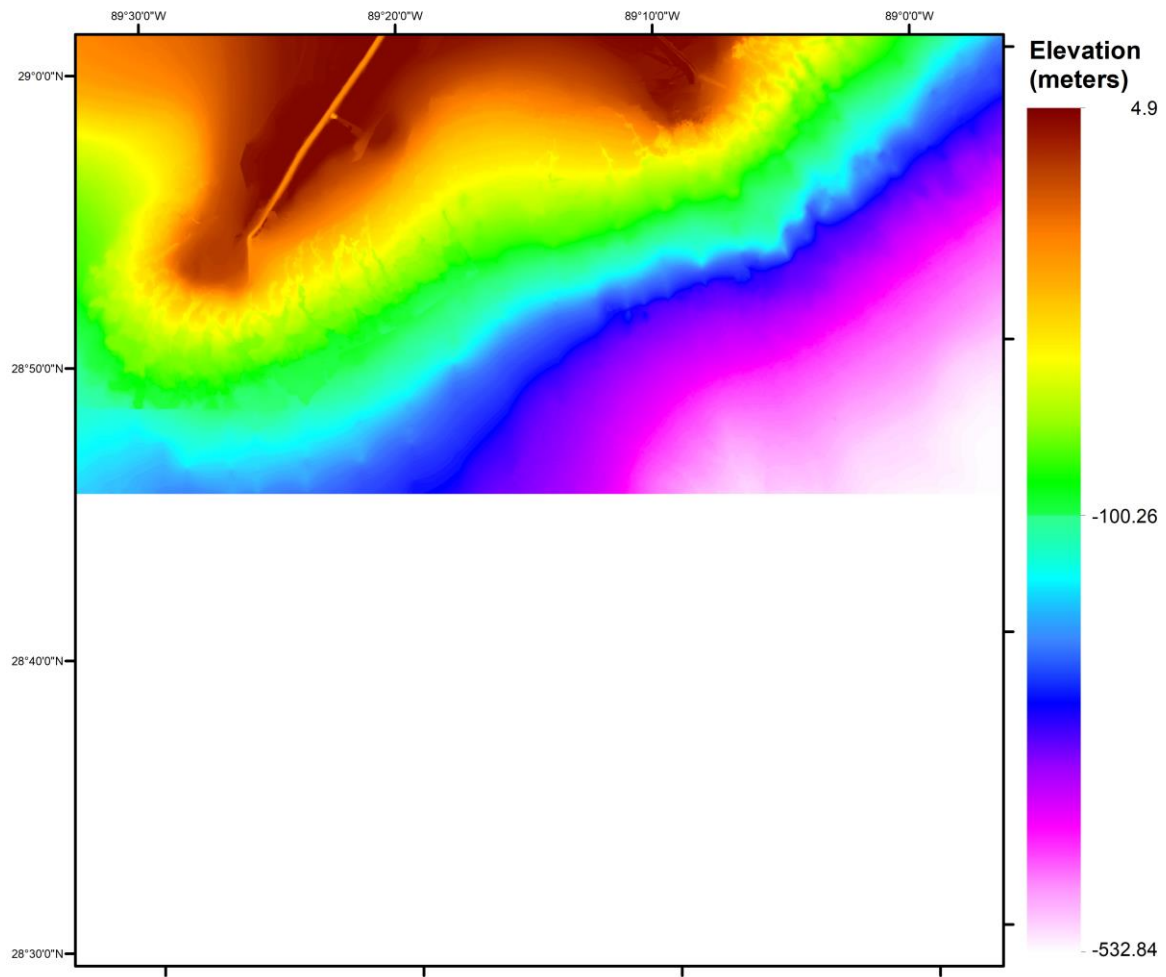


Figure A44. DEM visualization of a 0.5° x 0.5° cell from approximately 28.5°N to 29°N and 89.5°W to 89°W.

APPENDIX B: WETLAND VEGETATION COMMUNITY TYPE VISUALIZATIONS

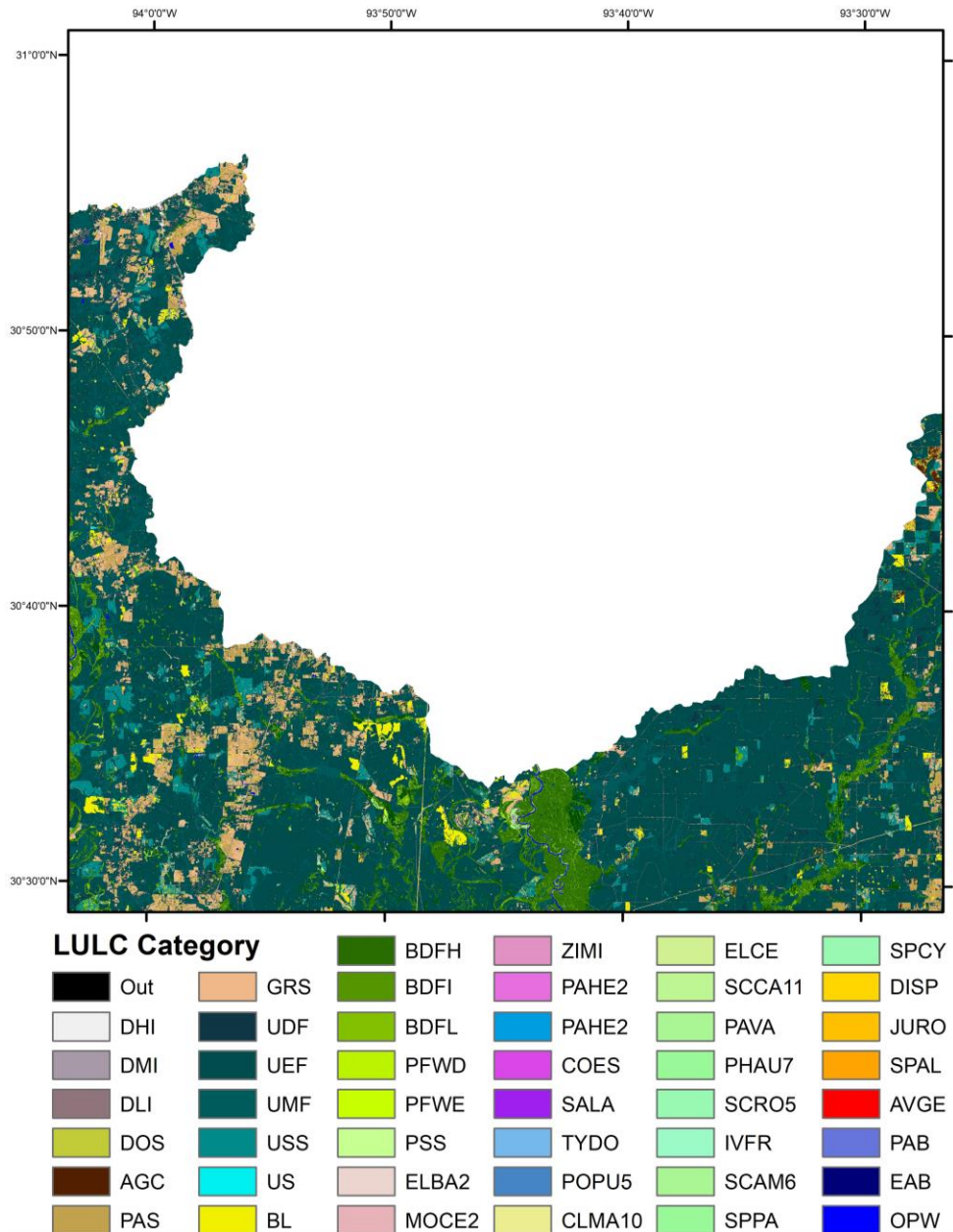


Figure B1. LULC visualization of a 0.5° x 0.5° cell from approximately 30.5°N to 31°N and 94°W to 93.5°W.

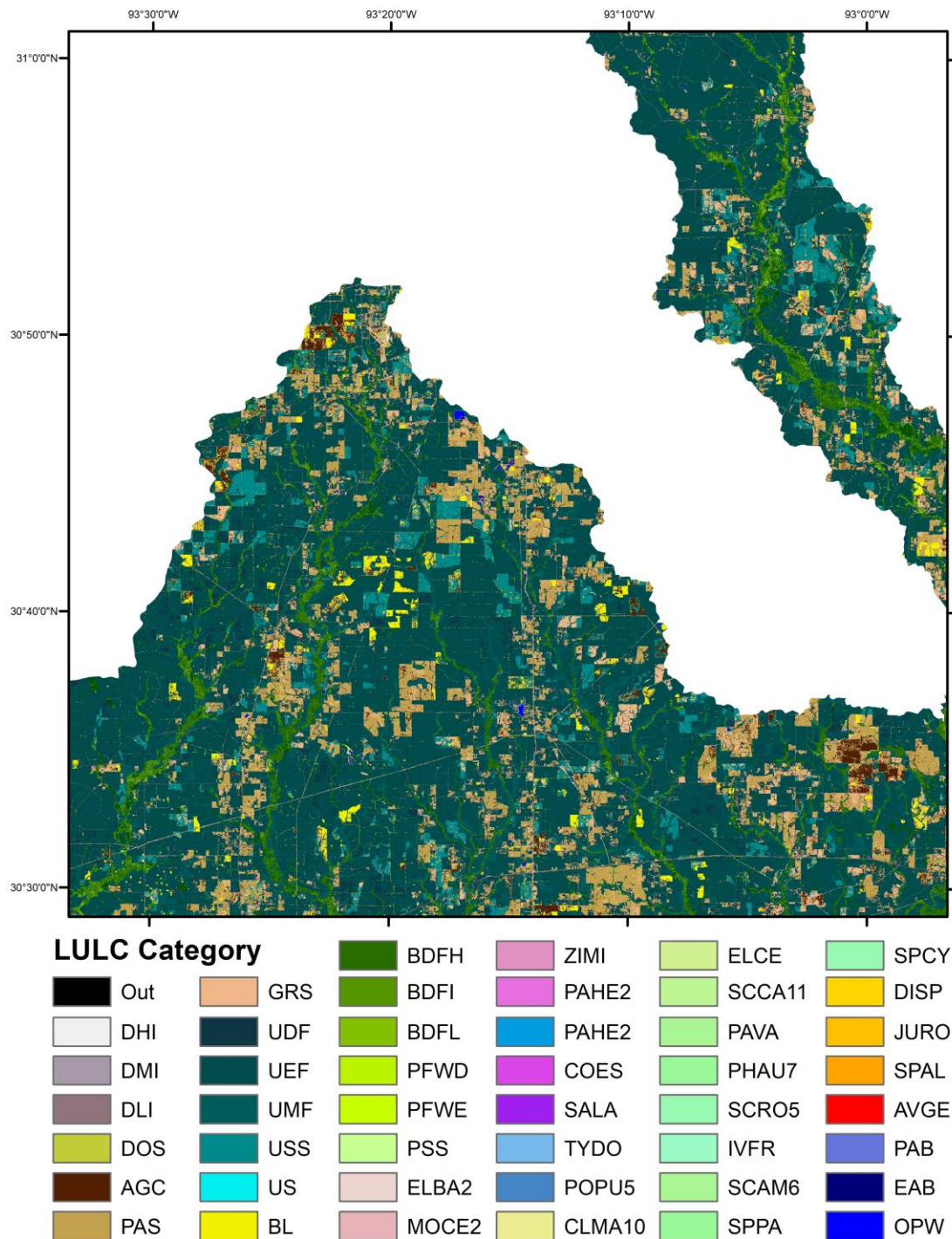


Figure B2. LULC visualization of a 0.5° x 0.5° cell from approximately 30.5°N to 31°N and 93.5°W to 93°W.

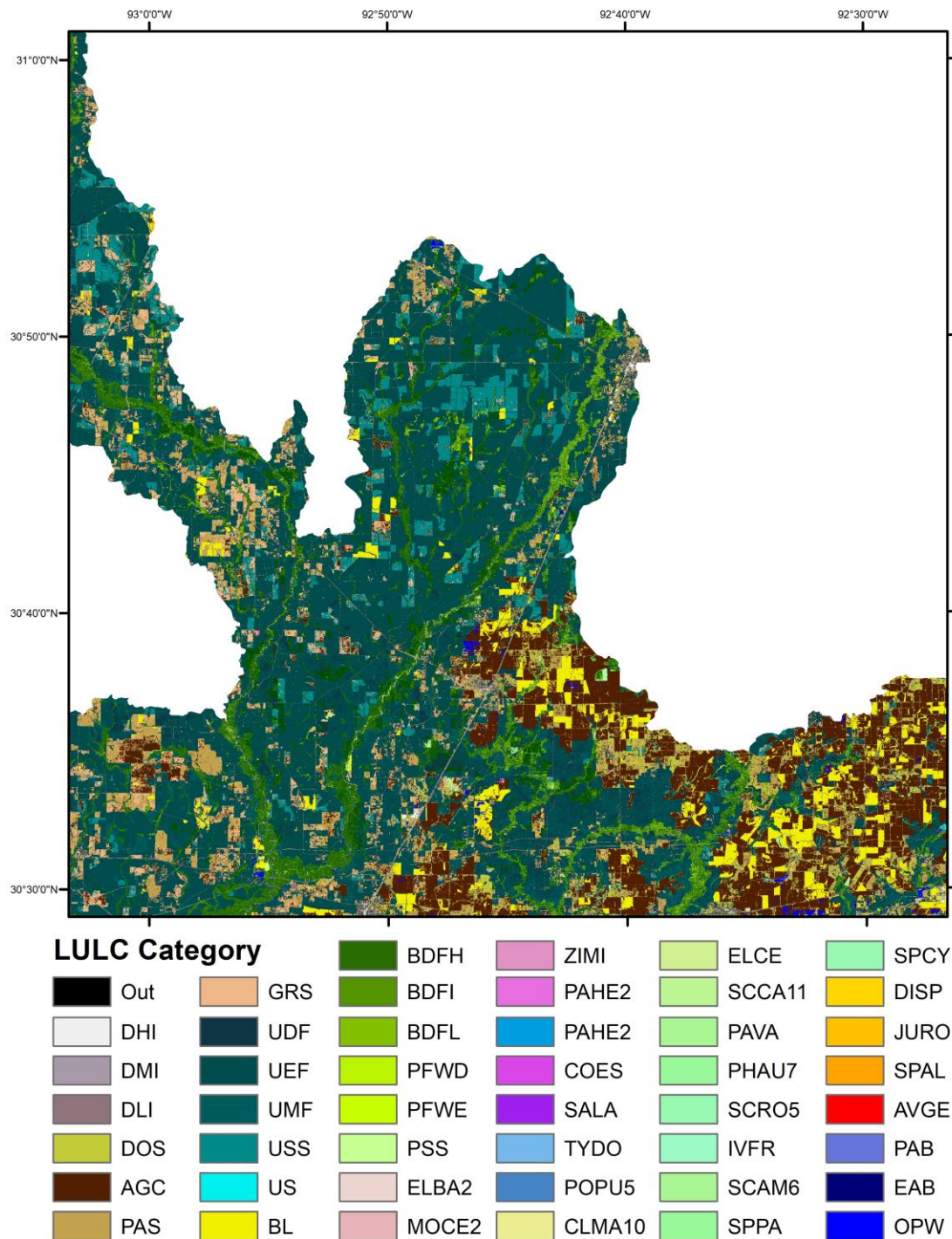


Figure B3. LULC visualization of a 0.5° x 0.5° cell from approximately 30.5°N to 31°N and 93°W to 92.5°W.

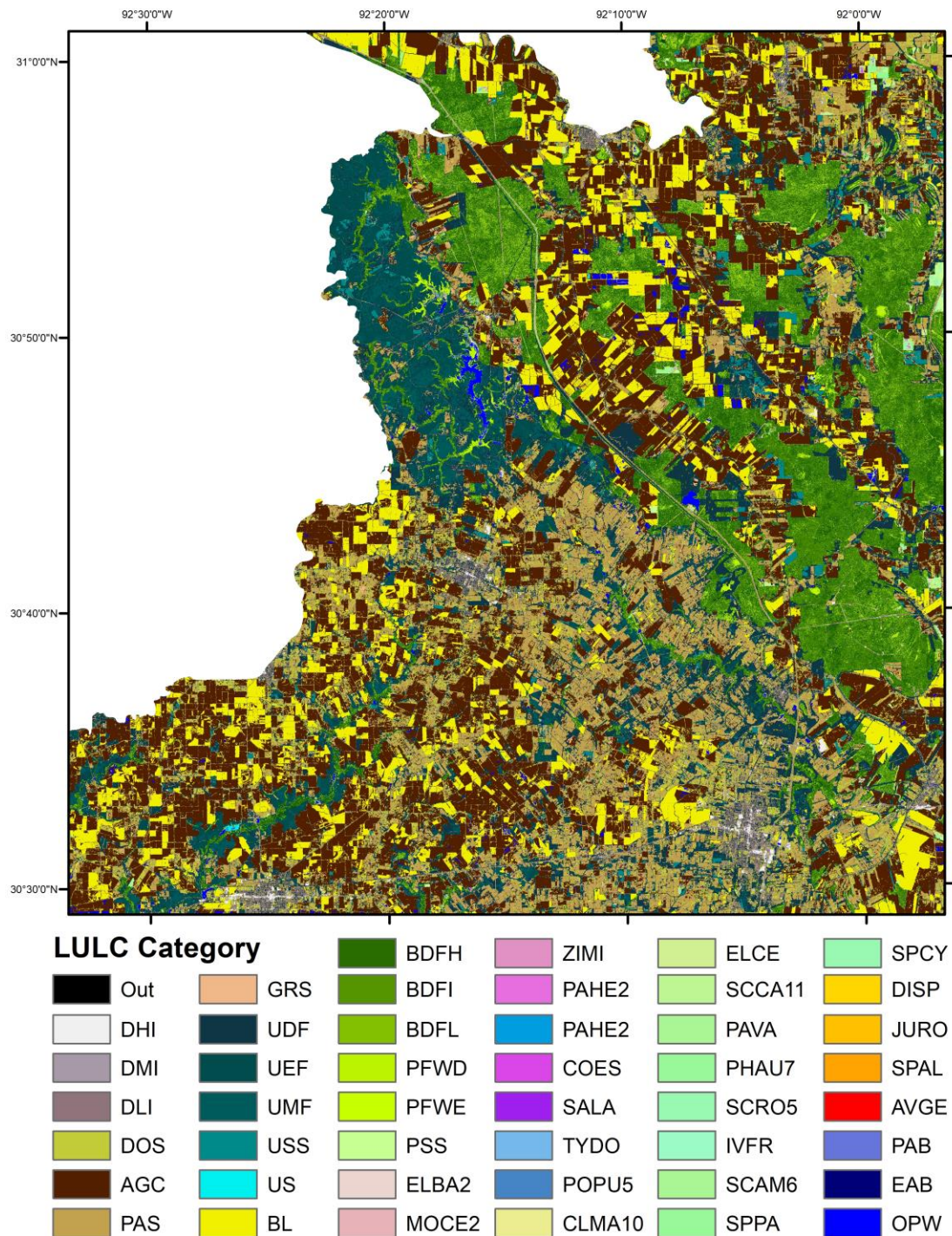


Figure B4. LULC visualization of a 0.5° x 0.5° cell from approximately 30.5°N to 31°N and 92.5°W to 92°W.

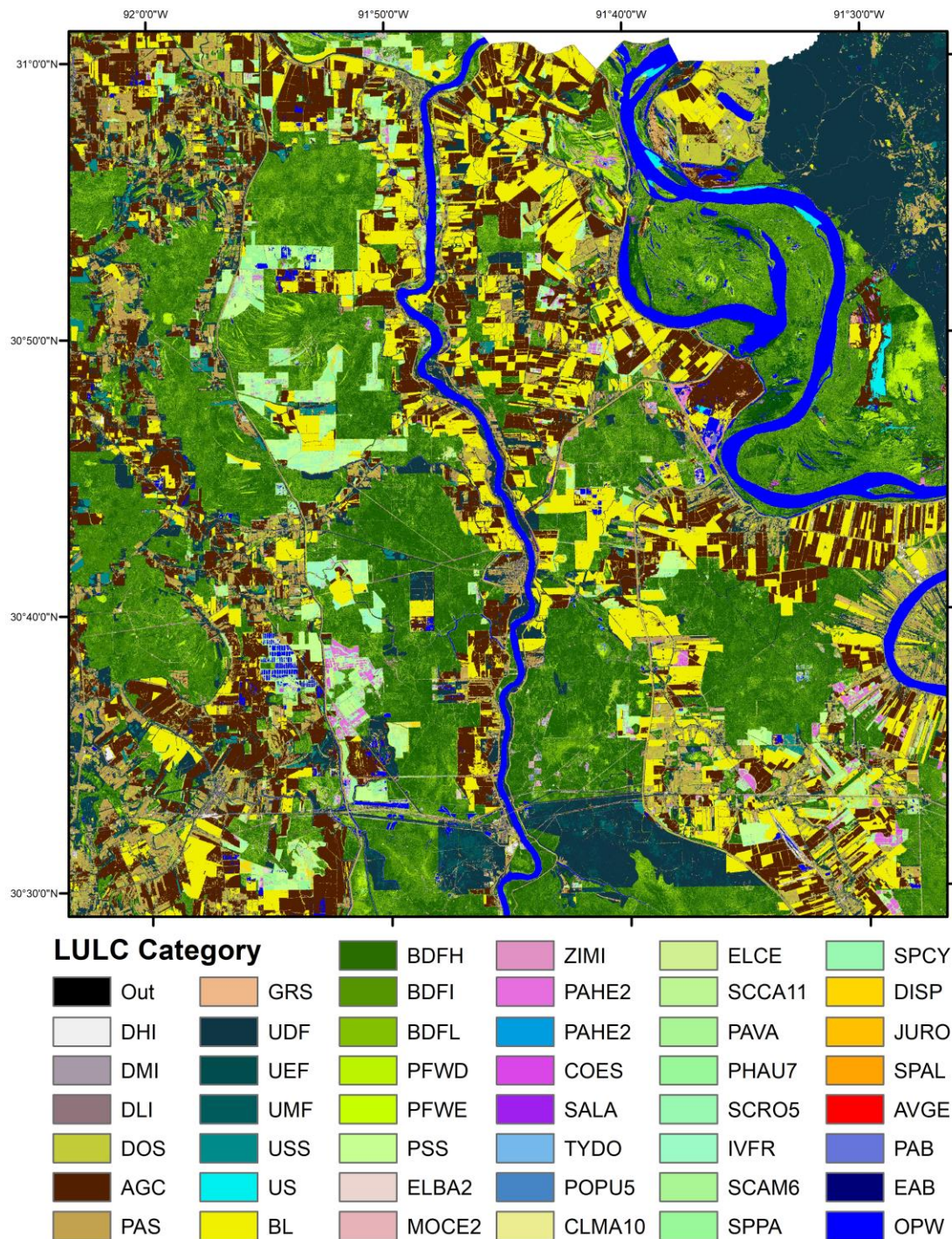


Figure B5. LULC visualization of a 0.5° x 0.5° cell from approximately 30.5°N to 31°N and 92°W to 91.5°W.

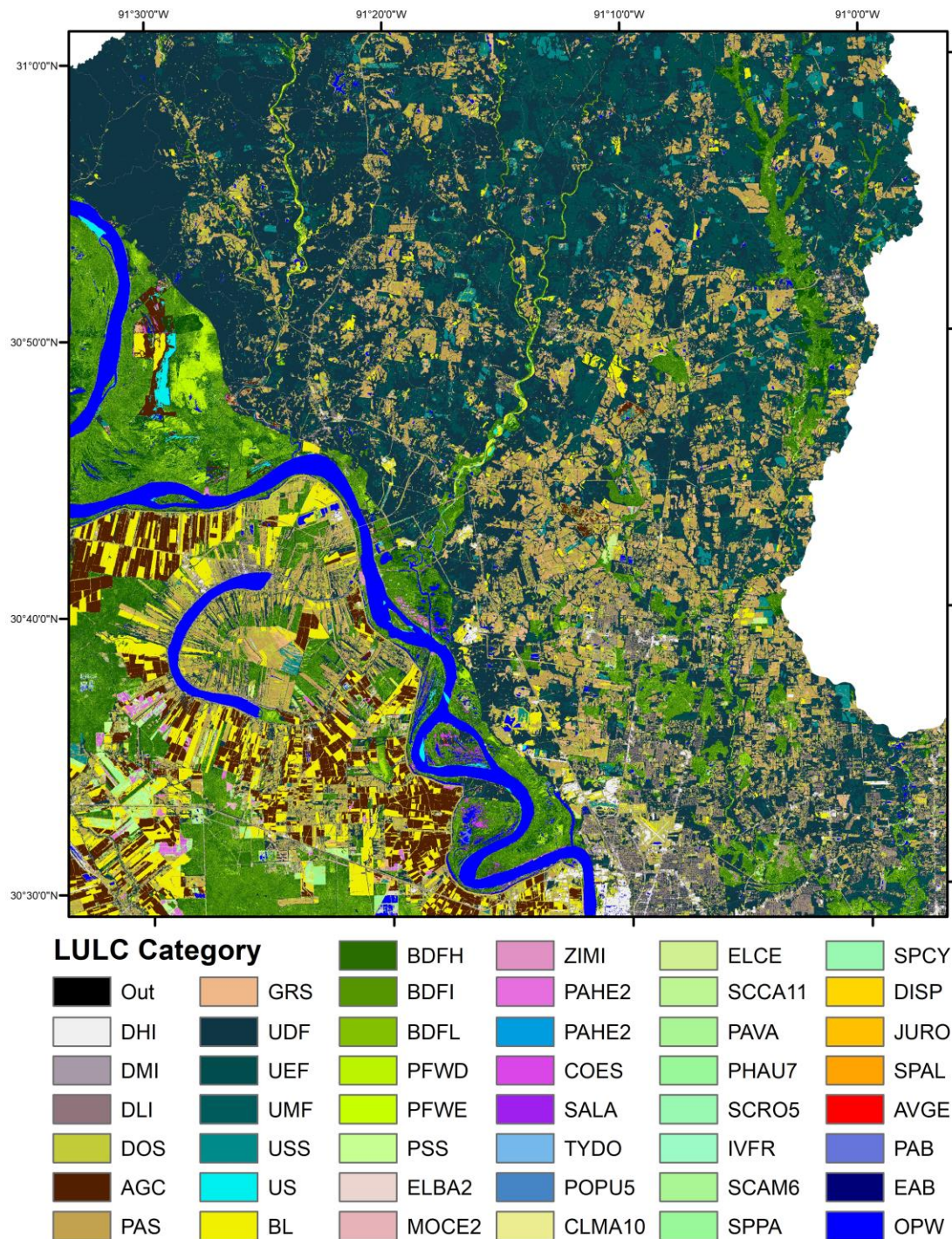


Figure B6. LULC visualization of a 0.5° x 0.5° cell from approximately 30.5°N to 31°N and 91.5°W to 91°W.

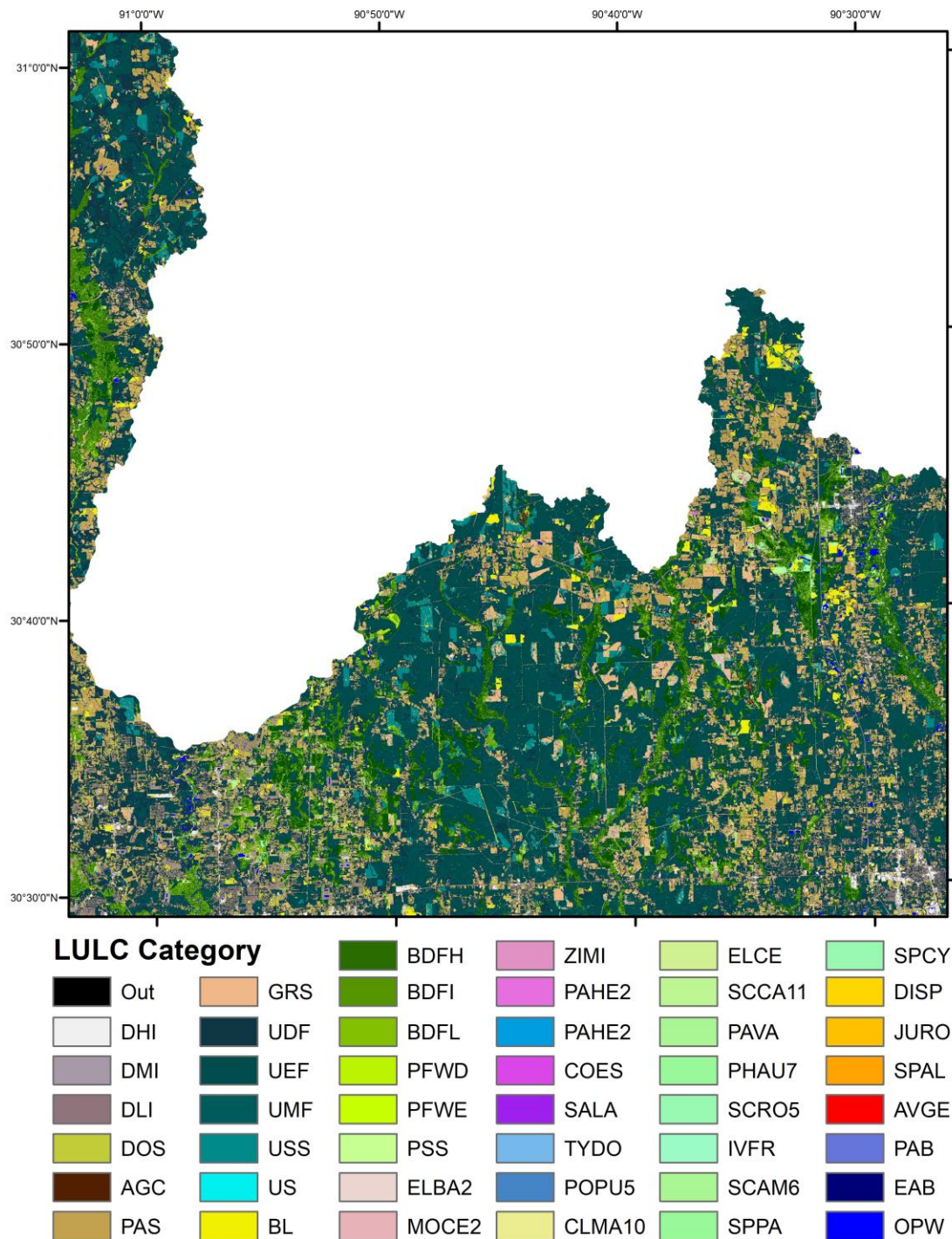


Figure B7. LULC visualization of a 0.5° x 0.5° cell from approximately 30.5°N to 31°N and 91°W to 90.5°W.

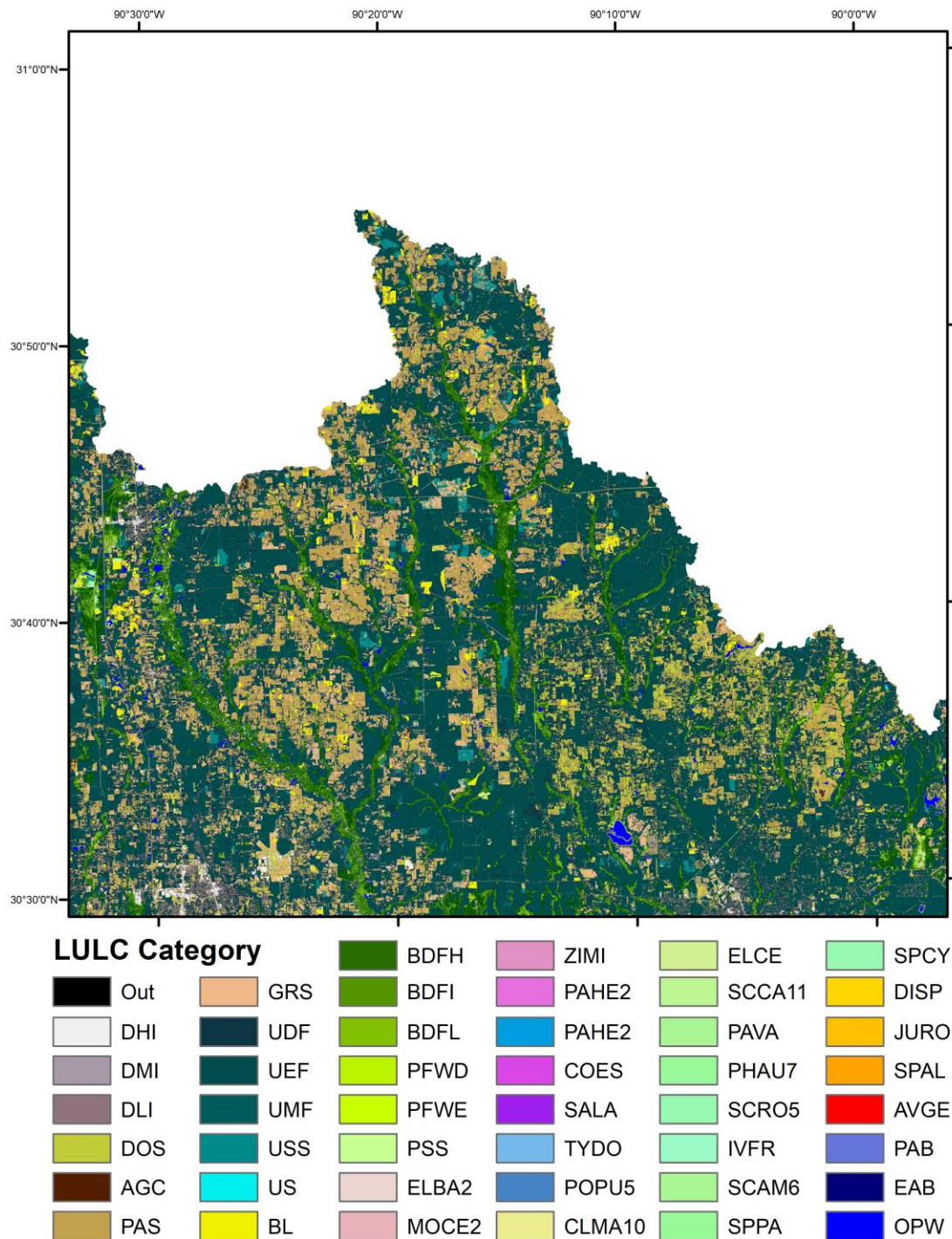


Figure B8. LULC visualization of a 0.5° x 0.5° cell from approximately 30.5°N to 31°N and 90.5°W to 90°W.

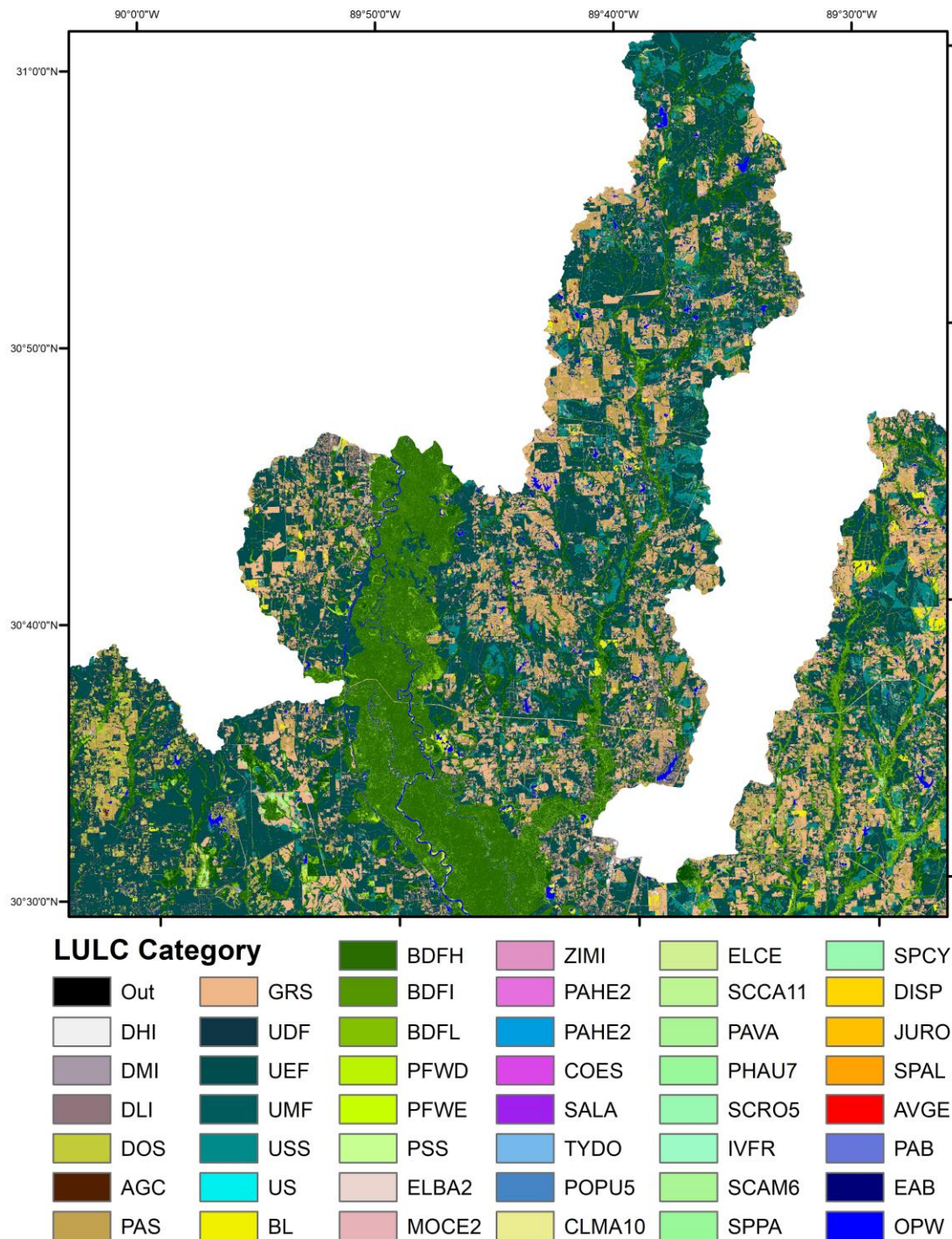


Figure B9. LULC visualization of a 0.5° x 0.5° cell from approximately 30.5°N to 31°N and 90°W to 89.5°W.

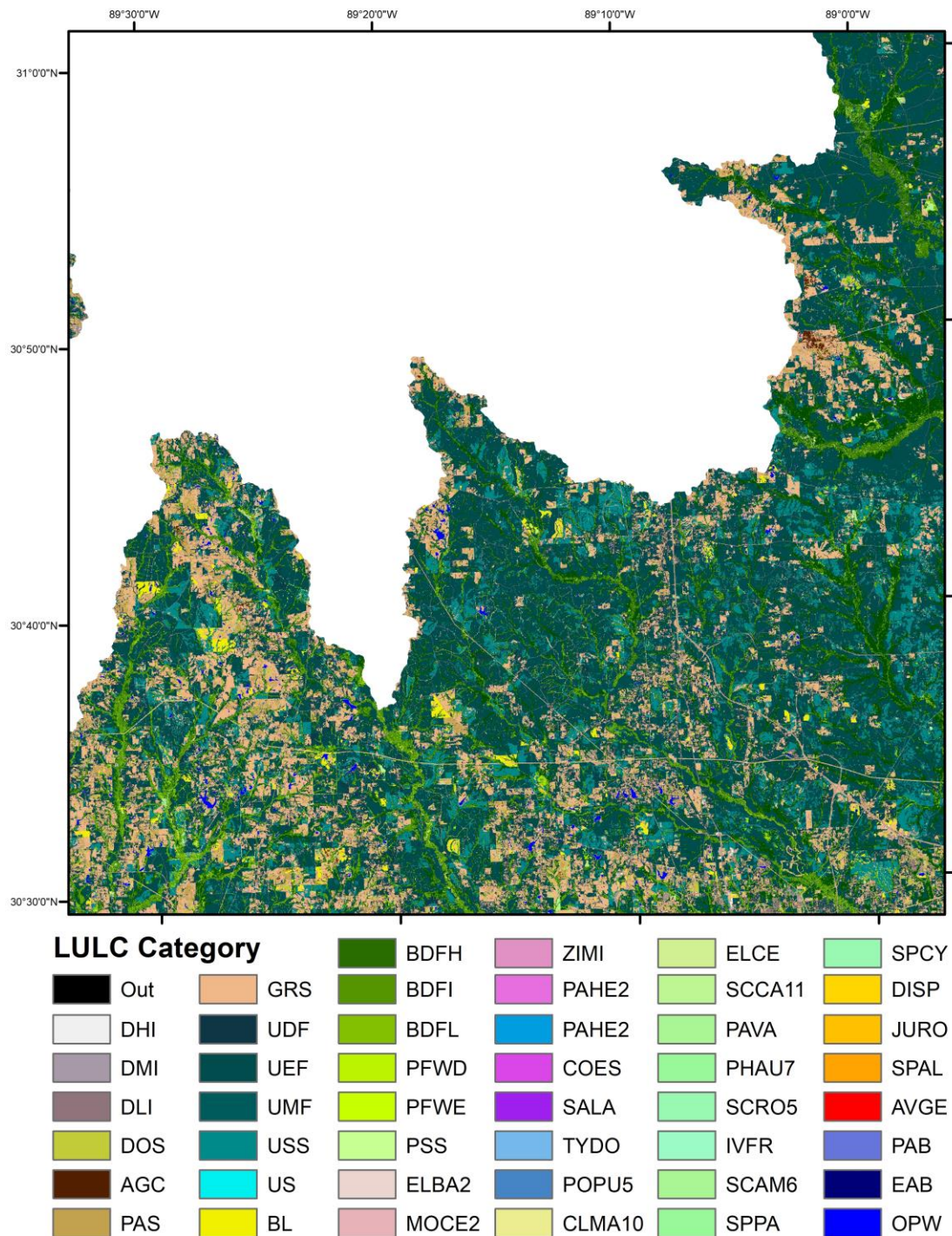


Figure B10. LULC visualization of a 0.5° x 0.5° cell from approximately 30.5°N to 31°N and 89.5°W to 89°W.

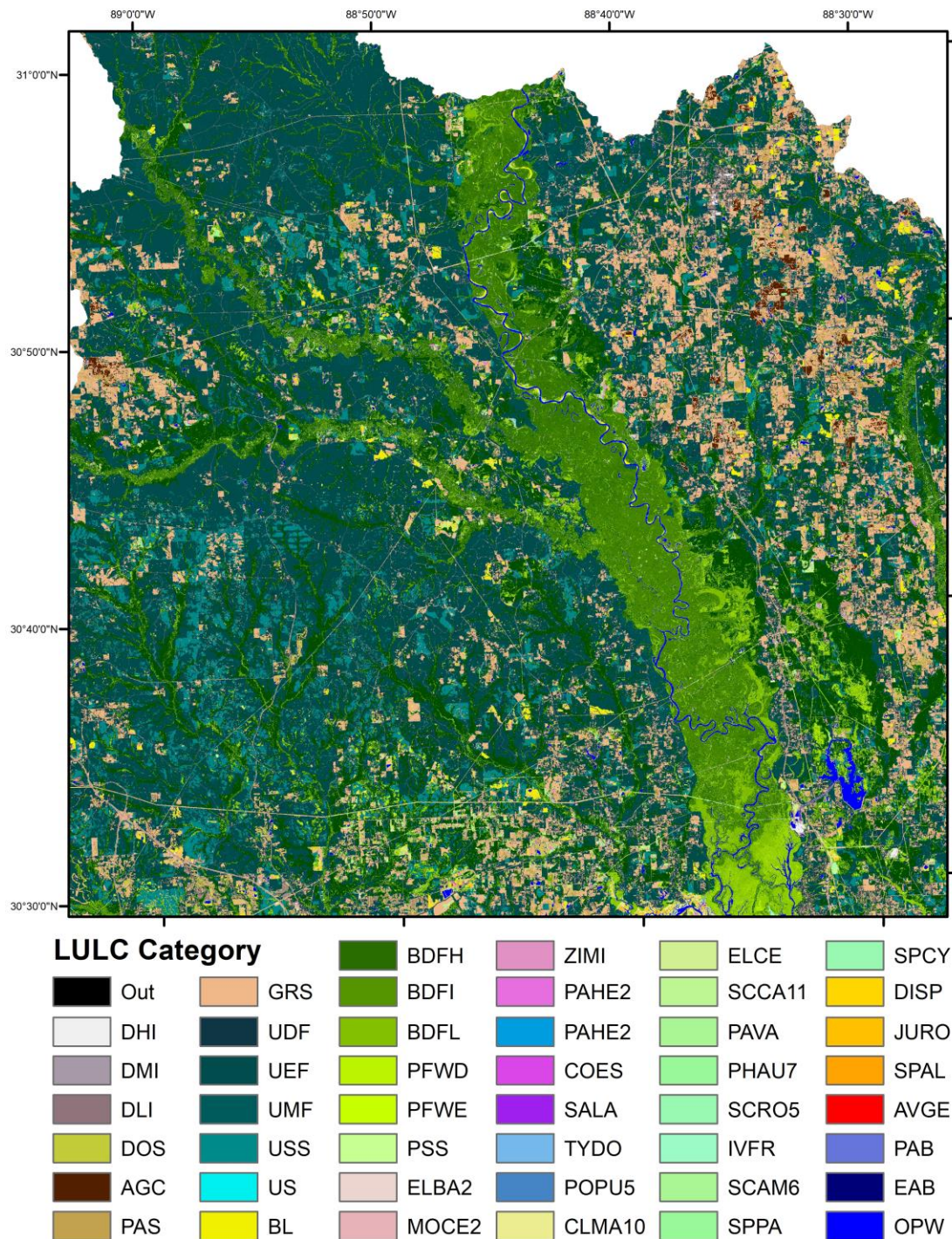


Figure B11. LULC visualization of a 0.5° x 0.5° cell from approximately 30.5°N to 31°N and 89°W to 88.5°W.

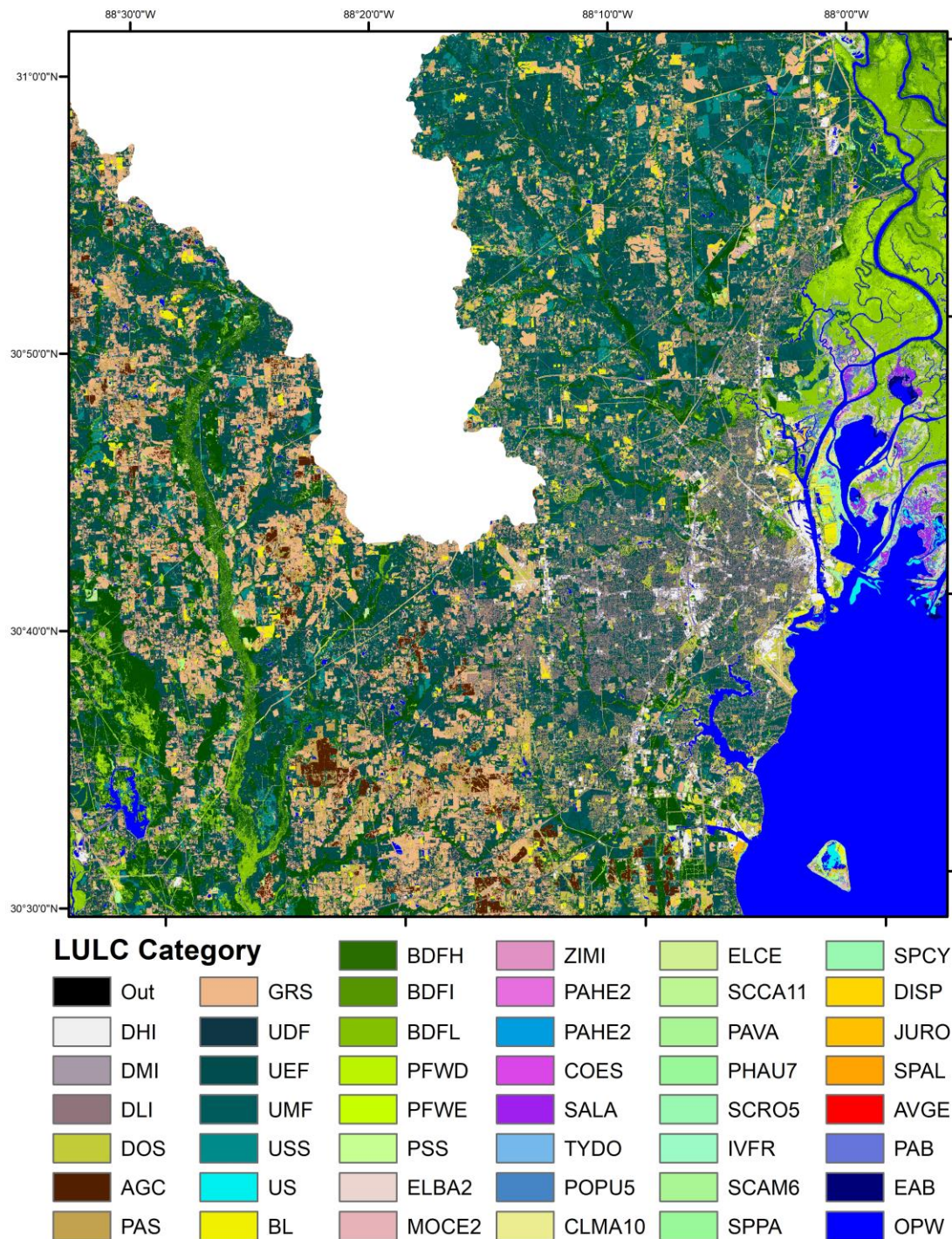


Figure B12. LULC visualization of a 0.5° x 0.5° cell from approximately 30.5°N to 31°N and 88.5°W to 88°W.

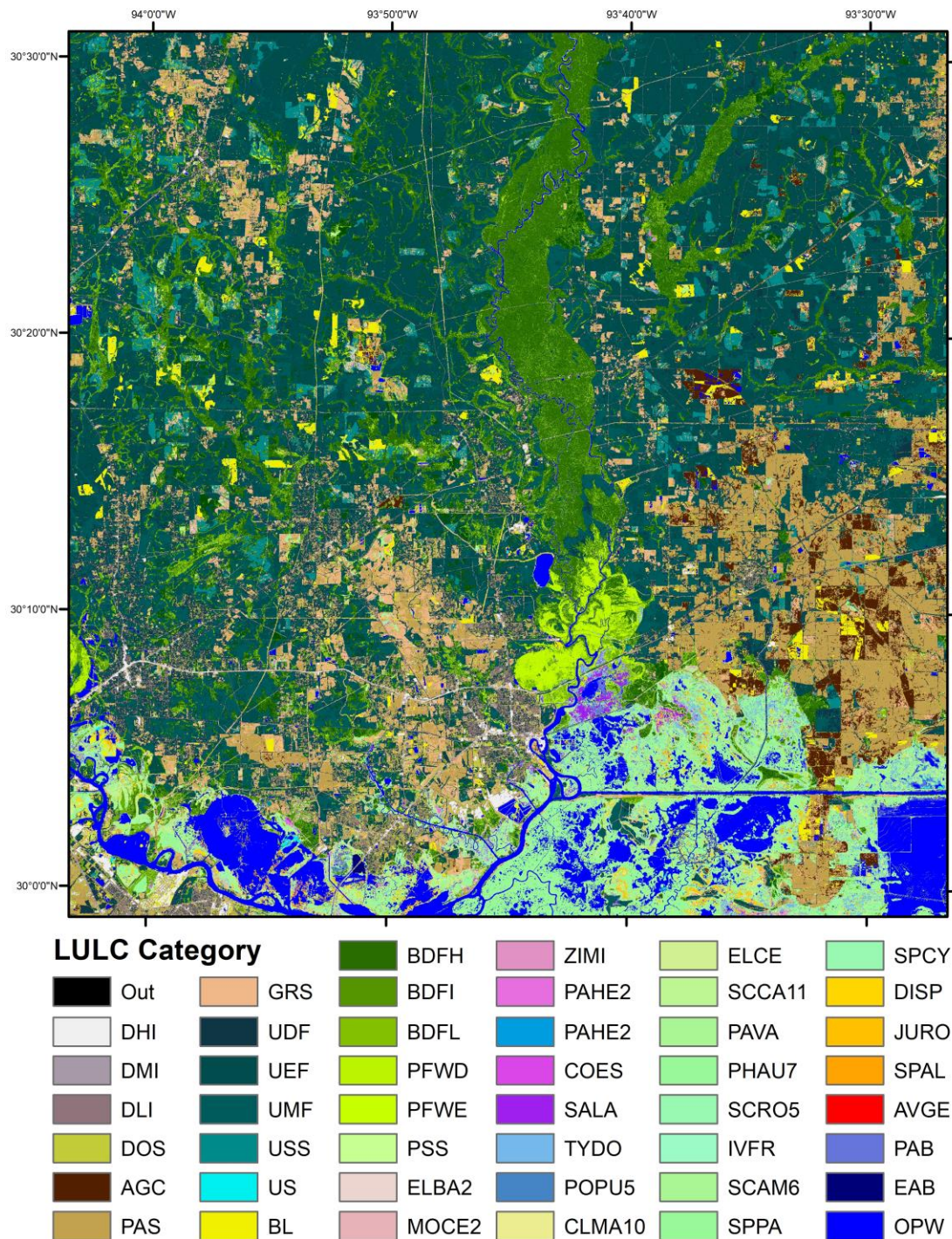


Figure B13. LULC visualization of a 0.5° x 0.5° cell from approximately 30°N to 30.5°N and 94°W to 93.5°W.

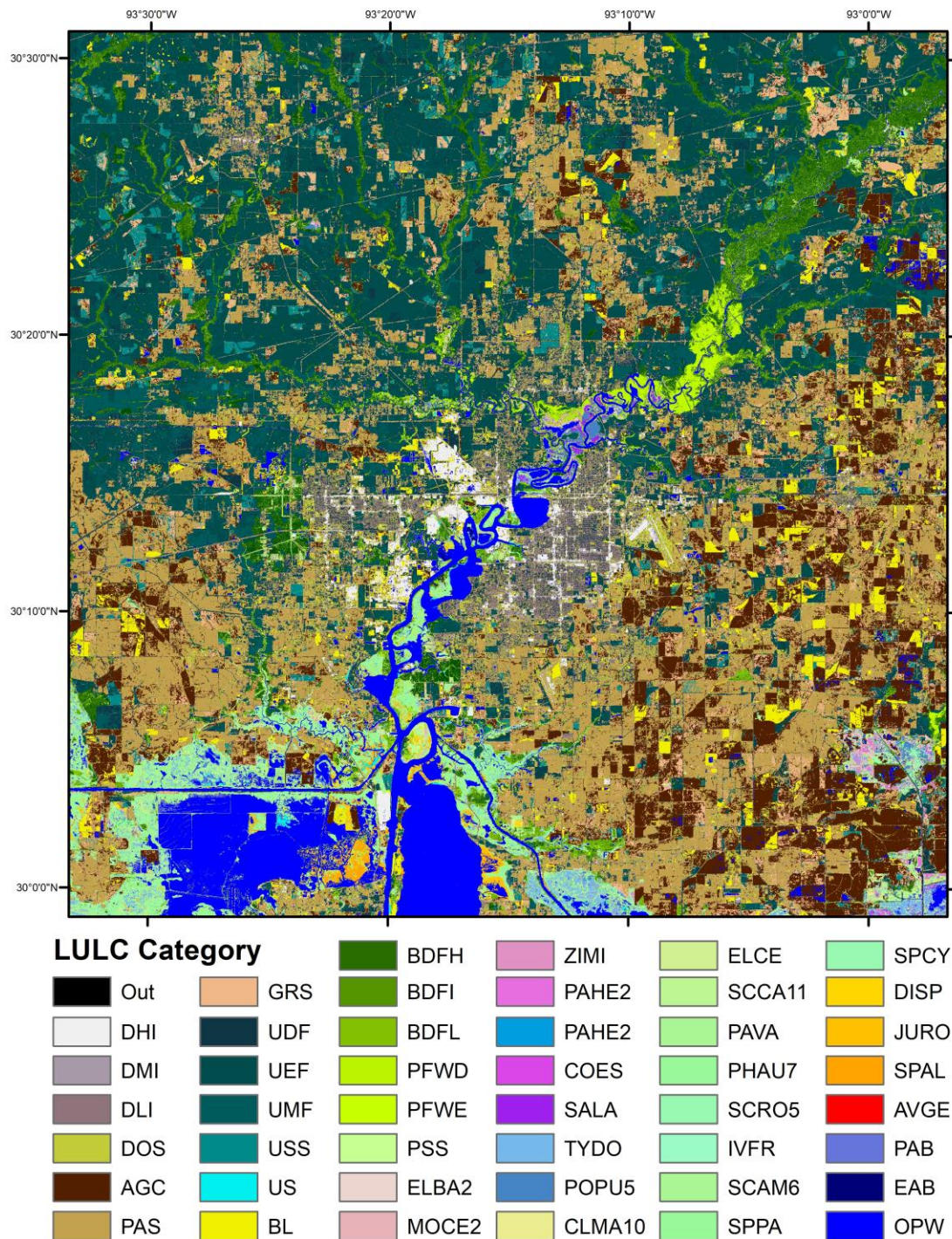


Figure B14. LULC visualization of a 0.5° x 0.5° cell from approximately 30°N to 30.5°N and 93.5°W to 93°W.

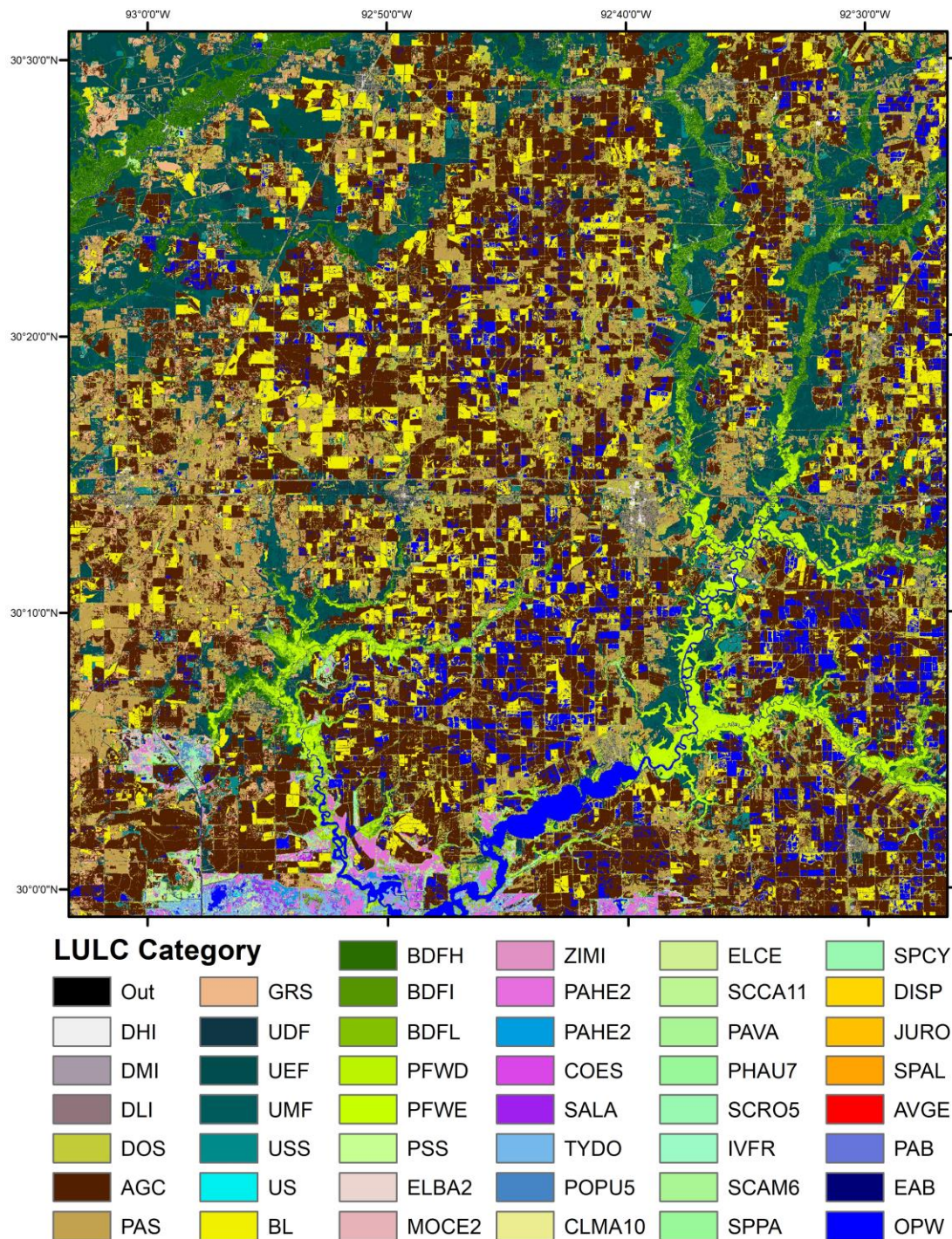


Figure B15. LULC visualization of a 0.5° x 0.5° cell from approximately 30°N to 30.5°N and 93°W to 92.5°W.

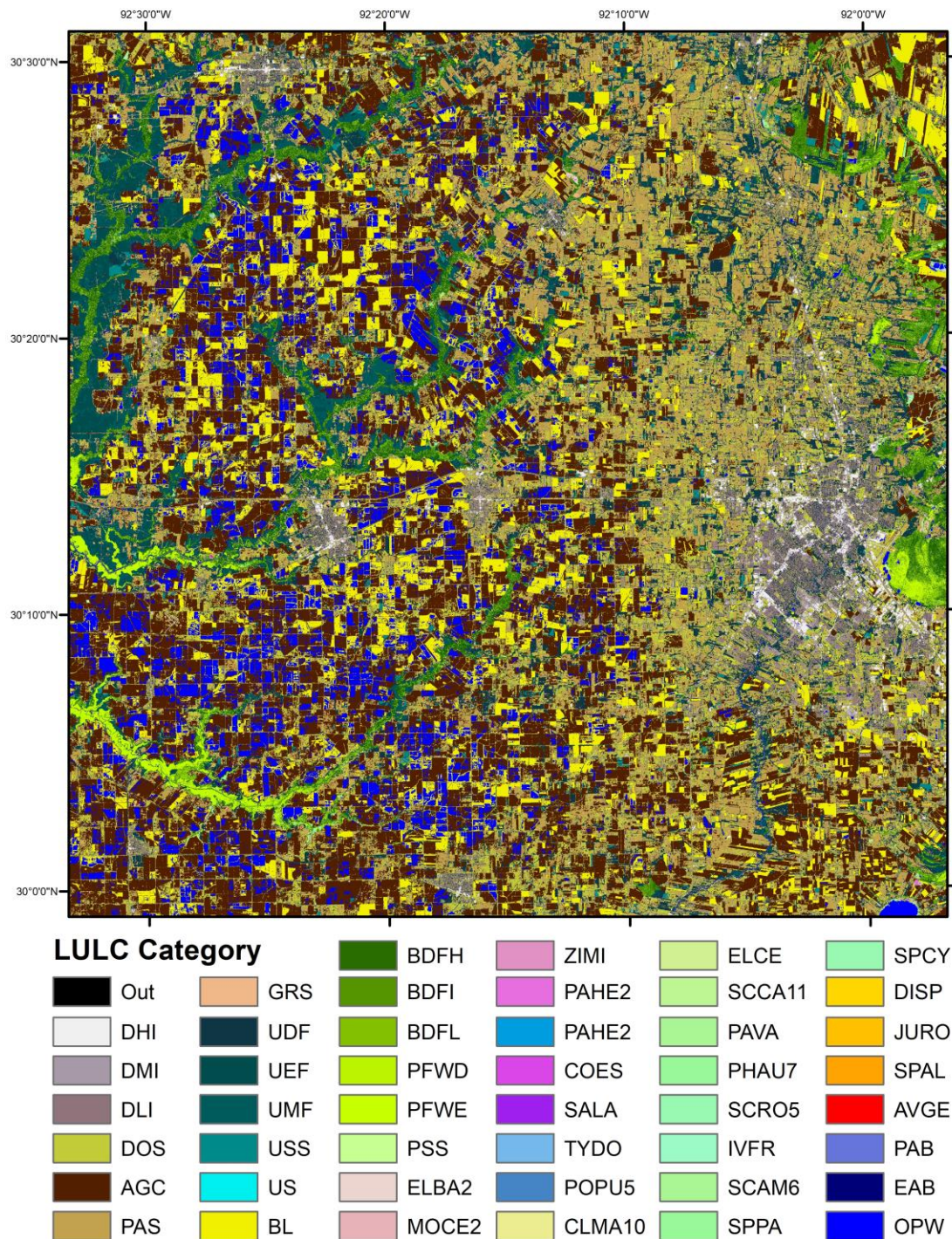


Figure B16. LULC visualization of a 0.5° x 0.5° cell from approximately 30°N to 30.5°N and 92.5°W to 92°W.

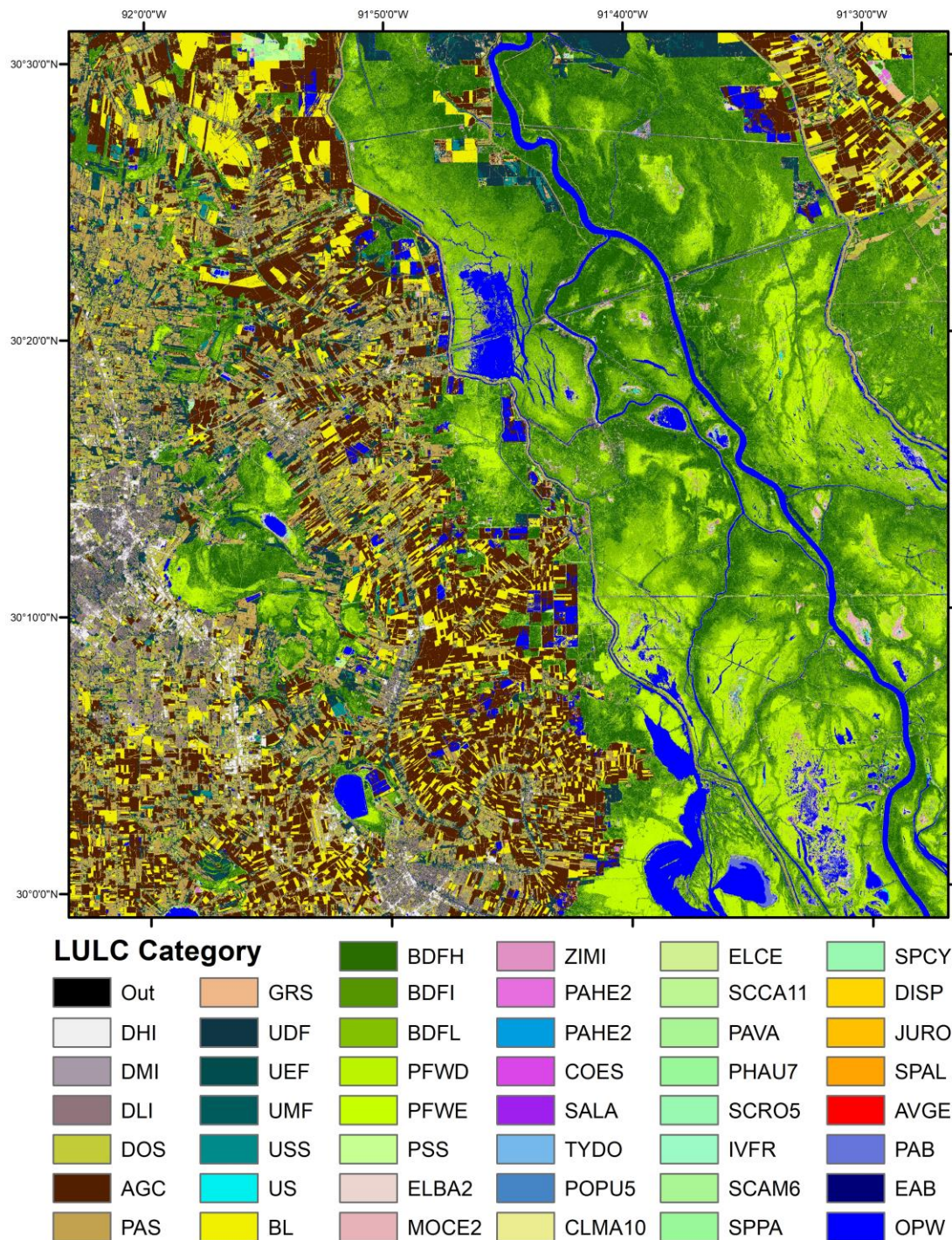


Figure B17. LULC visualization of a 0.5° x 0.5° cell from approximately 30°N to 30.5°N and 92°W to 91.5°W.

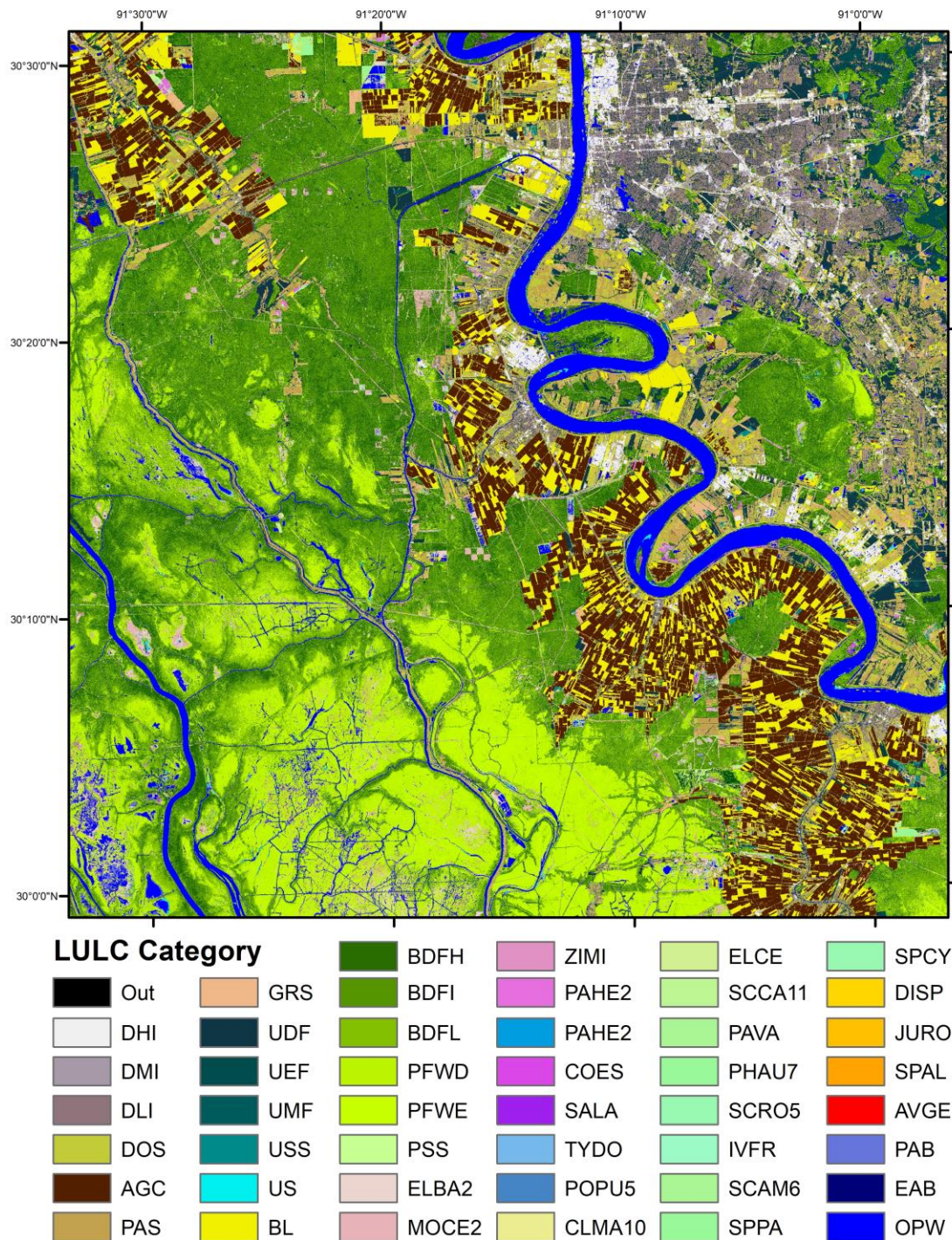


Figure B18. LULC visualization of a 0.5° x 0.5° cell from approximately 30°N to 30.5°N and 91.5°W to 91°W.

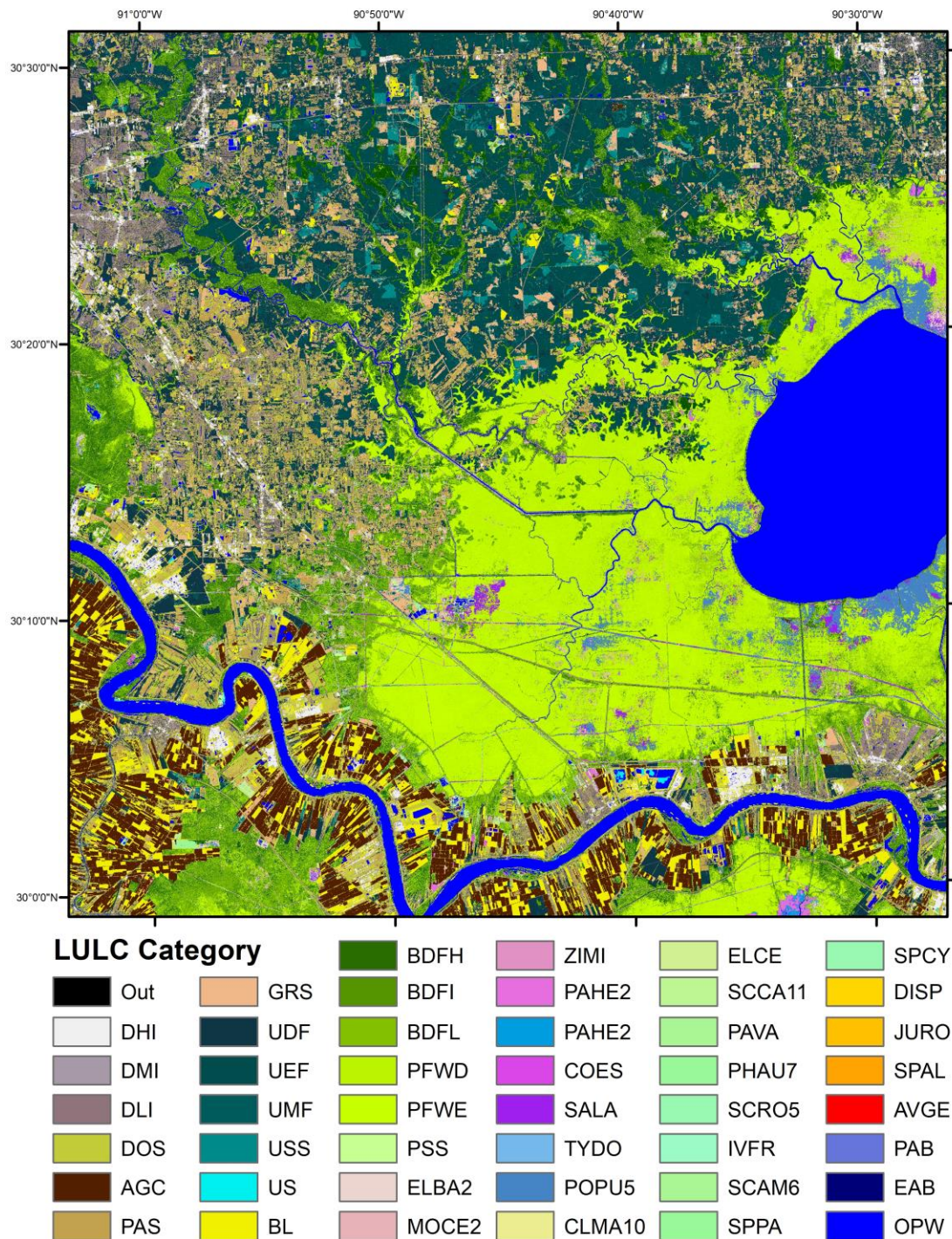


Figure B19. LULC visualization of a 0.5° x 0.5° cell from approximately 30°N to 30.5°N and 91°W to 90.5°W.

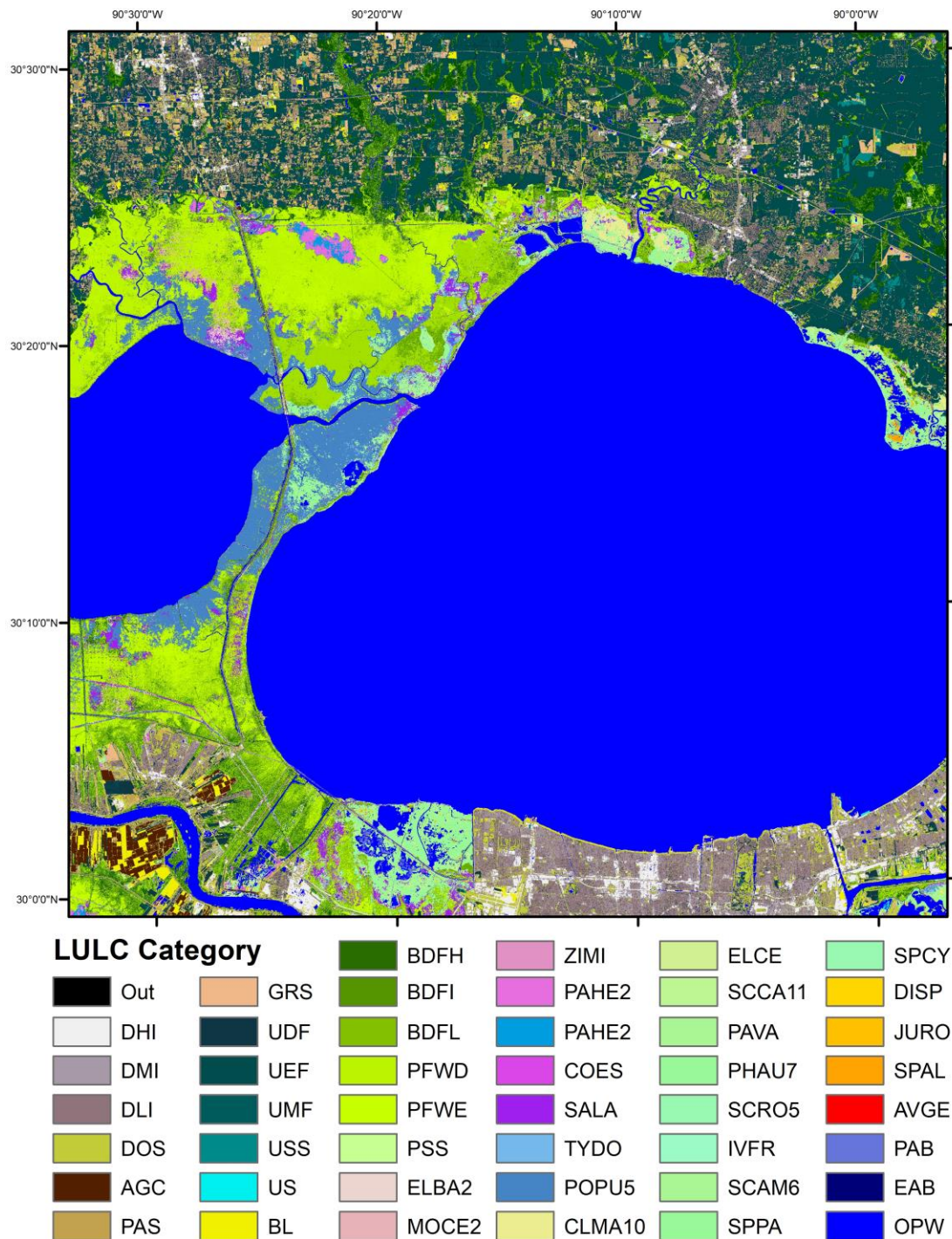


Figure B20. LULC visualization of a 0.5° x 0.5° cell from approximately 30°N to 30.5°N and 90.5°W to 90°W.

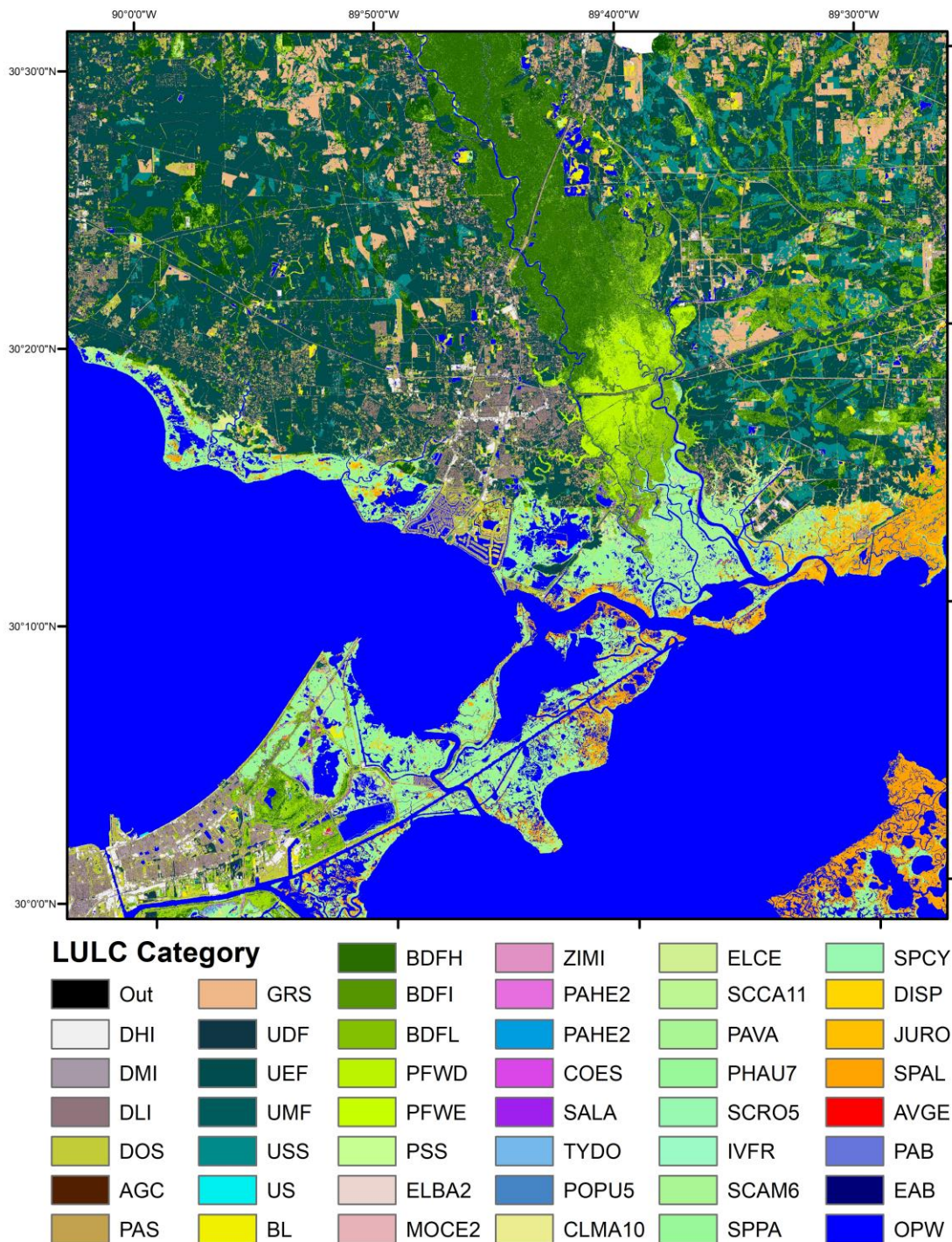


Figure B21. LULC visualization of a 0.5° x 0.5° cell from approximately 30°N to 30.5°N and 90°W to 89.5°W.

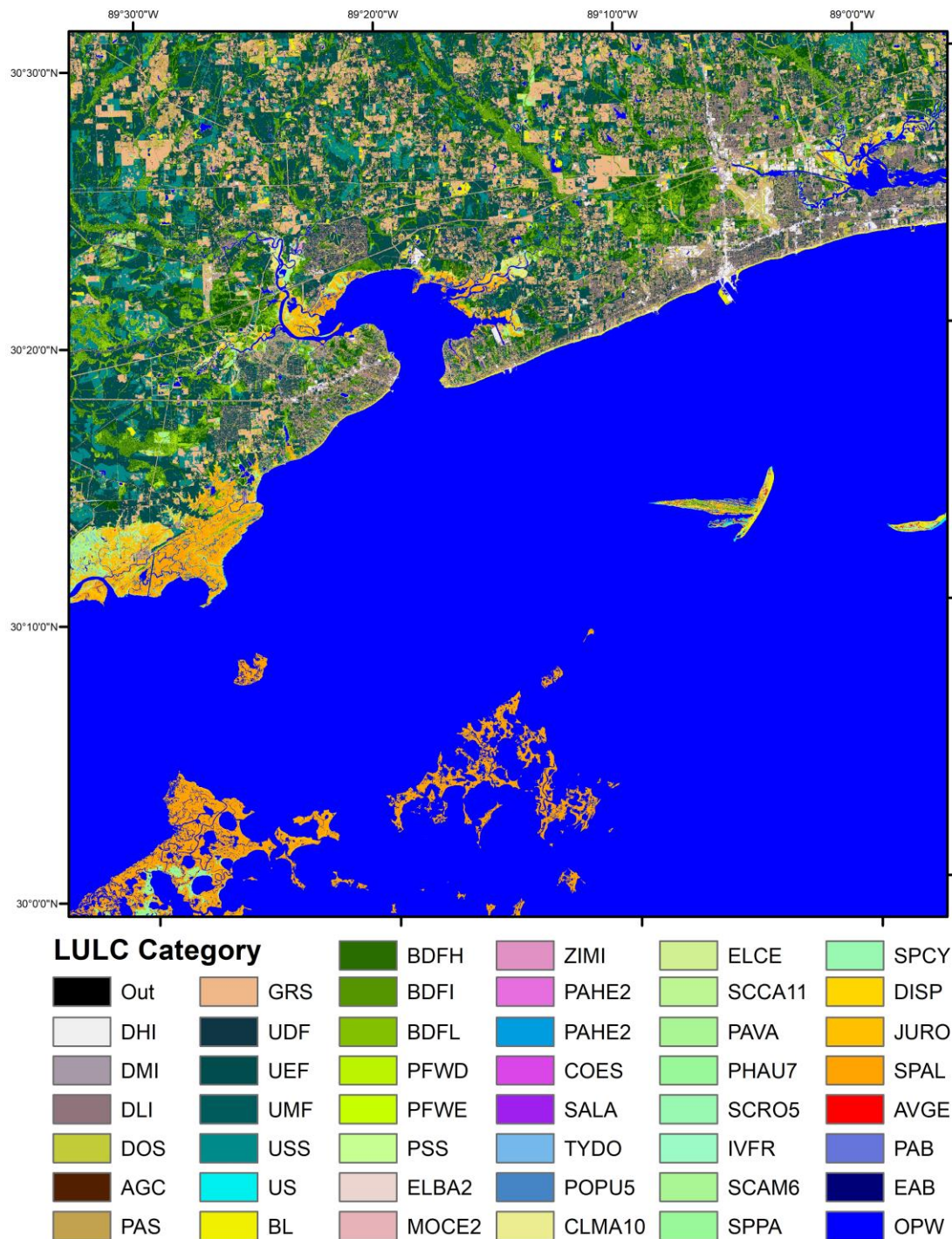


Figure B22. LULC visualization of a 0.5° x 0.5° cell from approximately 30°N to 30.5°N and 89.5°W to 89°W.

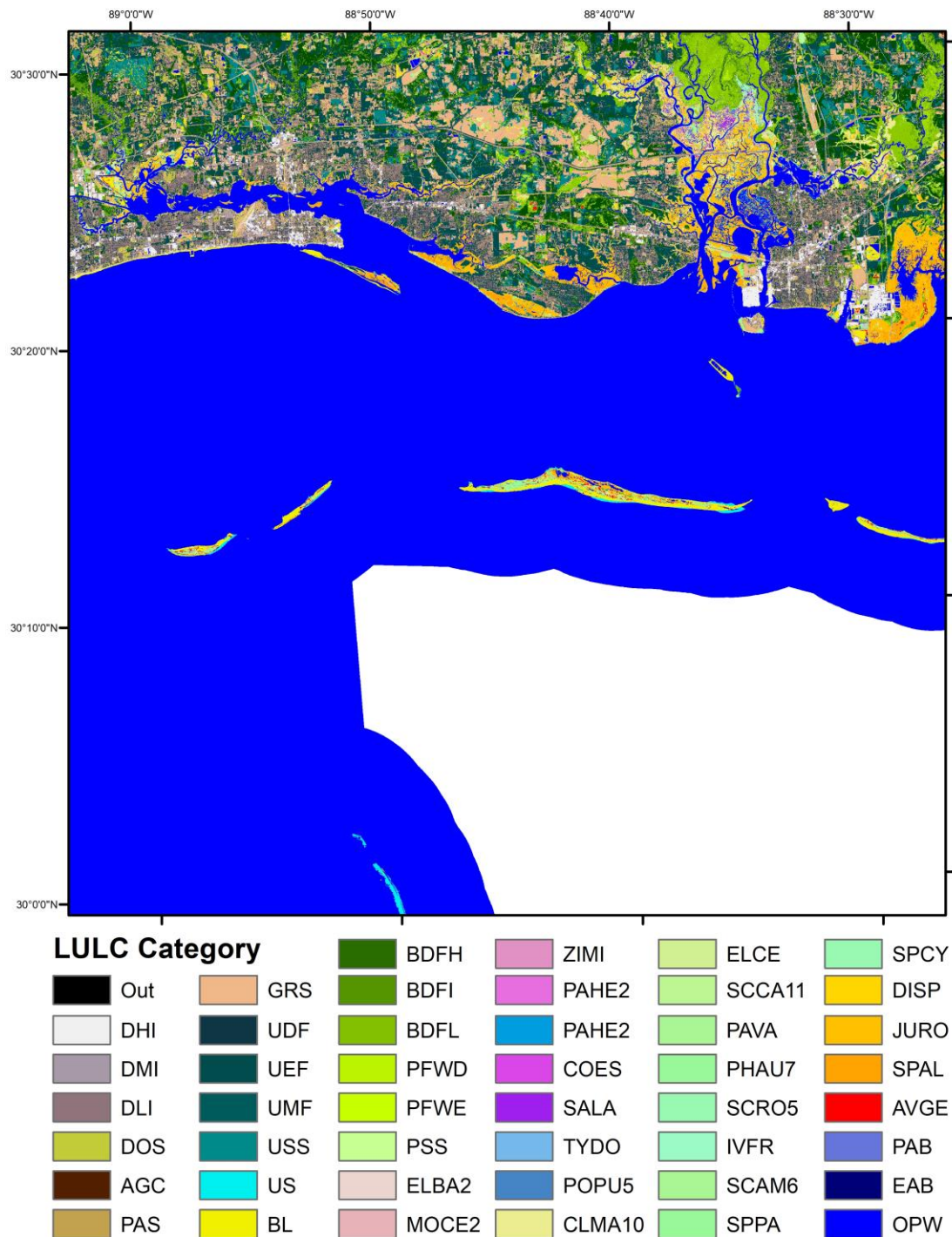


Figure B23. LULC visualization of a 0.5° x 0.5° cell from approximately 30°N to 30.5°N and 89°W to 88.5°W.

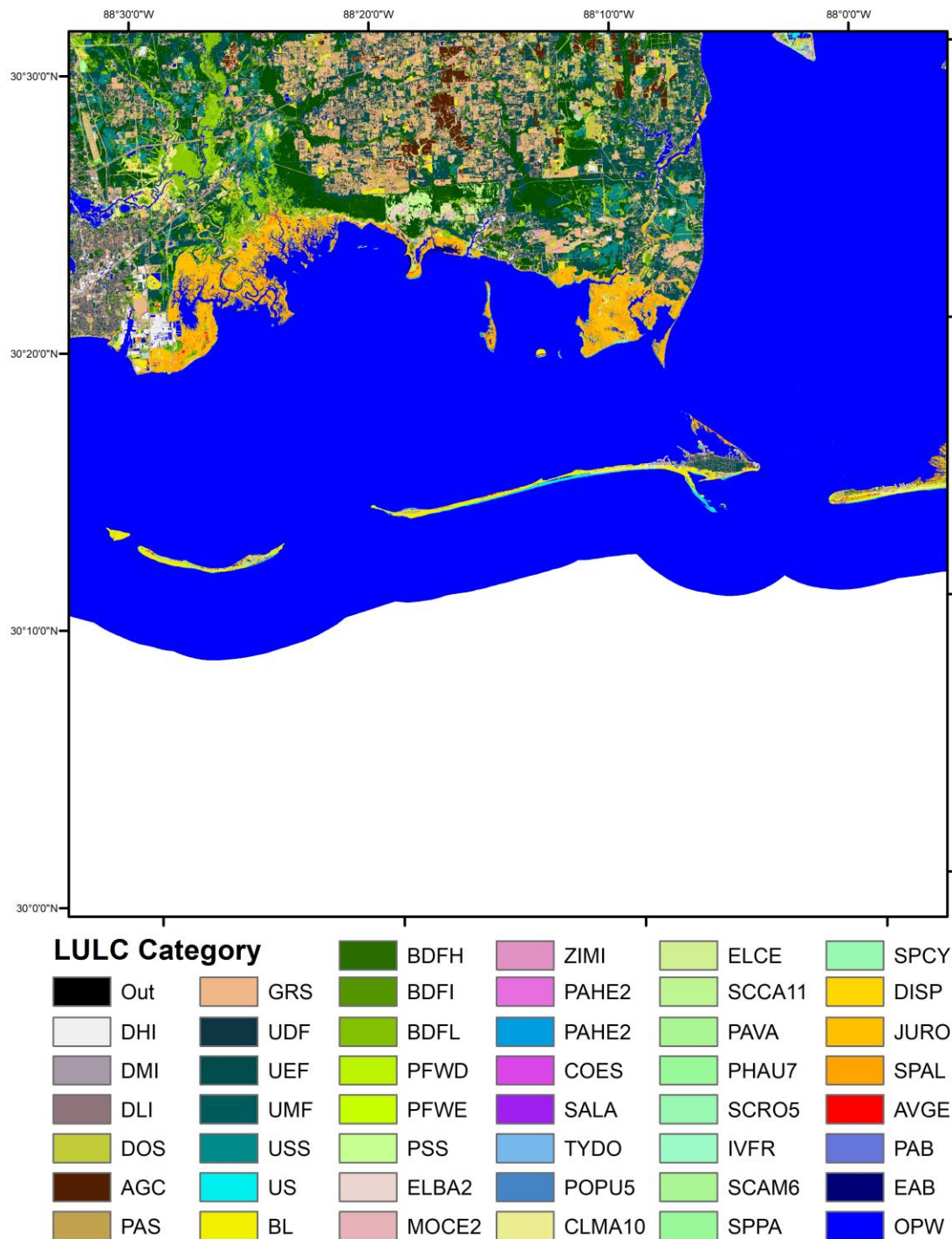


Figure B24. LULC visualization of a 0.5° x 0.5° cell from approximately 30°N to 30.5°N and 88.5°W to 88°W.

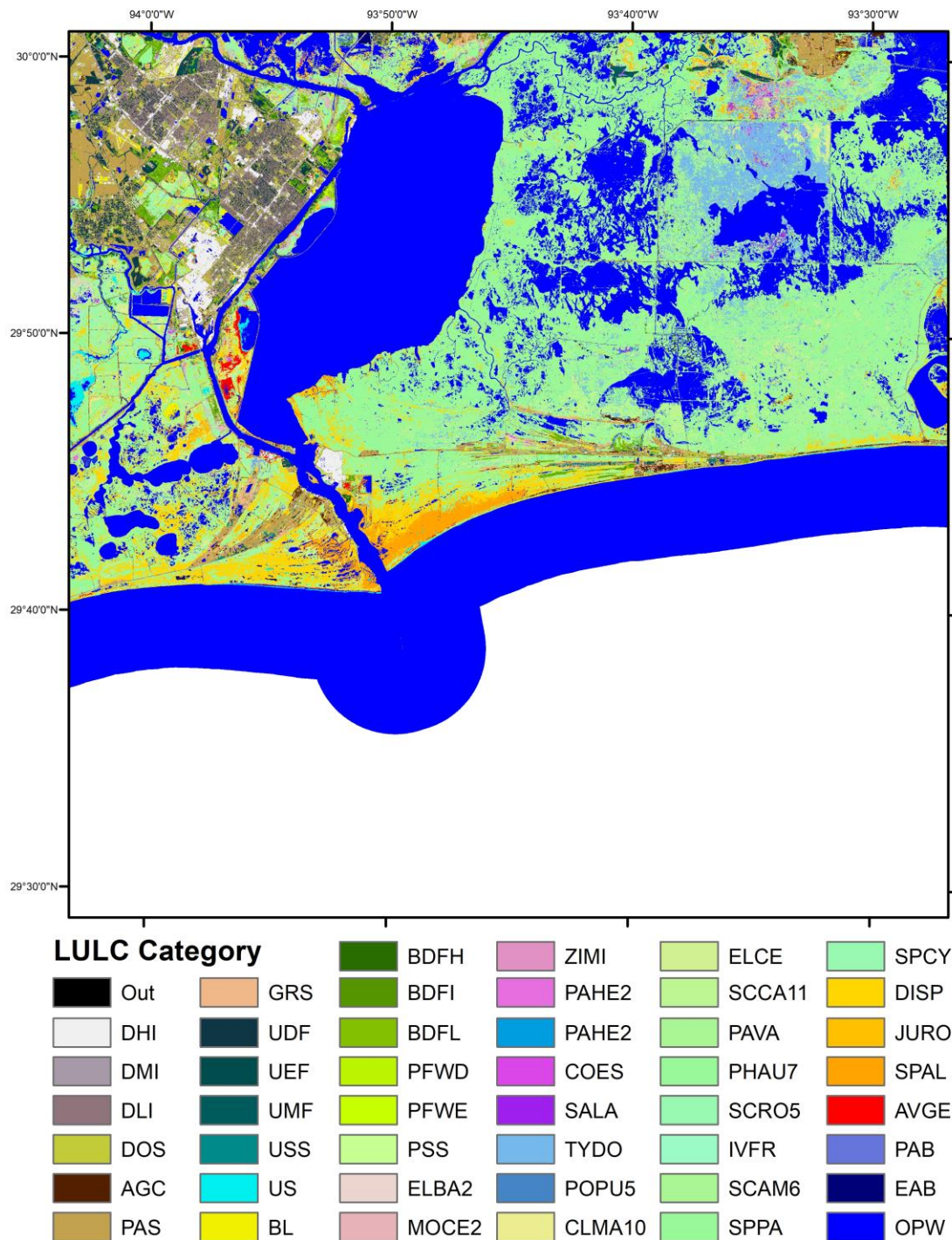


Figure B25. LULC visualization of a 0.5° x 0.5° cell from approximately 29.5°N to 30°N and 94°W to 93.5°W.

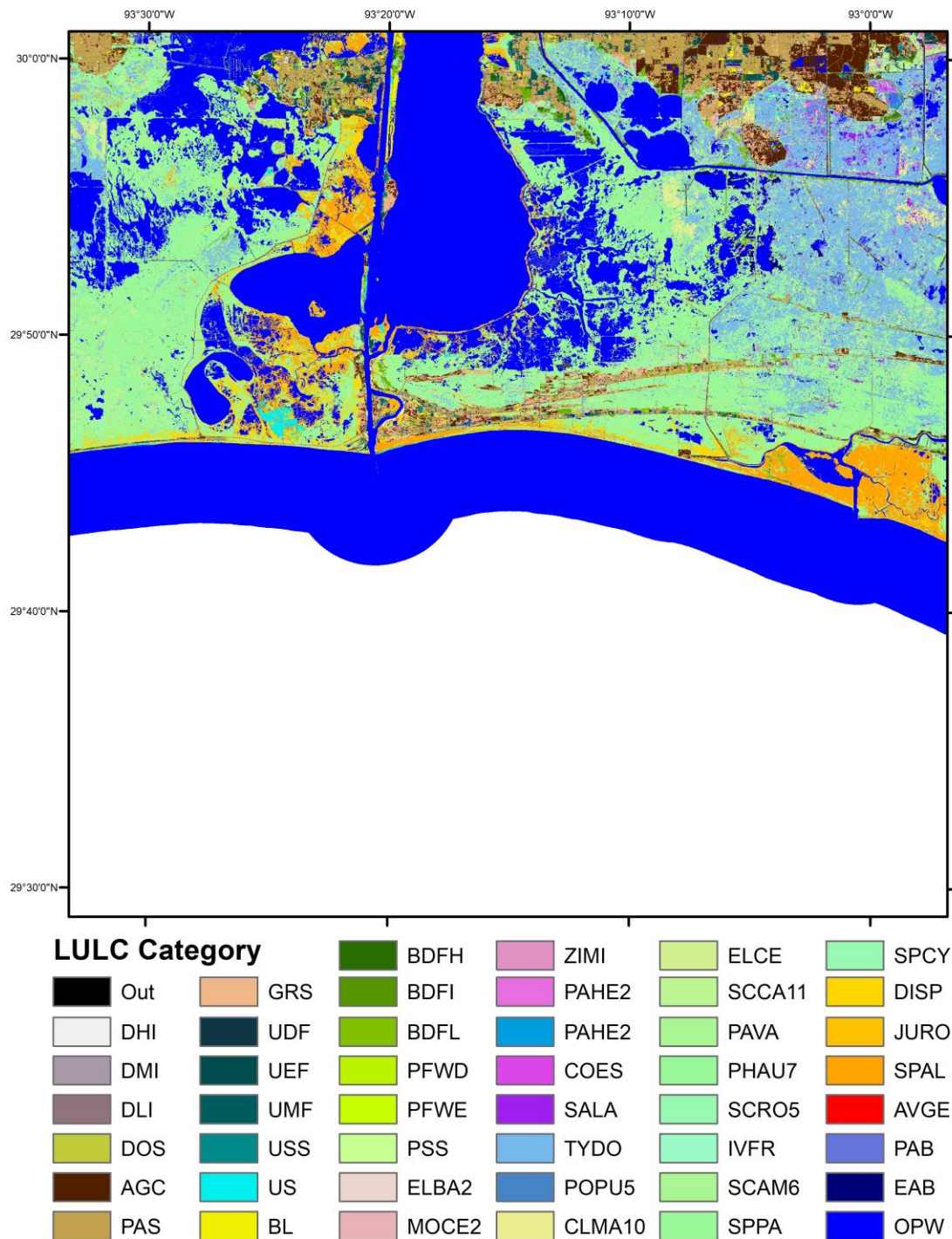


Figure B26. LULC visualization of a 0.5° x 0.5° cell from approximately 29.5°N to 30°N and 93.5°W to 93°W.

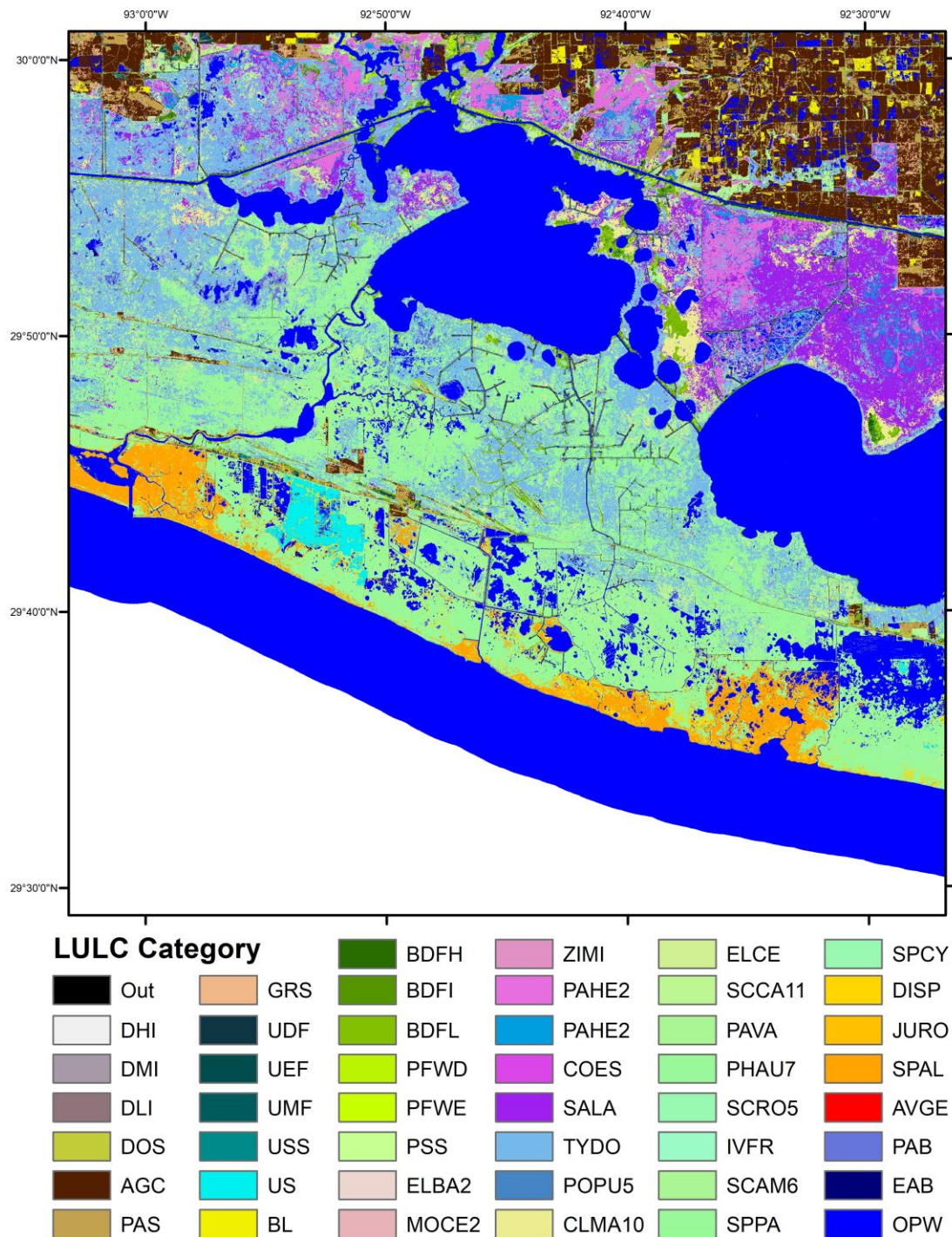


Figure B27. LULC visualization of a 0.5° x 0.5° cell from approximately 29.5°N to 30°N and 93°W to 92.5°W.

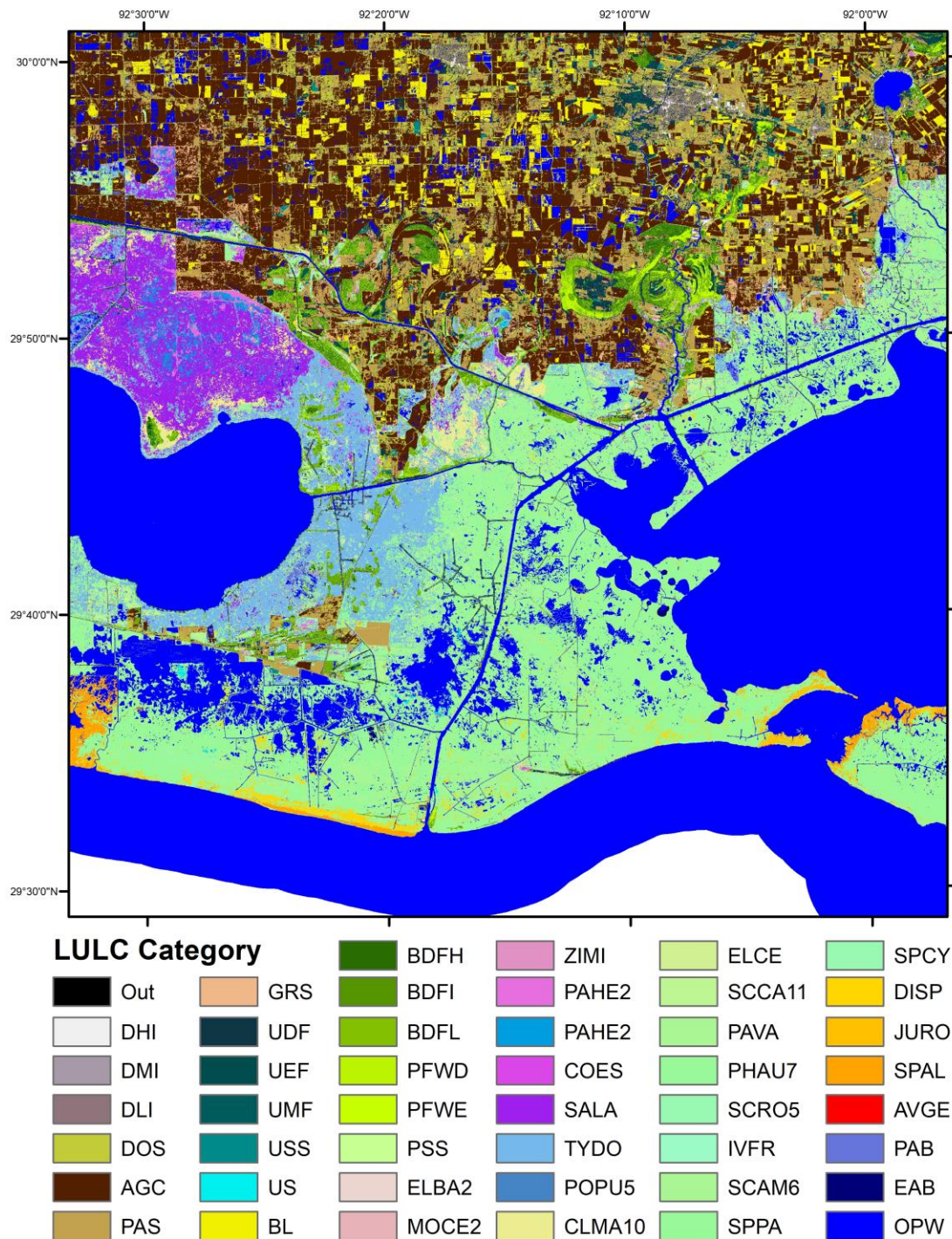


Figure B28. LULC visualization of a 0.5° x 0.5° cell from approximately 29.5°N to 30°N and 92.5°W to 92°W.

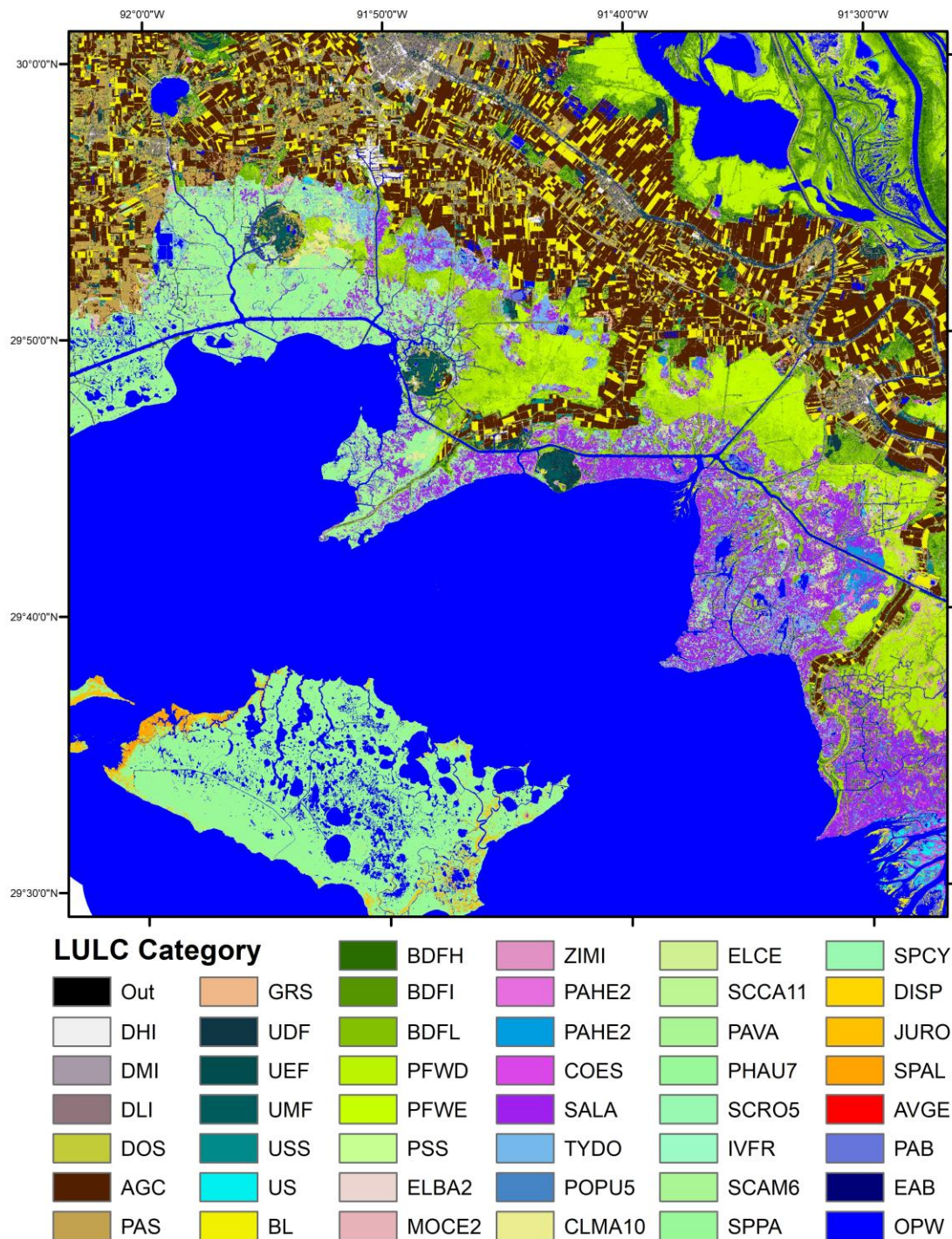


Figure B29. LULC visualization of a 0.5° x 0.5° cell from approximately 29.5°N to 30°N and 92°W to 91.5°W.

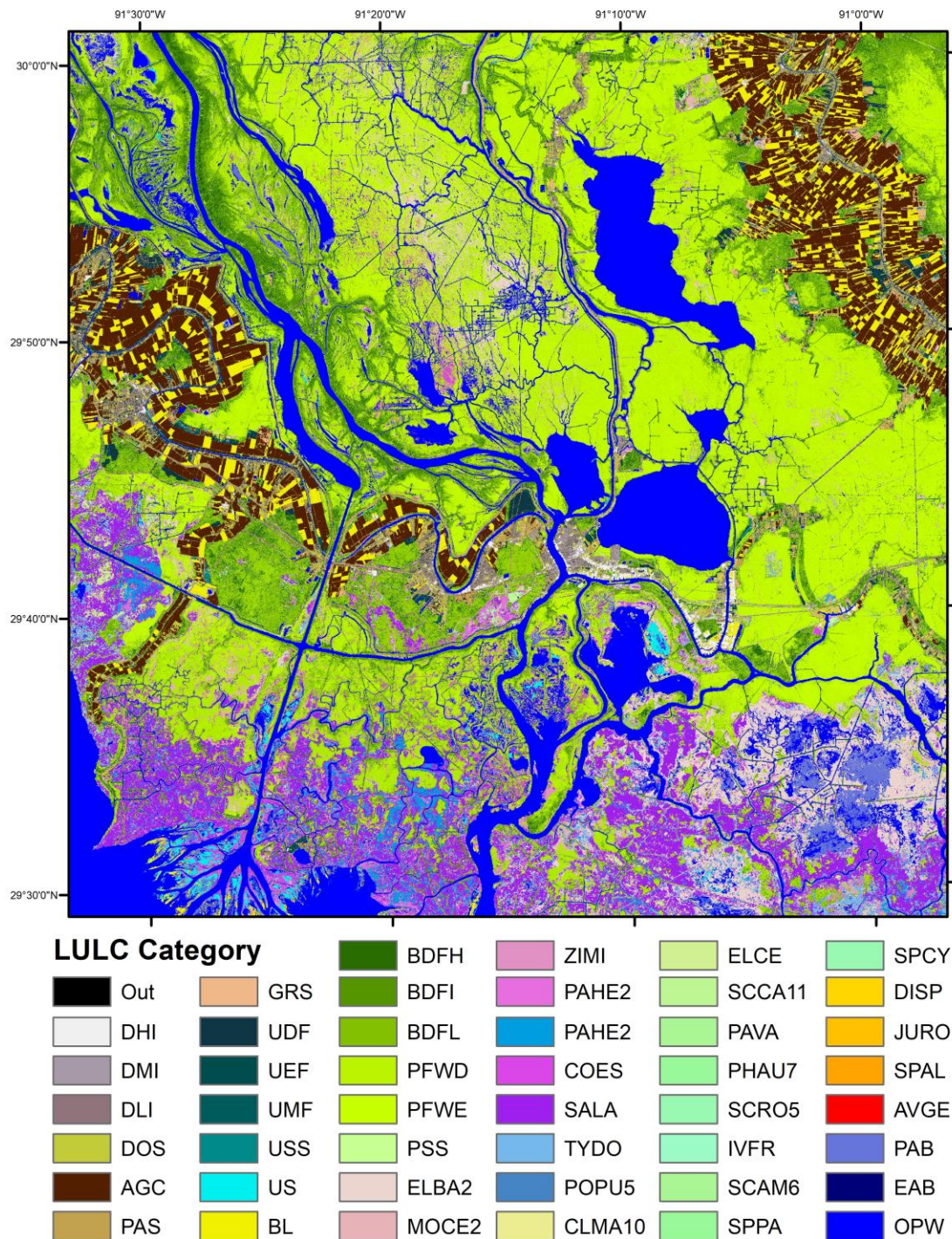


Figure B30. LULC visualization of a 0.5° x 0.5° cell from approximately 29.5°N to 30°N and 91.5°W to 91°W.

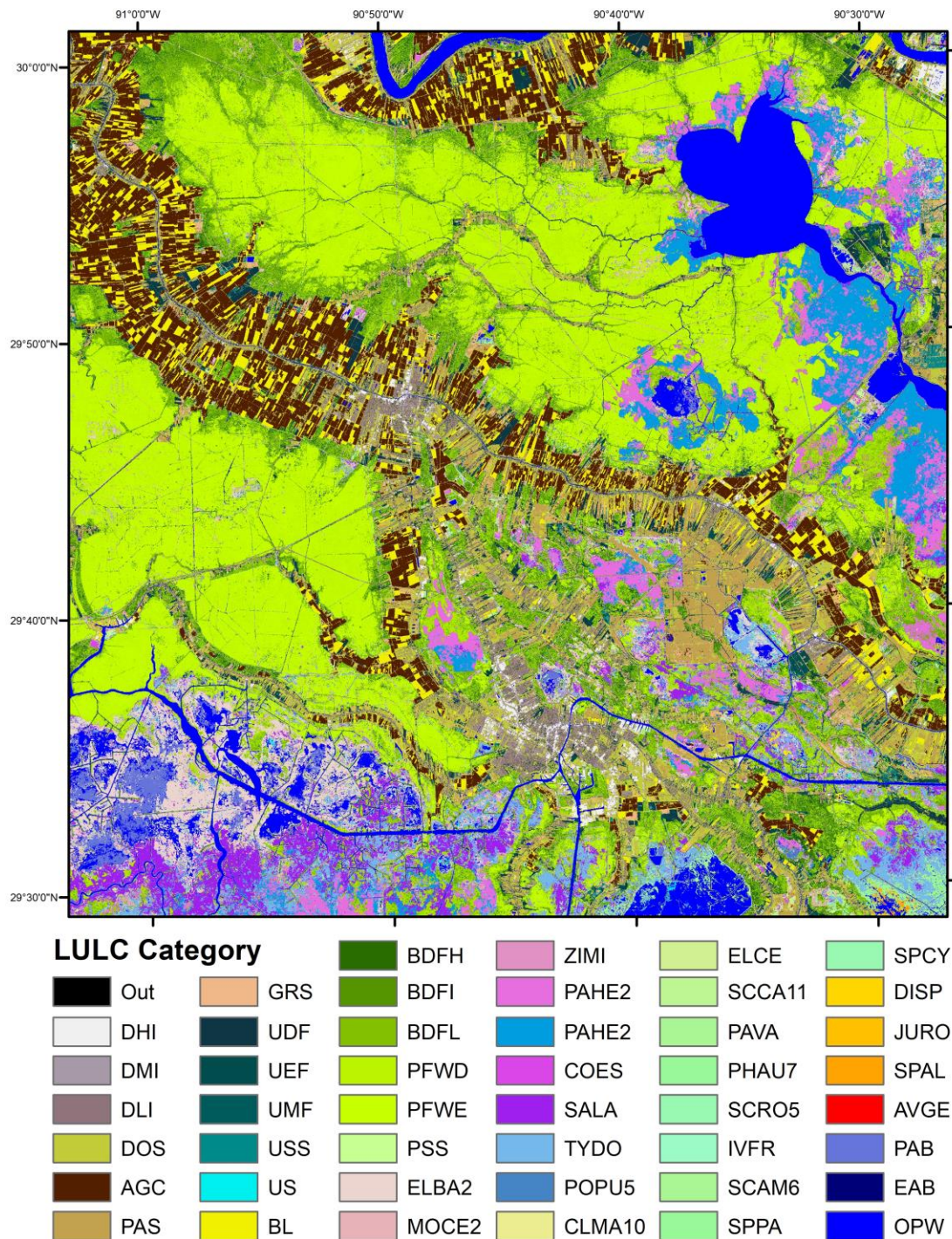


Figure B31. LULC visualization of a 0.5° x 0.5° cell from approximately 29.5°N to 30°N and 91°W to 90.5°W.

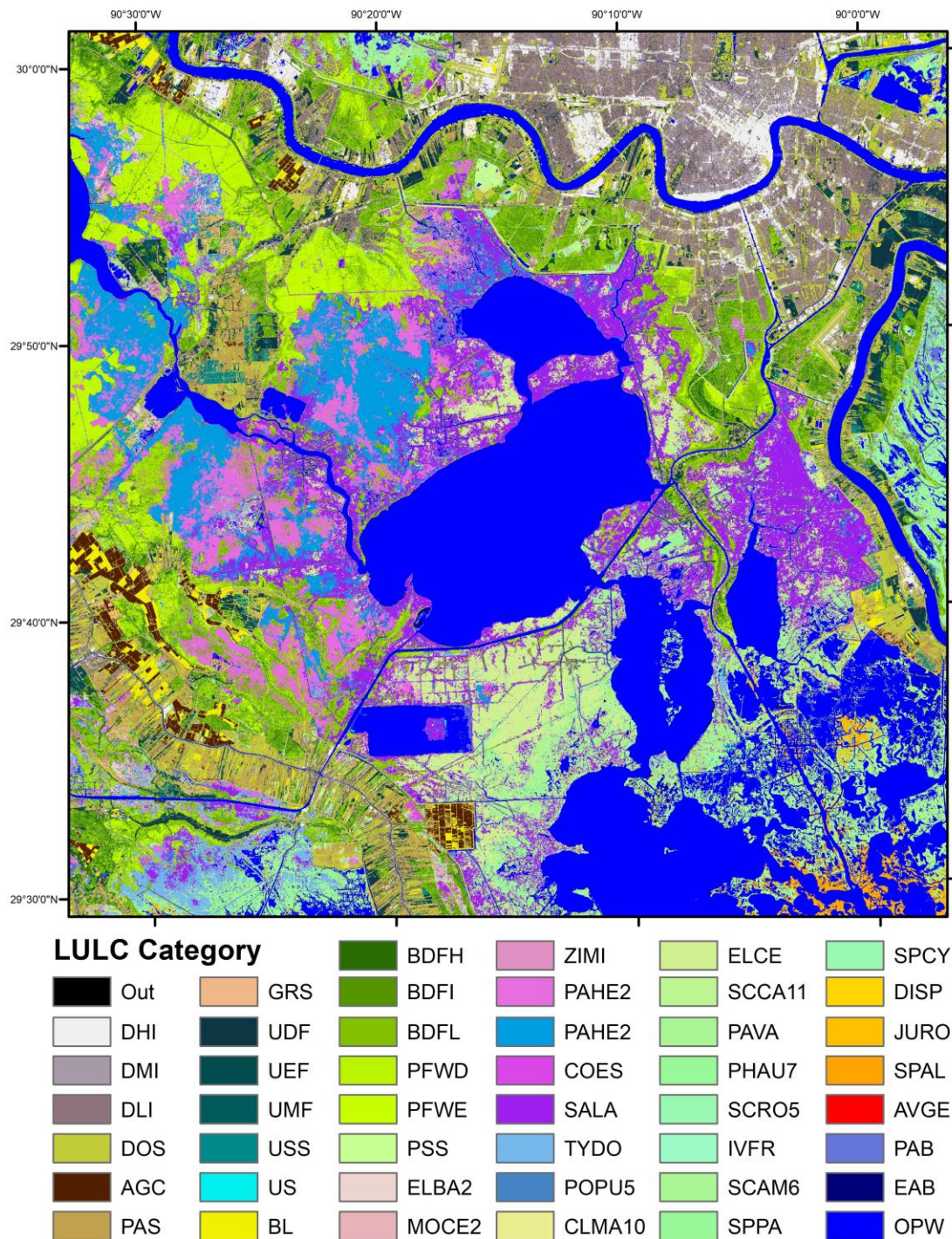


Figure B32. LULC visualization of a 0.5° x 0.5° cell from approximately 29.5°N to 30°N and 90.5°W to 90°W.

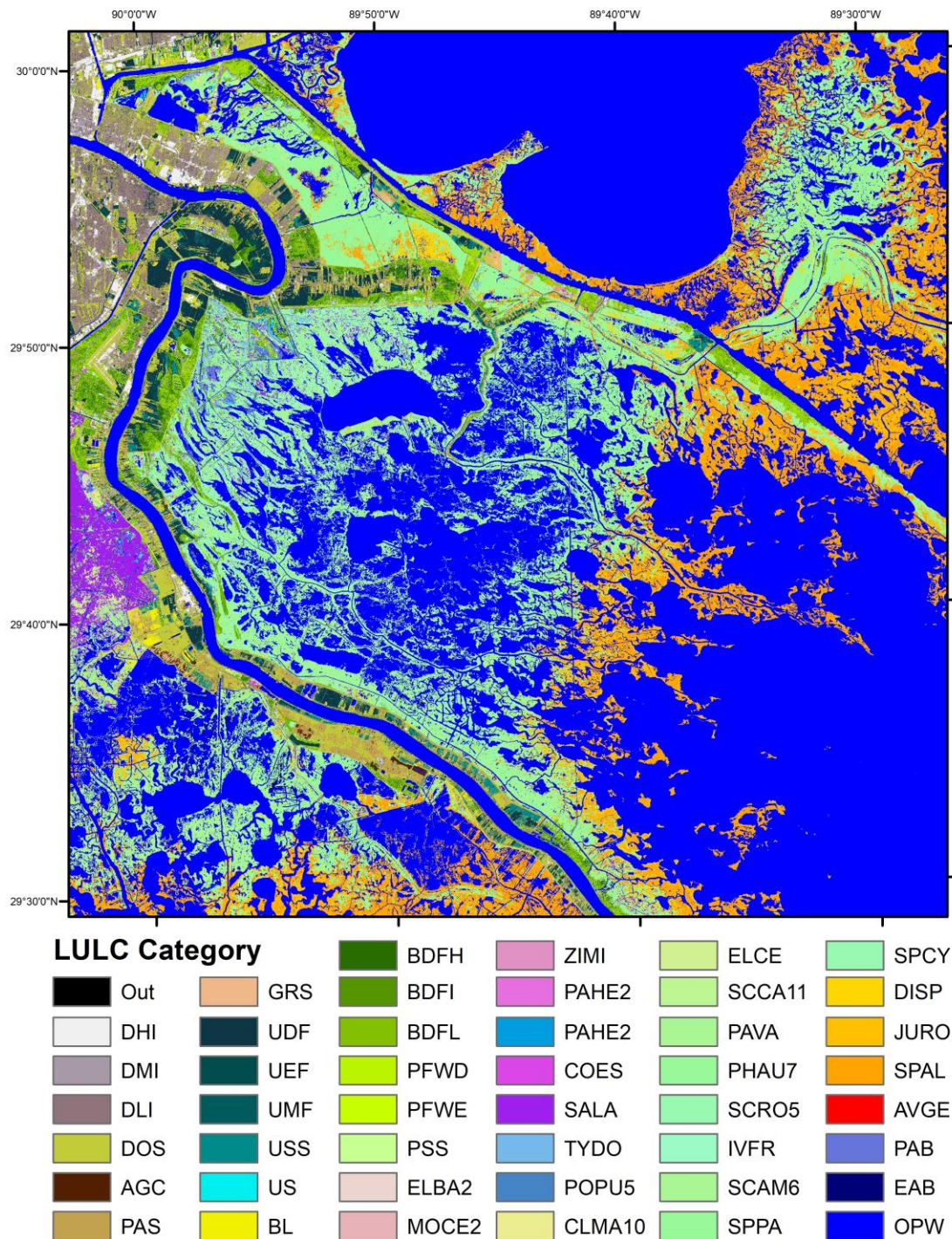


Figure B33. LULC visualization of a 0.5° x 0.5° cell from approximately 29.5°N to 30°N and 90°W to 89.5°W.

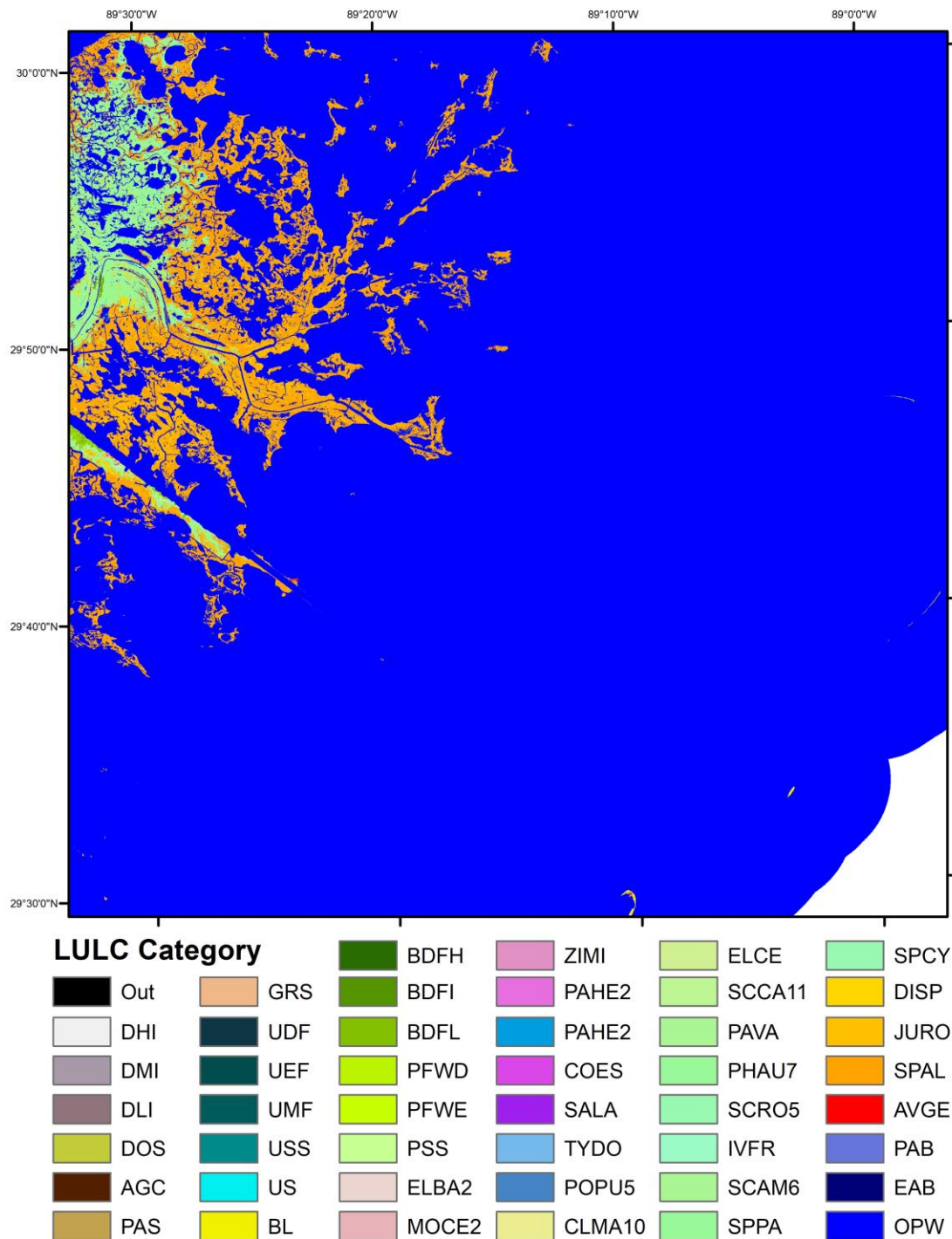


Figure B34. LULC visualization of a 0.5° x 0.5° cell from approximately 29.5°N to 30°N and 89.5°W to 89°W.

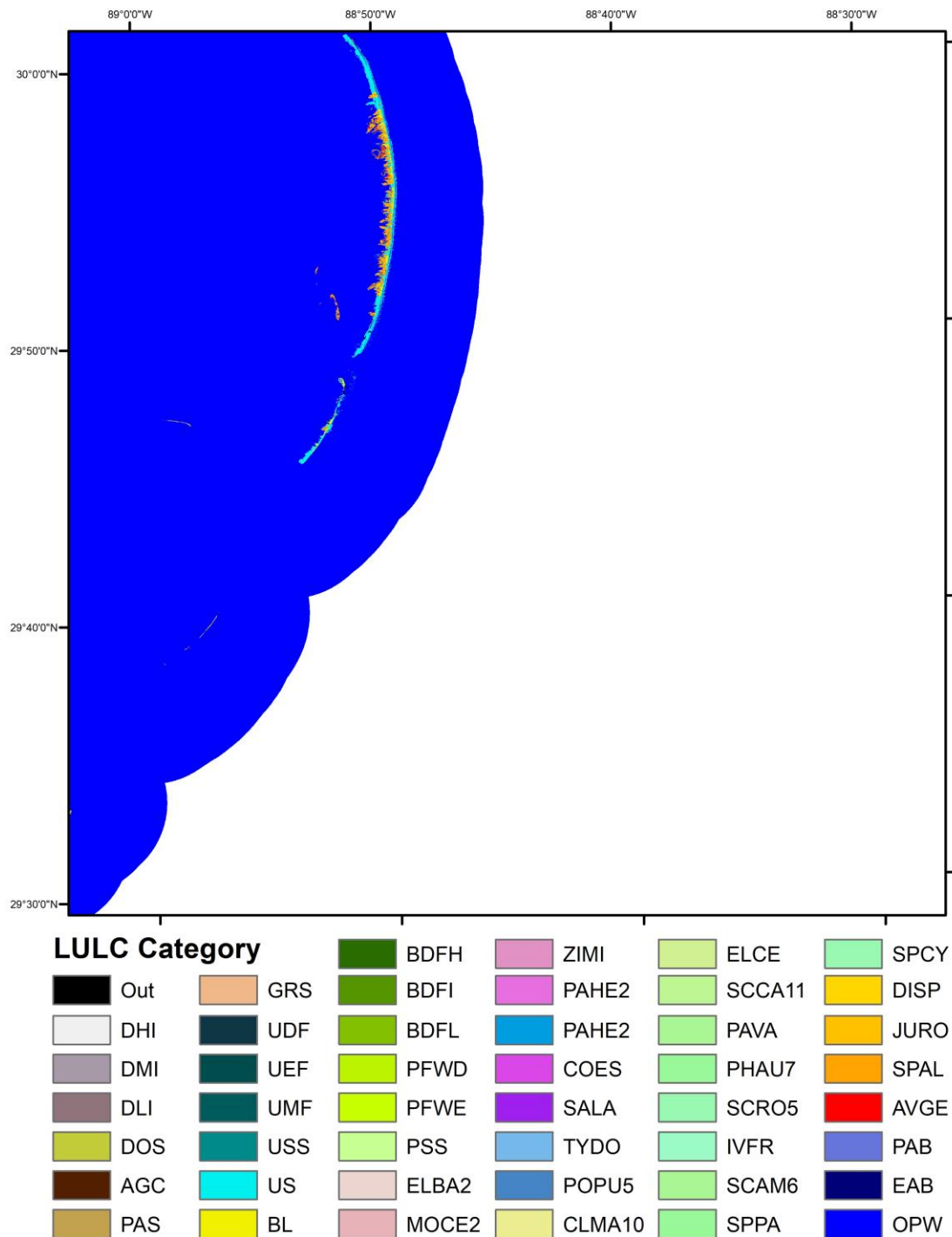


Figure B35. LULC visualization of a 0.5° x 0.5° cell from approximately 29.5°N to 30°N and 89°W to 88.5°W.

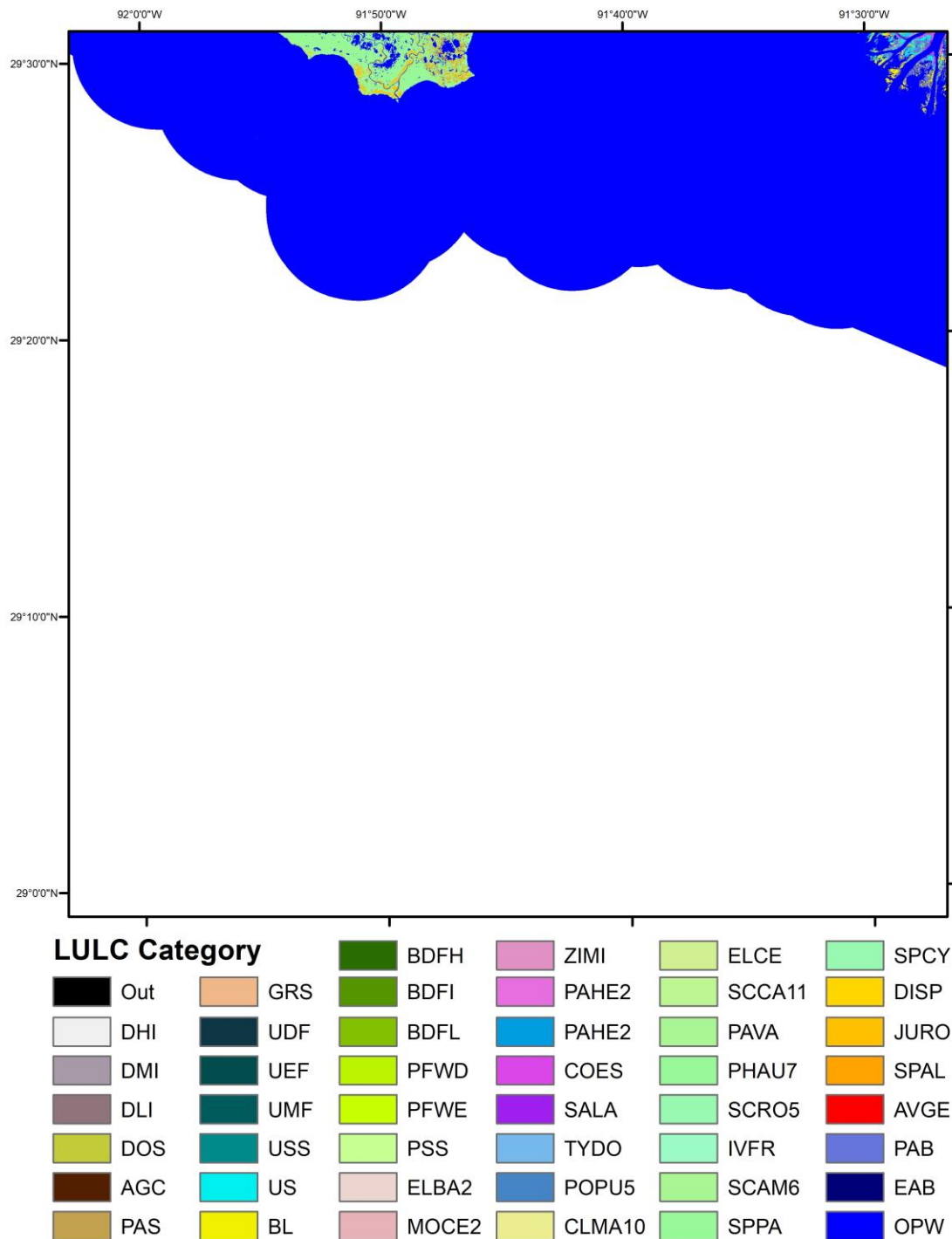


Figure B36. LULC visualization of a 0.5° x 0.5° cell from approximately 29°N to 29.5°N and 92°W to 91.5°W.

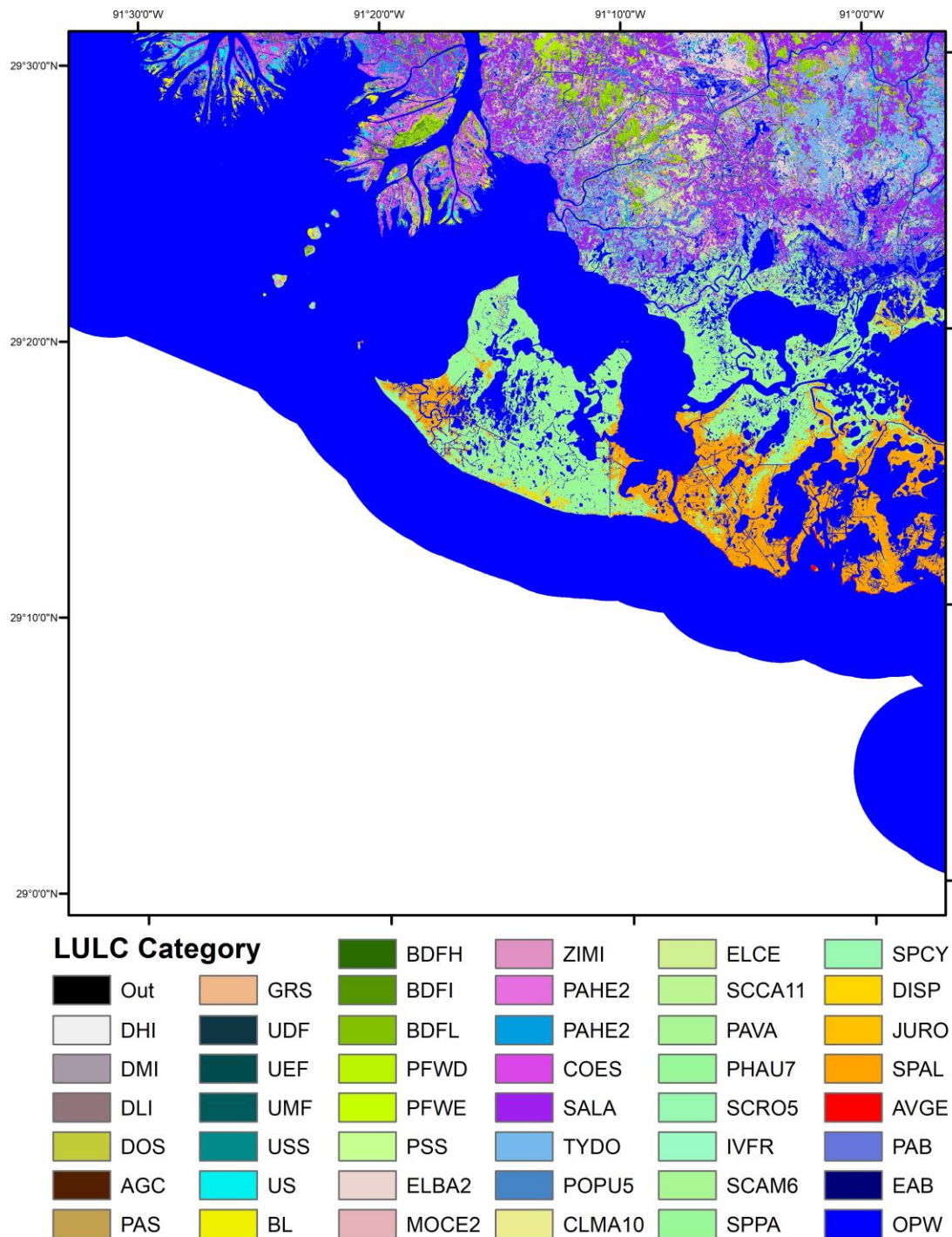


Figure B37. LULC visualization of a 0.5° x 0.5° cell from approximately 29°N to 29.5°N and 91.5°W to 91°W.

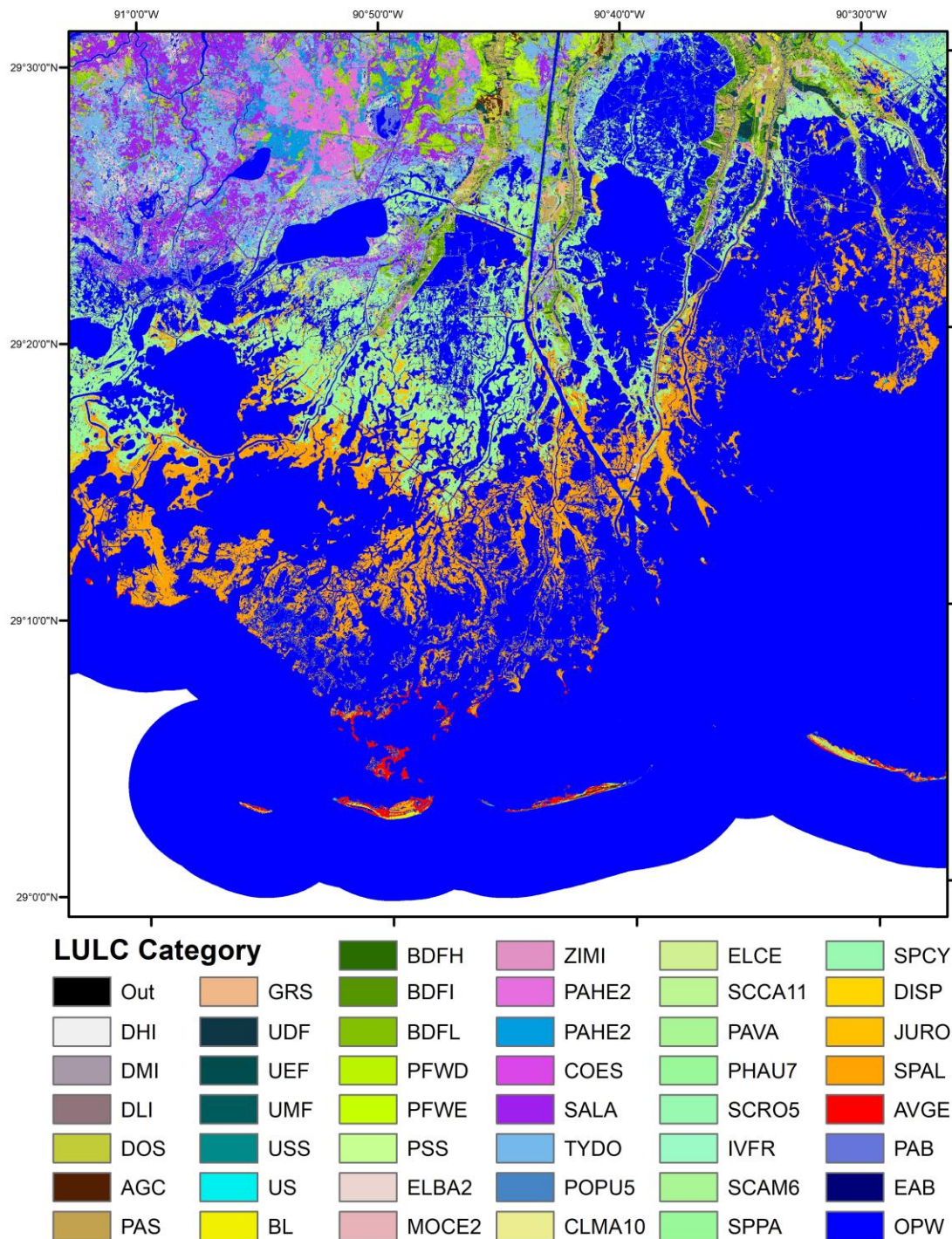


Figure B38. LULC visualization of a 0.5° x 0.5° cell from approximately 29°N to 29.5°N and 91°W to 90.5°W.

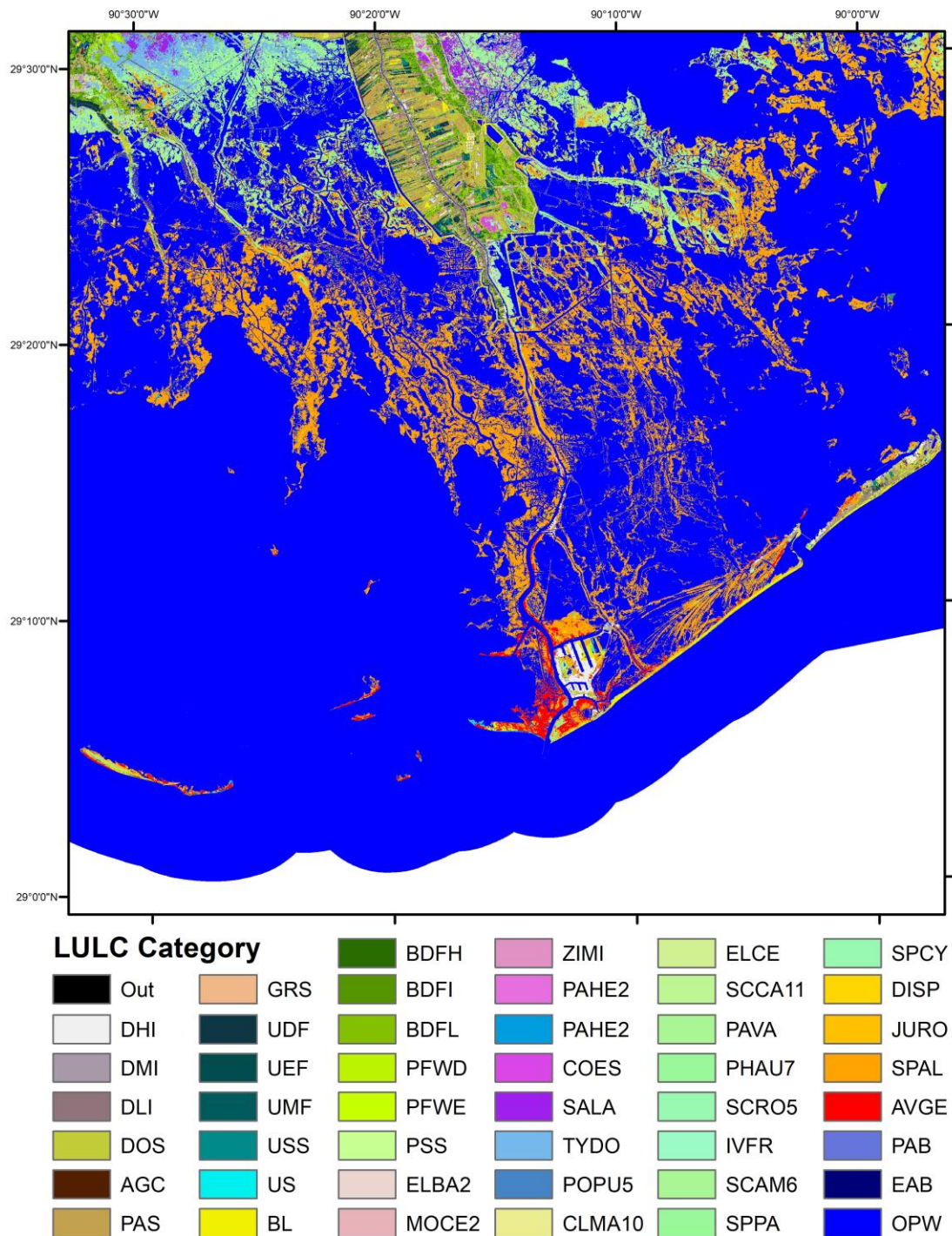


Figure B39. LULC visualization of a 0.5° x 0.5° cell from approximately 29°N to 29.5°N and 90.5°W to 90°W.

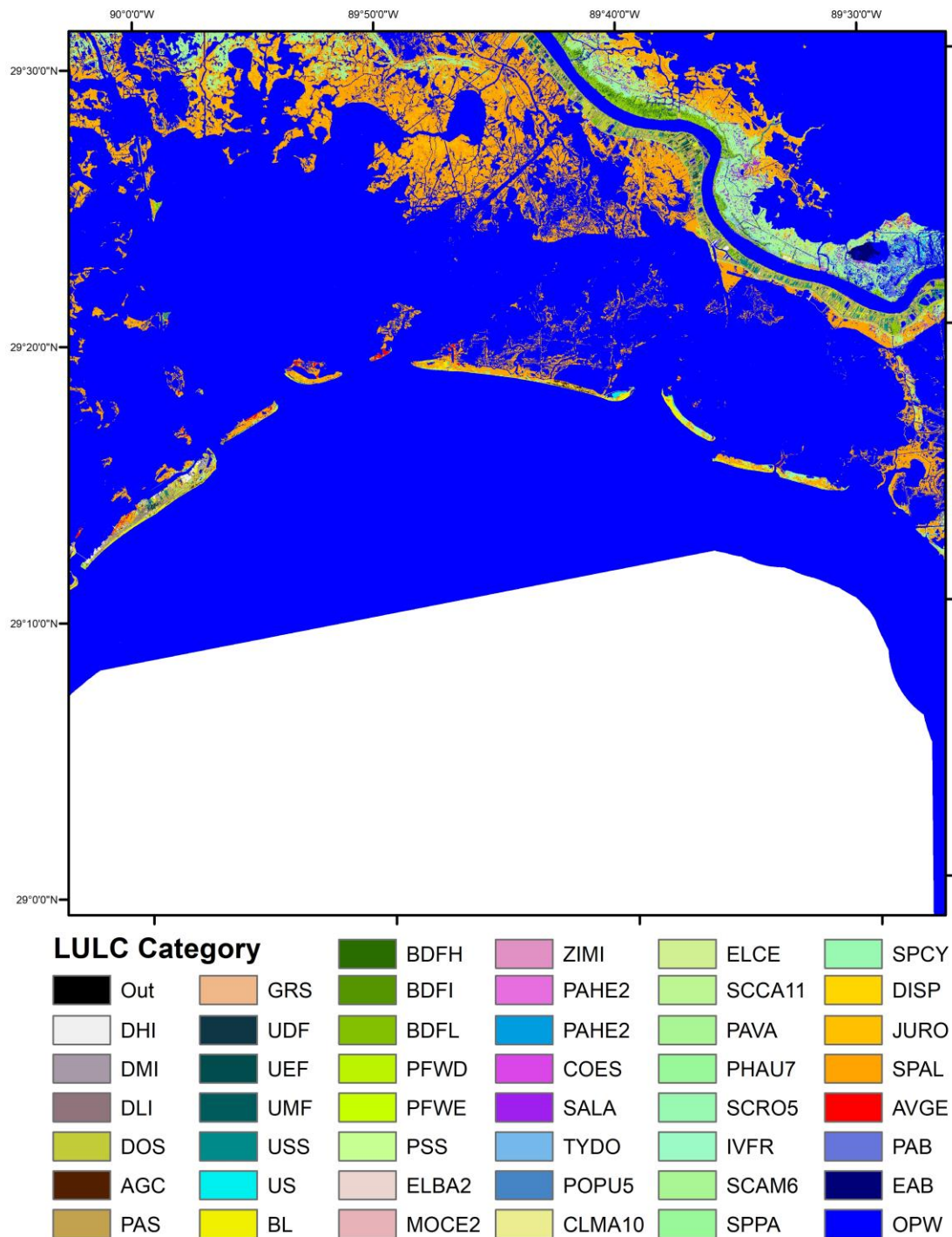


Figure B40. LULC visualization of a 0.5° x 0.5° cell from approximately 29°N to 29.5°N and 90°W to 89.5°W.

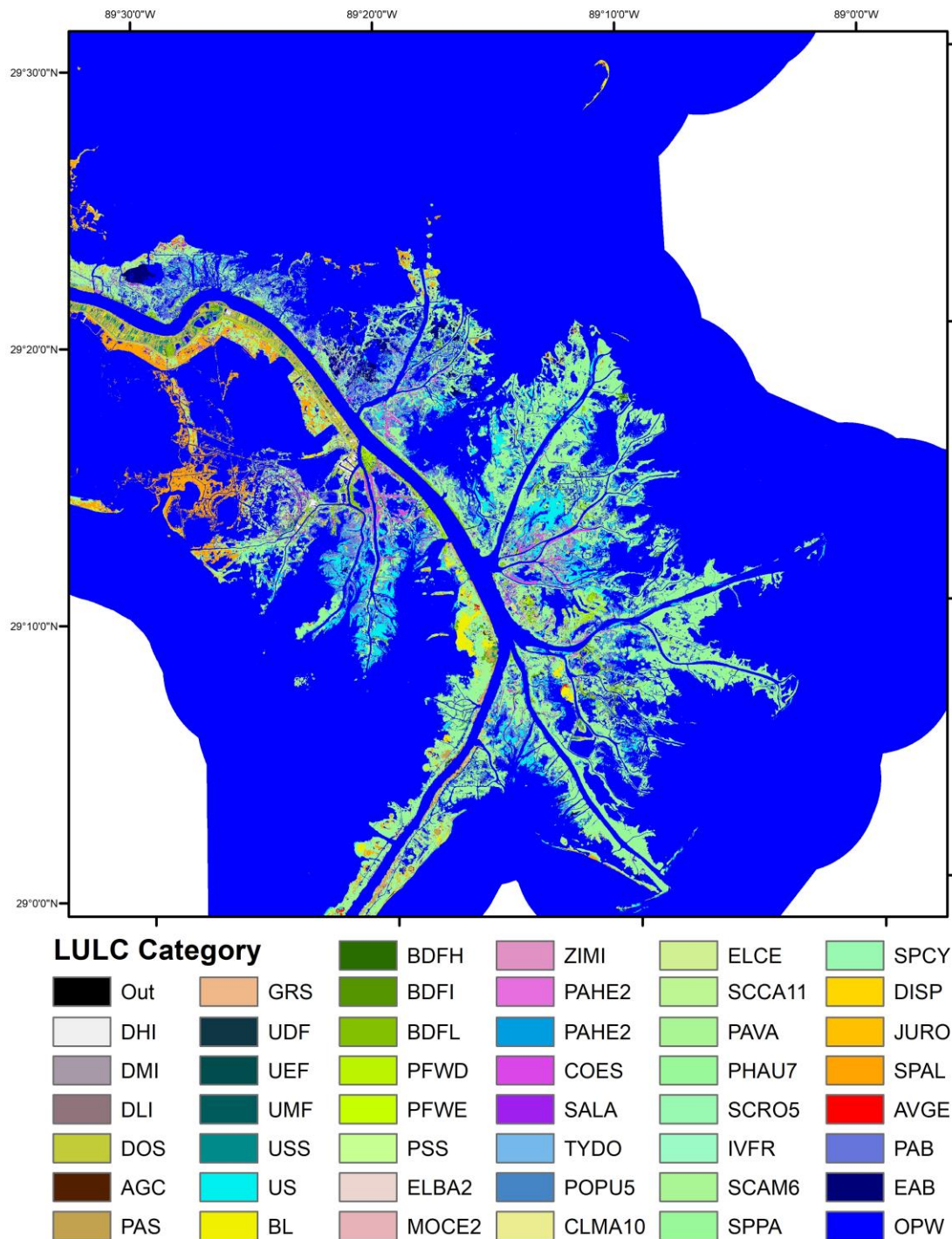


Figure B41. LULC visualization of a 0.5° x 0.5° cell from approximately 29°N to 29.5°N and 89.5°W to 89°W.

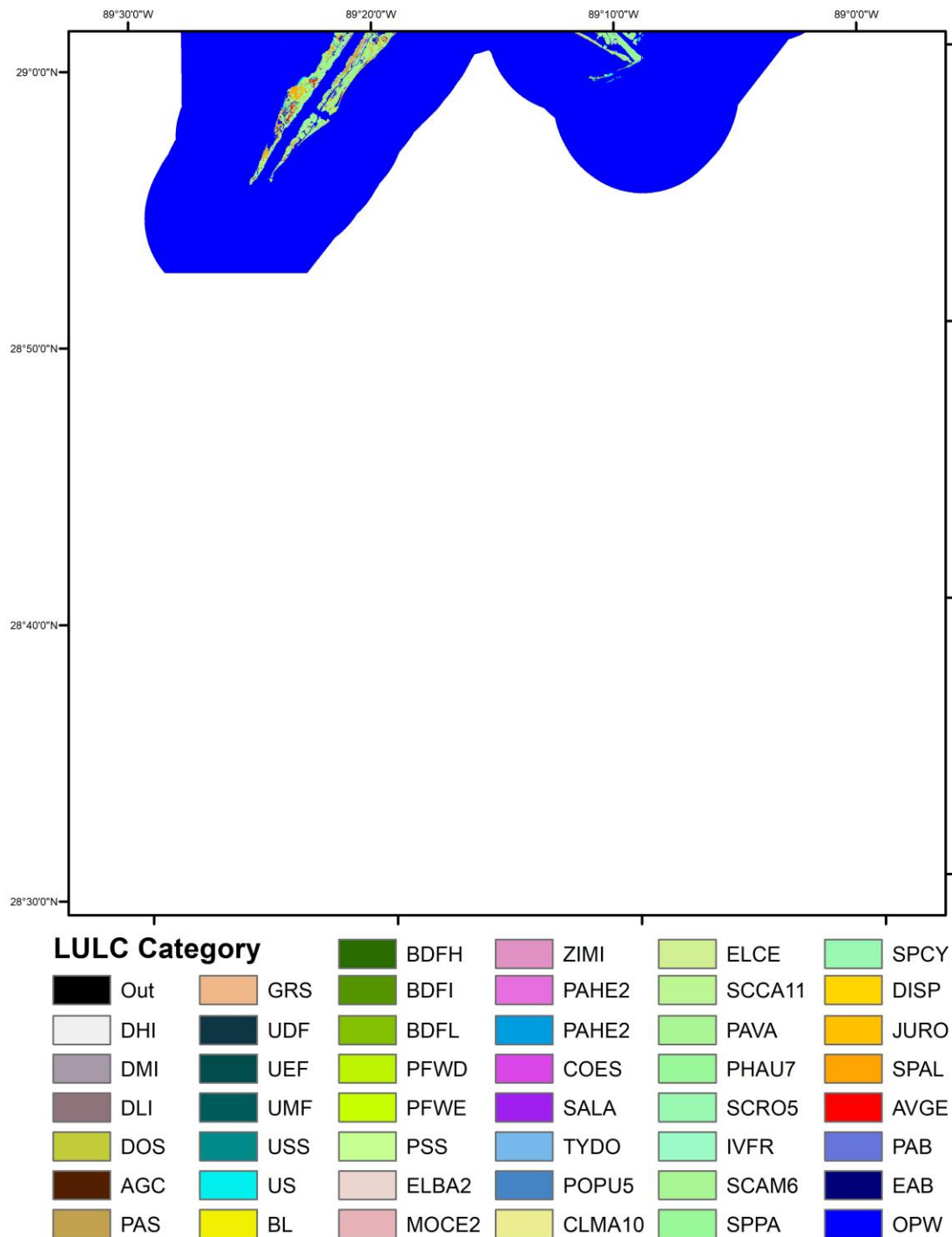


Figure B42. LULC visualization of a 0.5° x 0.5° cell from approximately 28.5°N to 29°N and 89.5°W to 89°W.